JAERI-M
94-038

BENCHMARK EXPERIMENT ON A COPPER SLAB ASSEMBLY BOMBARDED BY D-T NEUTRONS

March 1994

Fujio MAEKAWA, Yukio OYAMA, Chikara KONNO
Yujiro IKEDA, Kazuaki KOSAKO*
and Hiroshi MAEKAWA

日本原子力研究所
Japan Atomic Energy Research Institute

JAERI-Mレポートは，日本原子力研究所が不定期に公刊している研究報告書です。
入手の問合わせは，日本原子力研究所技術情報部情報資料課（〒319-11茨城県那珂郡東海村）あて，お申しこしください。なお，このほかに財団法人原子力弘済会資料センター（〒319-11 茨城県那珂郡東海村日本原子力研究所内）で複写による実費頒布をおこなっております。

JAERI-M reports are issued irregularly.
Inquiries about availability of the reports should be addressed to Information Division, Department of Technical Information, Japan Atomic Energy Research Institute, Tokai-mura, Naka-gun, Ibaraki-ken 319-11, Japan.

編集兼発行　日本原子力研究所
印　　刷　㈱原子力資料サービス

JAERI-M 94-038

Benchmark Experiment on a Copper Slab Assembly Bombarded by D-T Neutrons

Fujio MAEKAWA, Yukio OYAMA, Chikara KONNO
Yujiro IKEDA, Kazuaki KOSAKO* and Hiroshi MAEKAWA

Department of Reactor Engineering
Tokai Research Establishment
Japan Atomic Energy Research Institute
Tokai-mura, Naka-gun, Ibaraki-ken

(Received February 2, 1994)

Copper is a very important material for fusion reactor because it is used in superconducting magnets or first walls and so on. To verify nuclear data of copper, a benchmark experiment was performed using the D-T neutron source of the FNS facility in Japan Atomic Energy Research Institute. An cylindrical experimental assembly of 629 mm in diameter and 608 mm in thickness made of pure copper was located at 200 mm from the D-T neutron source. In the assembly, the following quantities were measured; i) neutron spectra in energy regions of MeV and keV, ii) neutron reaction rates, iii) prompt and decay gamma-ray spectra and iv) gamma-ray heating rates. The obtained experimental data were compiled in this report.

Keywords: Copper, D-T Neutron, Benchmark Experiment, Neutron Spectrum, MeV, keV, Reaction Rate, Gamma-ray Spectrum, Promt Gamma-ray, Decay Gamma-ray, Gamma-ray Heating Rate

---

* Nuclear Energy Data Center (NEDAC)

JAERI-M 94-038

D－T中性子照射による銅平板体系におけるベンチマーク実験

日本原子力研究所東海研究所原子炉工学部
前川　藤夫・大山　幸夫・今野　　力・池田裕二郎
小迫　和明*・前川　　洋

（1994年2月2日受理）

銅は核融合炉において，超伝導磁石あるいは第一壁に使われるなど，非常に重要な材料である。銅の核データの検証を目的として，日本原子力研究所FNSのD－T中性子源を使用してベンチマーク実験を行った。直径629 mm，厚さ608 mmの純銅製円柱状実験体系をD－T中性子源から200 mmに設置した。その体系内において，ⅰ）MeV，keVエネルギー領域の中性子スペクトル，ⅱ）中性子反応率，ⅲ）即発，崩壊γ線スペクトル，ⅳ）γ線核発熱率，を測定した。本レポートは得られた実験データをまとめたものである。

東海研究所：〒319－11　茨城県那珂郡東海村白方字白根2－4
＊㈶原子力データセンター

Contents

目　　次

1. Introduction

Engineering design activities of the International Thermonuclear Experimental Reactor, ITER, are now going on under international collaboration. In magnetic confinement fusion devices, copper is extensively used for various components. It is inevitable material in superconducting magnets and electric conductors. In one of the blanket designs of ITER, copper is also adopted in plasma facing components for first walls in front of blankets or divertor plates because of its superior thermal conductivity.

From a viewpoint of nuclear design, nuclear heating rate, displacement damage of copper and insulator dose are the main design parameters for superconducting magnet. Nuclear heating rate of copper for plasma facing materials are also crucial for cooling design of them. Hence accurate nuclear data constants of copper are required for nuclear design of first walls, blankets and shields. These data are usually retrieved from evaluated nuclear data libraries such as JENDL-3 [1] and FENDL [2]. For practical uses of these libraries, accuracy of them should be verified by analyzing benchmark experiments under D-T neutron fields. Through the verification, problems of the nuclear data are clarified or reliability of the data is proved.

Two integral experiments for copper with D-T neutrons were performed so far. One is the experiment [3,4] which is conducted as a part of the pulse sphere program at LLNL. In the experiment, a time-of-flight spectrum of neutrons and a pulse height spectrum of gamma-rays leaking from a copper sphere of 80 mm in diameter are measured with NE213 liquid organic scintillator. Minimum neutron energy of the time-of-flight spectrum is about 1 MeV, and the pulse height spectrum of gamma-rays is measured in an energy range between 0.2 and 6.5 MeV in recoiled electron energy. These spectra are compared with calculations with ENDF/B-V[5] and ENDL [6] libraries. Another experiment [7-11] was performed at OKTAVIAN in Osaka University. This experiment is also one of the series experiments of sphere. A leakage neutron spectrum down to 0.1 MeV is measured with time-of-flight technique and NE218 liquid organic scintillator from a copper spherical shell of 275 mm in thickness and 6.23 g/cm^3 in apparent density. Leakage gamma-ray spectrum above 0.5 MeV is also measured with NaI(Tl) scintillation detector. These spectra are compared with calculation with JENDL-3T[12], which is the test version of JENDL-3, and ENDF-B/IV [13].

A series of clean benchmark experiments with D-T neutrons were carried out at Fusion Neutronics Source [14] (FNS) in Japan Atomic Energy Research Institute (JAERI) for the purpose of verification of nuclear data. Experiments for lithium oxide [15,18,19], beryllium[16], carbon [17-19], concrete [20-22], iron [18,19,23,24] and tungsten [18,25] were completed so far. In these experiments, cylindrical slab assemblies are adopted, and measurements are performed at several points inside the assemblies. Measured quantities are neutron spectrum, reaction rate such as tritium production rate, foil activation, fission rate and gamma-ray heating rate.

Features of the clean benchmark experiments can be summarized as follows.

1. Since the experimental assemblies have cylindrical shape, two-dimensional transport codes are applicable in addition to Monte Carlo method.
2. The experimental assemblies are thick (typically 600 mm), and measured quantities are obtained at plural points in the assembly. Hence each measured data can be examined as a function of thickness of the material, and it is possible to trace penetration process of neutrons and gamma-rays.
3. Energy and intensity of source D-T neutrons vary with respect to emission angle. In the experiments in which D-T source is centered in a spherical assembly, as OKTAVIAN and LLNL experiments, neutrons emitted toward whole angle contribute to the measured spectra. The angle-dependency of source energy and intensity can not be simulated by one-dimensional analyses. Three-dimensional analyses are needed to simulate it. On the other hand, in our experiments with cylindrical slab assemblies, the angle-dependency of source neutrons can be completely simulated even in two-dimensional analyses.
4. The experimental room is large and room scattered background particles can be negligible, and analysis is needed only for the experimental assembly itself.
5. Because many quantities are measured with various experimental techniques, cross checking of the measured data is possible and reliability of the data can be confirmed.

As an extension of the clean benchmark experiments, an experiment on copper has been carried out. The following data were obtained in the experiment.

1. Neutron Spectrum (0.8 MeV < En) by NE213 Detector
2. Neutron Spectrum (3 keV < En < 1 MeV) by Proton Recoil Gas Proportional Counters
3. Neutron Reaction Rate by Foil Activation Technique
4. Prompt Gamma-Ray Spectrum by NE213 Detector
5. Decay Gamma-Ray Spectrum by NE213 Detector
6. Gamma-Ray Heating Rate by Thermoluminescent Dosimeters

In this report, the general description of the experiment are given in Chapter 2. In Chapter 3, details of each measurement are described and numerical data for all the experimental results are presented with their plots. The experiment is summarized in Chapter 4.

2. General Description of the Experiment

2.1 Experimental Assembly

The experiment was performed utilizing the D-T neutron source facility FNS (Fusion Neutronics Source) in JAERI. The experimental assembly was located in the first target room of FNS as shown in Fig. 2.1.1. The first target room had a grating floor structure to reduce room scattered background neutrons.

The experimental assembly was constructed in a quasi-cylinder by piling up copper blocks. The oxygen-free copper more than 99.99 % purity based on Japanese Industrial Standard C1020 was used. The dimension of the blocks are 50.7 x 50.7 mm square with length of 203.1, 101.5 or 50.7 mm. The equivalent diameter and thickness of the assembly are 629 and 608 mm, respectively, as shown in Figs. 2.1.2 and 2.1.3. The assembly was fastened into aluminum frames as shown in Fig. 2.1.2, and the frames and the assembly were mounted on a deck made of steel. A distance between the D-T neutron source and the front surface of the assembly was 200 mm.

In order to insert several detectors into the assembly, four experimental channels (drawers) were equipped. Some detectors had slender cylindrical shapes. When a cylindrical detector was located parallel to the central axis of the cylindrical assembly, a direction of the detector and that of neutron penetration were parallel. In this case, streaming effect of neutrons through the detector void might be expected in the measurement. Therefore the experimental channels were set so as to insert them from the side of assembly as shown in Fig. 2.1.3. All channels were made by thin sheaths and drawers of 0.2 mm thick stainless steel. Copper blocks of 49.2 mm square, slightly smaller than the standard size blocks, were loaded in these experimental channels. Some of these small blocks have holes of 21 mm square or 21 mm diameter circle to insert various detectors into the channel.

2.2 Neutron Source

Positive deuteron ions were extracted from an ion source with 50 kV voltage, and bent by an analyzing magnet to get single charged ion beam. Then the deuterons were accelerated by 300 kV voltage to 350 keV of the total energy. The deuteron beam was introduced to the first target room and bombarded to a tritium-titanium metal target. The beam current was controlled between 20 nA and 2 mA according to the measurement conditions. The maximum neutron yield was about 3 x 10^{11} neutrons/s for whole solid angle at beam current of 2 mA.

The tritium target structure is shown in Fig. 2.2.1. Titanium layer of 2 mg/cm^2 in

thickness and 20 mm in diameter was deposited on a copper base of 1 mm thickness. Tritiums of about 3.7 x 10^{11} Bq (10 Ci) were absorbed in the titanium layer. The copper base was surrounded by a stainless cover of 0.5 mm thickness, and cooling water was circulated in the gap of 1 mm between the copper base and the cover.

The longer pulse mode operation was applied to the measurement of prompt gamma-ray spectra. Arc current of a filament in the ion source were switched periodically to generate pulsing plasma. A beam divertor was used to cut off spilled d^+ ions. Finally, pulsed neutrons of about 1 ms in width and duty ratio of about 1/3 were obtained.

A pair of neutron and alpha-particle is generated associating with a D-T reaction. The absolute neutron yield can be determined by counting the number of the associated alpha-particles. Two systems of alpha-particle monitor [26,27] with silicon surface barrier solid state detectors are equipped in a beam drift tube. The absolute neutron yield can be determined with accuracy of ± 2 % by the alpha monitor. A long counter and a ^{232}Th fission counter are also settled as relative neutron yield monitors. The long counter is about 10 times much sensitive than the alpha counters. When a number of counts of the alpha monitors are not enough, the long counter calibrated to the alpha counters is used to determine the neutron yield.

Source neutron spectrum emitting from the target is shown in Table 2.2.1 and Fig. 2.2.2. The spectrum was calculated by MORSE-DD [28], simulating the real target structure as precise as possible. The calculated spectrum for 0-degree to the direction of the d^+ beam is normalized to the yield per unit solid angle, and then multiplied by 4π. Hence the energy integration of the spectrum with energy results in 1.1261. The reasons why the integral is more than the unity are as follows. i) Emitted neutrons are slightly enhanced to forward direction by D-T reaction kinematics, and ii) number of neutrons is multiplied by (n,2n) reactions with structural materials of the target. The spectrum of the target gamma-rays generated by interaction of neutrons and structural materials of the target calculated by MCNP [29] is shown in Table 2.2.2 and Fig. 2.2.3. Since the gamma-ray emission is almost isotropic, an integrated spectrum for whole solid angle was given. The energy-integral of the spectrum is 0.1637, i.e., 0.1637 photons are emitted isotropically, following one D-T reaction.

All experimental data contained in this report except decay gamma-ray spectra are normalized to unit source neutron. The unit source neutron does not mean the number of emitted neutrons from the target, but the number of D-T reactions at the target. When the experiment is analyzed, therefore, the source neutron spectrum and the gamma-ray spectrum have to be given by normalizing the total numbers of the source neutrons or photons to 1.1261 and 0.1637, respectively.

3. Experimental Procedures and Results

3.1 Neutron Spectrum

3.1.1 Neutron Spectrum in Energy Region of MeV

Detector Setup

A 14 mm-diameter spherical NE213 liquid scintillator [30] is used for the probe of neutron detection. An NE213 liquid of 1.38 x 10^3 mm^3 is contained in a spherical cell of Pyrex glass of 1 mm in thickness. A sectional view of the detector is shown in Fig. 3.1.1.1. The glass cell is sealed by melting glass in a nitrogen atmosphere, since the contamination due to oxygen degrades the scintillator properties. The sealed point is covered with an aluminum cap and cemented with epoxy resin. The scintillator is mounted on a photomultiplier tube with a quartz light guide of 11 mm diameter and 5 mm length. One side of the light glass is cut in a spherical shape so as to fit to the surface of the glass cell. The glass cell and the light guide are coated with the NE560 reflector paint made of MgO.

The measurements were carried out at the positions in the experimental drawers using special blocks with hole. The typical arrangement for the measurement in the drawer is shown Fig. 3.1.1.2. The R647-02 photomultiplier tube (Hamamatsu Photonics) was attached and the output signals from the anode were terminated by 100 kΩ register at the input of the pre-amplifier with 50 Ω output impedance. The signals were fed to a rise time discrimination circuit through the delay line amplifier. The rise time discrimination techniques (JAERI model 154A[31]) was used for the neutron gamma-ray separation. The rise time and pulse height data were taken in two dimensional array. The measurement was done twice with ten times different gains.

The gain drift of the system is frequently found due to the counting rate variation or temperature change. Therefore, we applied a gain-stabilizer for a stable measurement. The overall gain of the system was monitored by a peak produced by light emission of LED. The LED was connected through a 4 m glass fiber light guide. The difference between the expected position and observed one was fed back to a high voltage power supply. The schematic diagram for the electronic circuit was shown in Fig. 3.1.1.3. The measuring time for each experimental run was 2000 sec. The deuteron beam current was adjusted for the counting rate not to exceed 2000 cps because of dead time consideration.

Data Reduction

The data were stored into the PC/AX computer system in two dimensional data. The two dimensional data were separated into neutron and gamma-ray responses using two

dimensional data sorting kit. After separation of data, two pulse height spectra with two different gains were combined at about 2 MeV. This recoil proton spectrum was unfolded to neutron spectrum by FORIST code[32] using the neutron response matrix previously determined.[33] The response matrix is calculated by Monte Carlo method [30], while the responses in specially important energy regions, i.e., 13.6 to 14.8 MeV, are directly measured and replaced for the calculated response. The FORIST code provides the appropriate energy resolution function by internal iteration. The resolution function, defined as the window function W(E) in the code, is given together with the unfolded results for each run. The spectrum observed, $\Phi_{obs}(E)$, in this system is expressed as follows:

$$\Phi_{obs}(E) = \int_0^\infty \frac{1}{\sqrt{2\pi}\,\sigma(E)} \cdot \exp\left\{ - \frac{(E-E')^2}{2\sigma^2(E)} \right\} \cdot \Phi_{true}(E')\,dE' ,$$

where $\Phi_{true}(E)$: true neutron spectrum without any deformation, and

$$\sigma(E') = \frac{W(E') \cdot E'}{235} ,$$

and the denominator 235 is the conversion factor.[32]

Results and Error Assessment

The measured data are shown in Figs. 3.1.1.4 - 3.1.1.9 for four different positions inside the assembly and on the both surfaces of front and rear of the assembly. Tables 3.1.1.2 and 3.1.1.3 summarize the numerical results of the measured spectra with window functions described above. The obtained spectrum at the front is deformed by oscillation in unfolding code due to mismatching between the real detector response function and the used one. In this case, since the peak flux is more than two order larger than the flux around 5 - 10 MeV region, the flux error in this region is two order more sensitive to the error of the peak flux through the response function. In the deep position, it is seen that there are some small and broad oscillation below 8 MeV. This is partly arisen from the incompleteness of neutron and gamma-ray separation because a fraction of gamma-rays increase with the depth.

The accuracy of the neutron response in the neutron energy range of 13.6 to 14.8 MeV is about 2 % from the experimental confirmation. However, the calculated light output response corresponding to the proton energy below about 2 MeV gives a relatively poor representation. Hence, the errors increase in the lower energy range by accumulation of errors in the higher energy, especially in the case that 14 MeV neutrons are dominant. Table 3.1.1.1 shows the systematic errors which are estimated from the unfolded results measured for mono-energetic neutrons of 14.8 MeV. The error in the range below the peak energy is arisen from the mismatch of the response for 14.8 MeV neutrons due to the response error.

The fraction in the table denotes the ratio of the error in the interested energy range due to the response error to the peak flux around 14 MeV. Here the energy dependent error is represented as follows:

$$Error(\%) \text{ for } \Phi(E_n) = (\text{fraction}) \times \frac{\Phi_{peak}}{\Phi(E_n)} \times 100.$$

If the peak flux around 14 MeV is, for example, ten times larger than the flux below 10 MeV, the proton spectra in the range of 6 to 10 MeV might be distorted by -10 to -20 % , at maximum.

The energy calibration error also affects the unfolded results. The effects of variation in the energy axis are about 3 % above 10 MeV and less than 2 % for 1 to 10 MeV range, respectively. Lastly, the common error of 2 % is from the neutron source intensity which is a basis for all measurements in this experiment. The overall error comes to be 4 % for the flux above 10 MeV and 10 - 20 % below 10 MeV depending on the spectrum shape.

3.1.2 Neutron Spectrum in Energy Region of keV

A small counter head, a new data acquisition technique and the related electronics for proton-recoil gas proportional counter (PRC) were developed by Dr. E. F. Bennett at Argonne National Laboratory to measure the neutron spectrum inside the experimental assembly in the frame of the JAERI/USDOE collaboration program on fusion blanket neutronics [34-36].

Counter

This counter has a cylindrical shape as shown in Fig. 3.1.2.1. It was made from 0.41 mm thick SS-304 alloy. The outer diameter of the counter is only 19 mm so as to obtain a better resolution of position from the test assembly surface. On the other hand, the effective length of the counter is rather long (127 mm) in order to get more counts. The thickness of the anode wire was 20 μm. Field tubes were also added to define the active counter volume. This counter was inserted with the pre-amplifier into an experimental hole of 21 mm x 21 mm which was made vertically to the beam line.

Two identical counter heads were filled by different gases in order to measure the neutron spectrum from a few keV to 1 MeV. One counter was filled by hydrogen gas at 0.5677 MPa (5.789 kgf/cm^2) with 1 percent CH_4 for the low-energy component (from a few keV to 150 keV) and the another at 0.6102 MPa (6.222 kgf/cm^2), 50-50 mixture of hydrogen and argon with 1.8 percent nitrogen for the upper energy component (from 150 keV to 1 MeV). Argon reduces range of recoiled proton since it has larger stopping power. The iron resonance at 27 keV and the thermal peak at 626 keV of $^{14}N(n,p)^{14}C$ reaction were utilized for the energy calibration.

Electronics and Data Acquisition system

A new data acquisition technique [37] was developed to reduce time of measurement and data process. In the conventional technique, several high voltage runs are separately performed for one measurement, but the new technique can take data by single measurement run using high voltage sweep with a ramp shape. The block diagram of the data acquisition system is shown in Fig. 3.1.2.2.

A preamplifier was required to be inserted into an experimental hole of 21 mm x 21 mm to measure the in-situ neutron spectra. A special size preamplifier of 20 mm x 20 mm x 200 mm was devised based on an original ANL designed preamplifier. It was also redesigned to operate at +45 V / -15 V to mitigate overload events by higher energy neutrons by a sufficient margin.

An analog programmable high-voltage DC/DC converter supplies the high voltage for the counter. An analog function generator, which produces time dependent analog profile

(sawtooth), serves as driver to the DC/DC converter to change the high voltage. As the result, output high voltage slowly changes with the period of 165 sec between the upper and lower voltages during the acquisition. The generated high voltage is monitored using a dividing resistance, which scaled down high voltage by about 1/500. The about 500 Hz test pulses with the rise time larger than that of any pulse from ionizing events are fed to the preamplifier. The pulse height of the test pulse also changes like sawtooth with the period a few seconds.

There are two analog pulse amplifiers required for pulse shape discrimination against gamma ray events. One is an integration amplifier (Y-amplifier) with output proportional to input pulse height, i. e. the energy of recoiled proton. This amplifier is modified using R-C filtering [38] in order to reduce the effects by overload signals. The other amplifier, called X-amplifier, has much shorter shaping time constants than the Y-amplifier. Its output is proportional to the input pulse height and the reciprocal of the rise time of input pulse.

The outputs of Y-amplifier, X-amplifier and the dividing resistor are digitized to 4096 channel maximum by one analog digital converter using a multiplexer and logical circuits. The digitized data are taken to an EPSON-PC286V personal computer (CPU: 80286) through an interface board of LSI 8255A. The data acquisition program calculates 1) the ratio of the X-amplifier output to the Y-amplifier, which is proportional to the reciprocal of the rise time of the event, 2) a gas multiplication corresponding to the high voltage and 3) the energy (in log-scale) of recoiled proton using the output of Y-amplifier and the gas multiplication on line. The ratio of X/Y and the energy are stored to a two dimensional array (32 channel x 512 channel).

Measurement and Data Processing

The measurement was performed at the front and rear surface and at the depths of 76, 228, 380 and 532 mm from the copper assembly surface. The counters were inserted from the side perpendicularly to the direction of the D-T neutrons. The high voltage changed from 3000 to 4200 V and from 2400 to 3000 V in hydrogen and hydrogen/argon counters, respectively.

In off-line data processing, the recoil proton events and test pulse events were selected using the rise time information for each proton recoil energy. The test pulse events were used in order to estimate dead time loss and to normalize recoil proton events. Neutron spectra $\Phi(E)$ was derived using the following equation,

$$\Phi(E) = \frac{1}{N \cdot S \cdot \sigma(E)} \cdot \frac{E}{\sigma(E)} \cdot \frac{dD(E)}{dE} \quad ,$$

where N : hydrogen atom number

S : source neutron

$\sigma(E)$: n-p scattering cross-section

D(E) : recoil proton spectrum.

The measured spectra are shown in Figs. 3.1.1.4 - 3.1.1.9, and the numerical values are given in Tables 3.1.2.1 and 3.1.2.2.

Error Assessment

Possible error sources of this technique are gas pressure (Hydrogen atomic number), n-p scattering cross section, fitting error for differentiation of recoil proton spectrum due to count statistics and calibration of recoil energy. The fitting error is the largest, which is about 3 - 10 % above 10 keV, while the other errors are expected to be less than 1%. Moreover, neutron spectra below 10 keV tend to become smaller due to the uncertainty of the W-value, which is the average energy lost by the incident particle per ion pair formed. The error due to W-value is not included in the experimental errors.

3.2 Neutron Reaction Rate

The reaction rates were measured by the foil activation technique. In order to give spectral indices for wide energy range, plural reactions with different threshold energy were considered along with some (n,γ) reactions. In Table 3.2.1, reactions are listed with their effective threshold energies. The general use of the common dosimetry reactions, e.g., $^{27}Al(n,\alpha)^{24}Na$, $^{56}Fe(n,p)^{56}Mn$, $^{58}Ni(n,p)^{58}Co$, $^{58}Ni(n,2n)^{57}Ni$, $^{90}Zr(n,2n)^{89}Zr$, $^{93}Nb(n,2n)^{92m}Nb$, $^{115}In(n,n')^{115m}In$, $^{197}Au(n,\gamma)^{198}Au$ and so forth, was of particular importance, because of facilitating the comparative study of neutronics products on different material configurations.

Activation Foils and Irradiation

Sample size was 10 mm in diameter and 1 mm in thickness for activation foils except Indium and gold. Indium foils had a dimension of 10 x 10 x 1 mm^3. In order to minimize the self-shielding effect for the $^{197}Au(n,\gamma)^{198}Au$ reaction, gold foils with a size of 10 mm x 10 mm x 0.001 mm were adopted. The other ordinary threshold foils were set in the experimental drawer channels for the axial distribution measurement.

The foils were irradiated for about 10 hours with D-T neutrons and total neutron yields at the target are 5.3 x 10^{15} n. Neutron production rate was monitored by the associated α-particle counting method. The irradiation history was recorded by using the multi-channel scaling (MCS) for the decay correction during irradiation.

Reaction Rate Determination

After the irradiation, γ-rays were measured with Ge detectors. As described, a large number of foils were subjected in this system to realize a precise spacial distribution of reaction rate. Four Ge detectors were used and relatively calibrated to the standard detector. The detecting efficiencies for the relative detectors were calibrated with the standard detector by using the same activity sample which was irradiated at the experiment. This scheme facilitated whole counting time without loosing any accuracy in the experimental error for the efficiency.

Reaction rate, **RR**, were derived from the γ-ray counts with necessary corrections. The **RR** is given as,

$$\mathbf{RR} = \frac{\lambda \cdot C \cdot A}{\varepsilon \cdot W \cdot N_a \cdot a \cdot b \cdot Y \cdot S_a \cdot \mu \cdot (1-\exp(-\lambda \cdot t_i)) \cdot \exp(-\lambda \cdot t_c) \cdot (1-\exp(-\lambda \cdot t_m))},$$

where,

λ: decay constant (/sec),

C: γ-ray peak counts,

A: atomic mass,
ε: detector efficiency,
W: sample weight,
N_a: Avogadro's number,
a: natural abundance of the target element,
b: γ-ray branching ratio,
Y: neutron source strength (/sec)
S_a: correction factor for the decay during irradiation,
μ: γ-ray self absorption correction factor,
t_i: irradiation time,
t_c: cooling time,
t_m: collection time.

The neutron yield fluctuation monitored with the MCS was used for the correction of S_a. The correction of μ was assumed to be treated by one dimensional model. The decay data for the half-life (decay constant) and γ-ray branching ratio were taken from Ref. 39). The neutron strength, Y, was time averaged neutron productions monitored with the fission chambers. The natural background γ-ray subtraction was sometime critical for weak activities (^{57}Ni, ^{115m}In, ^{89}Zr, ^{92m}Nb) located in the deep positions in the assemblies. In that case, the contributions were carefully subtracted from the net peak counts. Counting loss due to coincidental sum-peak in the cascade γ-rays was corrected.

Experimental Error and Uncertainty

Major sources of the error for the reaction rate were the γ-ray counting statistics (0.1 to several %) and the detector efficiency (2 to 3 %). The error for sum-peak correction was estimated less than 2 % depending on the decay mode and fraction of multiple γ-ray cascade. The error for the decay correction was reflected from the error of half-life of the activity. If the half-life was accurate, the error for the saturation factor should be less than 1 % even for the short half-life activities.

The other errors associated with foil weight, γ-ray self-absorption, irradiation time, cooling time and counting time were negligibly small. The error for neutron yield was estimated to be 2 %. The overall error for the major part of reaction rate ranged from 3 to 6 %. Some data for high threshold reaction in the deep positions suffered from poor counting statistics due to low activation rate.

Highlights of the Measured Reaction Rate Distributions

In Table 3.2.2, the results for the reaction rates are given with experimental errors. A

corresponding plot of the reaction rate distribution is shown in Fig. 3.2.1. As the spectral indices point of view, the ratio of the reaction rates plays very effective role. The ratios of reaction rate to the $^{115}In(n,n')^{115m}In$ is shown in Fig. 3.2.2. In this figure, all of reaction rates at the position of front surface (200 mm) are normalized to be 1.0, in order to focus the spectral sensitivity of respective reactions. Highlights observed form the experimental value are given as follows:

(i) The threshold type reaction show almost same trend of the decreasing distribution profile as the depth of the detector increase in the copper assembly. Figure 3.2.2 gives more precise index for the high energy neutron flux. The $^{64}Zn(n,p)^{64}Cu$, $^{56}Fe(n,p)^{56}Mn$ and $^{90}Zr(n,2n)^{89}Zr$, shown in Fig. 3.2.2, are the threshold reaction with higher threshold energy than that of reference $^{115}In(n,n')^{115m}In$ reaction. The ratios of reactions with higher threshold energy decrease more rapidly than those with lower threshold energies. This corresponds the difference in the reaction sensitivity to the low energy neutrons which are enhanced in the deeper location. From this ratio analysis, a spectrum change can be roughly investigated.

(ii) The reaction rate for the ^{64}Cu production, however, exhibits a difference in the distribution at locations deeper than 200 mm from the surface of the assembly. This is due to the increase of contribution from the $^{63}Cu(n,\gamma)^{64}Cu$ reaction relative to the $^{65}Cu(n,2n)^{64}Cu$ reaction, both of which produce the same ^{64}Cu radioactivity.

It is understandable by the consideration that the 14 MeV neutron flux decrease as the depth increase, resulting in the less contribution of the $^{65}Cu(n,2n)^{64}Cu$. On the other hand, contribution from $^{63}Cu(n,\gamma)^{64}Cu$ to the total ^{64}Cu production increase because the (n,γ) is, in general, sensitive to low energy neutrons. The reaction rate ratio shown in Fig. 3.2.2 gives more clear picture of the $^{63}Cu(n,\gamma)^{64}Cu$ domination for ^{64}Cu production at the deep location of the assembly. It is obviously understood that the ^{64}Cu at 600 mm depth is produced by the $^{63}Cu(n,\gamma)^{64}Cu$ reaction, more than three orders of magnitude of largely than that by the $^{65}Cu(n,2n)^{64}Cu$ reaction. This particular reactions associated with copper are of importance in understand the radioactivity production distribution in the copper materials. The present results give straightforward experimental data for the activation analysis.

(iii) The distribution profile of the $^{197}Au(n,\gamma)^{198}Au$ reaction rate is quite different from those of other threshold reactions. This is simply because the most sensitive energy for (n,γ) reaction, in general, is at the resonance or the thermal energy, as mentioned for $^{63}Cu(n,\gamma)$ reaction. This is shown in enhanced way in Fig. 3.2.2. At the position of 500 mm depth, the ratio of reaction rate to that of $^{115}In(n,n')$ is more than 400. Indirectly this graph indicates that the neutron spectrum at the deep location is dominated by the slow neutron, and 14 MeV neutron fraction seems negligibly small.

3.3 Gamma-Ray Spectrum

Gamma-rays to be measured as benchmark data for fusion neutronics can be classified into two components; prompt and decay gamma-rays. The prompt gamma-rays are emitted when a nucleus in an excited state produced by a neutron interaction transits to its ground state. The half life of the nucleus is usually shorter than nano-second. The decay gamma-ray emission follows an alpha or a beta decay of an unstable nucleus, or emitted by a transition of a meta-stable nucleus to its ground state. The half life of the decay is usually longer than one second. Because half lives of prompt and decay gamma-rays largely differ from each other, importance of the two kinds of gamma-rays on the engineering is also quite different. Prompt gamma-rays are related to the design parameters during operation of fusion devices, while decay gamma-rays are related to those after shutdown. Data bases and calculation codes used for these design parameters are also different. Therefore prompt and decay gamma-rays should be clearly separated each other in benchmark experiments for fusion neutronics.

Measurements of prompt and decay gamma-ray spectra are described in sections 3.3.1 and 3.3.2, respectively.

3.3.1 Prompt Gamma-Ray Spectrum

Gamma-Ray Spectrometer

The following properties are required as an in-situ gamma-ray spectrometer.

i) It is possible to separate gamma-ray events from neutron events.
ii) The detector hardly emits gamma-rays by itself.
iii) The detector response has an energy dependency of incident gamma-rays.
iv) Sensitivity is isotropic.
v) It should be as small as possible to avoid perturbation of the measurement neutron and gamma-ray fields.

A liquid organic scintillation counter NE213 [40] is selected for the purpose. A sectional view of the counter is shown in Fig. 3.3.1.1. Outer dimensions of the counter are 48 mm in diameter and 262 mm in length. The scintillator is a sphere of 40 mm in diameter, and contained in a Pyrex glass cell. Composition of the counter is almost as that of usual scintillation counters, but an optical fiber is equipped for gain stabilization. Light pulses from an external light source can be introduced to the light guide through the optical fiber.

Electric Circuit

The electric circuit used in the measurement is shown in Fig. 3.3.1.2. Dynode signals from Photomultiplier Tube (PMT) are fed to a pre-amplifier, and the output signals are put

into two Delay Line Amplifiers (DLAs) at the same time. Gains of the two DLAs are different by about 10 times to obtain energy spectra of wide dynamic range. Uni-polar pulse signals from each DLA are fed to a Rise-Time-to-Pulse-Height-Convertor and discriminated into neutron and gamma-ray signals according to difference of the rise time of signals to make gate signals for gamma-ray events. Pulse height signals of gamma-rays from DLA are selected using the gate signals at Linear Gates, and stored in a Multichannel Analyzer.

In general, a gain of a photomultiplier tube drifts with counting rate or temperature change. To suppress the gain drift, a gain stabilization system is equipped. Light pulses of constant intensity generated by a light emitting diode in a thermostat are injected into the PMT through the light guide of scintillator. Drift of the detector pulses to the light pulses is monitored and the high voltage applied to the PMT is fed back to keep the pulse height always constant. The light pulse signals mixed in a pulse height spectrum from gamma-rays are rejected from the spectrum by anti-coincidence. The gain is kept in about accuracy of 1 % by the gain stabilization system.

Rejection of Decay Gamma-Rays by Long Pulse Method

As mentioned above, in a measurement of prompt gamma-rays, it is important to clearly reject decay gamma-rays which are regarded as the background. In a case of copper in D-T neutron fields, decay gamma-rays from ^{62}Cu and ^{64}Cu generated by the following two reactions are dominant as the background.

^{63}Cu(n,2n)^{62}Cu	σ_{14MeV}= 570 mb	$T_{1/2}$=9.73 m	E_γ=0.511 MeV	I_γ=195.6 %
^{65}Cu(n,2n)^{64}Cu	σ_{14MeV}= 953 mb	$T_{1/2}$=12.7 h	E_γ=0.511 MeV	I_γ=38.6 %

As shown in Fig. 3.3.1.3, intensity of these decay gamma-rays changes at every moment depending on a history of neutron irradiations for the experimental assembly. If the decay gamma-rays are measured before or after the measurement of prompt gamma-rays, it is very difficult to determine the averaged amount of decay gamma-rays during the measurement of prompt gamma-rays. Hence the pulsed neutron method is applied to accurately determine the background.

A period, between the times when D-T neutrons are injected into the experimental assembly and when neutrons disappear from the assembly due to captures and leakages, is almost equal to several hundreds μs, corresponding to the slowing down time of D-T neutrons to thermal neutrons. Prompt gamma-rays following neutron reactions are emitted by several hundreds μs after injection of D-T neutrons. Pulsed neutrons of several hundreds μs in width are generated and the periods of measurement for foreground and background gamma-rays are determined as shown in Fig. 3.3.1.3. Intensity of decay gamma-rays emitted by activated nuclei which half-lives are usually longer than one second can be regarded as constant during

the measurement period of foreground and background runs. Pulse height spectra (PHS) for the foreground and the background runs are measured at the same time with different time-gate. Pulse height spectrum without decay gamma-rays is accurately derived subtracting the background spectrum from the foreground one.

Measurement

Prompt gamma-ray spectra were measured in the experimental channels at four positions; 76, 228, 380 and 532 mm from the front surface of the assembly. The center of the scintillator of the NE213 gamma-ray spectrometer was set to the position on the central axis of the assembly. The accelerator was operated in the arc-pulse mode with pulse width of 0.75 ms and repetition rate of 1.98 ms. Deuteron beam current was adjusted to between 20 nA and 10 μA depending on the measurement positions to keep the counting rates constant. The maximum counting rate was limited about 2000 cps for sum of neutron and gamma-ray events of high-gain circuit. Absolute neutron yields were determined by using the alpha-counter mentioned in the chapter 2. In the measurements at positions of 76 and 228 mm, since the number of counts of the alpha-monitor was less than 1000, the neutron yields were determined by the long-counter. The long-counter is about 10 times more sensitive than the alpha-counter, and it was calibrated to the alpha-counter. Energy calibration of measured pulse height spectra was performed with the Compton edge of 1.275 MeV gamma-rays of Sodium-22. Signals from a high precision research pulser were fed into the pre-amplifier to determine zero pulse height.

Data Processing

Measured PHSs for high and low gains were connected to one PHS for both foreground and background runs. The background PHS were subtracted from the foreground PHS. The obtained PHS were unfolded using the FORIST code [32] to derive energy spectra higher than 0.25 MeV. The response matrix used in the unfolding process was calculated by using the MARTHA code [41]. The original MARTHA code was the Gamma-Ray Response Matrix Calculation Code for NaI(Tl) Scintillator, but the cross section data in the code used was replaced for NE213 scintillator. The obtained gamma-ray spectra at four positions are shown in Fig. 3.3.1.4 and Tables 3.3.1.1 - 3.3.1.4. The errors in the figure and tables are statistical ones only. The FORIST code provides a window function W(E) with the spectrum. The window function corresponds to the energy resolution of the unfolded spectrum in full width at half maximum in percentage. If a true spectrum and an observed spectrum is expressed as $\Phi_{true}(E)$ and $\Phi_{obs}(E)$, respectively, they are related with the next equation.

$$\Phi_{obs}(E) = \int_0^{\infty} \frac{1}{\sqrt{2\pi}\sigma(E)} \cdot \exp\left\{ - \frac{(E-E')^2}{2\sigma^2(E)} \right\} \cdot \Phi_{true}(E')dE'$$

where

$$\sigma(E) = \frac{W(E) \cdot E}{235} .$$

Namely, the obtained spectra are broadened by Gaussian distribution of which standard deviation is (window function / 235.5).

Error Estimation

Error sources are estimated as follows.

Neutron Yield	±2 - 3 %
Response Functions	+0 - 8 %
Perturbation Effect by the NE213 Counter	+0 - 10 %
Statistics Error	±4 - 10 %

Errors for the neutron yield include calibration errors of long counter. Errors for response functions are estimated by measuring gamma-rays from calibrated standard sources up to energy of 2.754 MeV [40]. It is found that the measured spectra obtained through the unfolding process are larger by 0 - 8 % comparing with actual intensities of the sources. Perturbation effect caused by the insertion of the NE213 detector is examined by Monte Carlo calculations with and without detector modeling. When the detector is modeled, the calculated spectra become larger by 0 - 10 % in the energy range higher than 0.2 MeV compared to the cases without modeling. Statistics errors are given in Tables 3.3.1.1 - 3.3.1.4.

The error sources due to response functions and perturbation effect are systematic errors, and the statistic error is a random error. In the error of neutron yield, both systematic error for the calibration of the alpha-monitor and long counter and random error of counting statistics are included. As a whole, the measured spectra are observed roughly 0 - 15 % larger than the true spectra. Errors except statistical ones are not included in Tables 3.3.1.1 - 3.3.1.4 and Fig. 3.3.1.4.

Uncorrected Factors in the Measured Spectra

The following parasitic and contaminated gamma-rays are not corrected from the measured gamma-ray spectra, because it is impossible to separate.

(i) The NE213 liquid scintillator is contained in a boric-silicic glass (Pylex glass). The

next reaction takes place in boron-10 of the glass mainly for low energy neutrons.

$$^{10}B(n,\alpha)^{7}Li^{*}, \quad ^{7}Li^{*} \rightarrow ^{7}Li + \gamma\,(0.478\ MeV)$$

The gamma-rays of 0.478 MeV are not produced by the copper but by the detector itself. Annihilation gamma-rays arising from electron pair creations are seen at energy of 0.511 MeV in an usual gamma-ray spectrum. Gamma-ray peaks observed around 0.5 MeV in the measured spectra are formed by the 0.487 MeV gamma-rays and the annihilation gamma-rays. As the depth of detection position increases, a fraction of low energy neutron increases and the $^{10}B(n,\alpha)^{7}Li^{*}$ reactions occur more frequently. And then, the contribution of 0.478 MeV gamma-rays becomes dominant around 0.5 MeV.

(ii) The organic scintillator NE213 consists of hydrogen and carbon. Hydrogens emit gamma-rays following neutron capture reactions.

$$^{1}H(n,\gamma)^{2}H^{*}, \quad ^{2}H^{*} \rightarrow ^{2}H + \gamma\,(2.225\ MeV)$$

This gamma-rays of 2.225 MeV also disturb measured gamma-ray spectra. According to the another experiment, a ratio of observed gamma-rays from $^{10}B(n,\alpha)^{7}Li^{*}$ reactions to those from $^{1}H(n,\gamma)^{2}H^{*}$ reactions for the NE213 counter has been found to be about 20. Hence small bumps at 2.2 MeV seen in the measured spectra at 380 mm and 532 mm can be identified as the gamma-rays associated with the $^{1}H(n,\gamma)^{2}H^{*}$ reactions.

(iii) Target gamma-rays, that is, gamma-rays generated by neutron interactions with the structural materials of the target, are emitted along with neutrons. The target gamma-rays are also included in the measured spectra. According to an estimation by a transport calculation, the followings are found. The target gamma-rays contribute most to the spectrum at 76 mm. At that position, fractions of the target gamma-rays to those generated by neutron interactions with copper are roughly summarized as follows.

$E\gamma < 2.5$ MeV	1.5 - 3 %
$2.5 < E\gamma < 8$ MeV	3 - 5 %
$8 < E\gamma < 10$ MeV	5 - 10 %

At the measurement positions deeper than 228 mm, the contribution of the target gamma-rays can be negligible as it is less than 1 %. But at the position of 76 mm, it should be considered in transport calculations.

3.3.2 Decay Gamma-Ray Spectrum

Measurement

Spectra of decay gamma-rays emitted from activated nuclei were measured after an irradiation as a function of cooling time. The method of measurement is basically almost the same as that of prompt gamma-ray spectrum. The different points are as follows.

The NE213 spectrometer was located in a experimental channel at 76 mm from the front surface of the assembly. The similar electric circuit was used as Fig. 3.3.1.2, but output signals from the DLA were put directly into the ADC with single gain and without pulse shape discrimination. An irradiation was carried out with deuteron beam current of 2 μA resulting in a neutron generation rate of 2 x 10^8 neutrons/sec. The irradiation was continued for 20 minutes. Just after stop of the irradiation, sequential measurements of pulse height spectrum was started in turn. A time chart of the measurement is shown in Table 3.3.2.1. The memory of the MCA which store digitized data from ADC was switched one after another for the series of measurement. It took about 5 seconds to switch the memory. The maximum counting rate was about 4700 cps for the measurement just after the irradiation.

Data Processing

Background pulse height spectra were subtracted from foreground ones, and the pulse height spectra were unfolded to derive gamma-ray energy spectra in just the same method as the prompt gamma-ray measurement. The obtained spectra were normalized as gamma-ray flux [1/ sec / cm^2] when the assembly was irradiated for 20 minutes with a neutron generation rate of 10^{10} neutrons/sec.

Background pulse height spectra were measured twice for 7 minutes just before the irradiation, pre-measurement, and from 187 to 248 minutes after stop of the irradiation, post-measurement. Since this experiment was performed after the other experiments in a day without enough cooling time, activated nuclei generated in the previous experiments had not been sufficiently disintegrated in the pre-measurement. Hence background of post-measurement was used in the present experiment. Because the used background were measured after about 3 - 4 hours since the stop of irradiation, gamma-rays which half lives were more than a few hours were also contained in the background spectrum and they were subtracted from the foreground spectrum.

Results

The measured spectra are shown in Table 3.3.2.2 - 5 and Fig. 3.3.2.1. In the figure, remarkable peaks at 0.5 MeV and their Compton continua between 0.2 and 0.4 MeV were seen. In an energy range of 0.6 - 4 MeV, several components of gamma-rays are seen.

These gamma-rays are integrated in four energy ranges; 0.4 - 0.65 MeV, 0.65 - 1.0 MeV, 1.0 - 1.4 MeV and 1.4 - 3.0 MeV. The results are shown in Table 3.3.2.6 and Fig. 3.3.2.2 - 5. Since the integrated spectra between 0.4 - 0.65 MeV which correspond to the peaks at 0.5 MeV were well fitted with a line of 9.74 minutes of half life as seen in Fig. 3.3.2.2, the component can be attributed to annihilation gamma-rays from ^{62}Cu produced by ^{63}Cu(n,2n) reactions.

Gamma-rays between 1.4 and 3.0 MeV can be fitted with two component of 2.24 and 13.91 minutes of half lives as shown in Fig. 3.3.2.5. The component of 13.91 minutes is thought as gamma-rays of about 2 MeV energy from ^{62m}Co produced by ^{65}Cu(n,α) reactions. The other component of 2.24 minutes is regarded as gamma-rays of 1.779 MeV from ^{28}Al. Silicon-28 and aluminum-27 are contained in the scintillator cell made of glass and aluminum cap of the detector, respectively. Nuclei of ^{28}Al can be produced by ^{28}Si(n,p)^{28}Al and ^{27}Al(n,γ)^{28}Al reactions. Hence the component of 2.24 minutes is not attributed to the copper but to the scintillation detector itself, and an attention have to be paid to the peaks which are seen around 1.8 MeV until about 20 minutes in Fig. 3.3.2.1.

The integrated spectra between 1.0 and 1.4 MeV can be separated into three components of 2.24, 9.74 and 13.91 minutes as shown in Fig. 3.3.2.4. The three components are interpreted as follows; (i) 2.24 minutes: Compton continua of 1.779 MeV gamma-rays from ^{28}Al, (ii) 9.74 minutes: gamma-rays of 1.173 MeV from ^{62}Cu produced by ^{63}Cu(n,2n) reactions and (iii) 13.91 minutes: gamma-rays of 1.164 and 1.173 MeV from ^{62m}Co produced by ^{65}Cu(n,α) reactions.

As for the integrated spectra between 0.65 and 1.0 MeV shown in Fig. 3.3.2.3, because many Compton continua from gamma-rays with energies higher than 1 MeV from the spectra, the source of gamma-ray emission can not identified.

3.4 Gamma-Ray Heating Rate

Principle of Measurement

Gamma-ray heating rate is defined as absorbed dose of gamma-rays in a medium. To measure the gamma-ray heating rate, a method which utilize a plural kinds of thermoluminescence dosimeter (TLD) was proposed [42] by Tanaka, et al. The principle is described in the Ref. 42), and examples of the application of the method in D-T neutron fields are described in Ref. 18), 19) and 33). Here, brief explanations are given. Absorbed doses of gamma-rays in a medium measured by different kinds of TLDs monotonously increase as a function of effective atomic numbers of the TLDs. Hence the absorbed dose of the medium can be derived by interpolating absorbed doses measured by several kinds of TLDs.

Irradiation

Since the atomic number of copper is 29, three kinds of TLDs which effective atomic numbers (Z_{eff}) are around 29 are selected; MSO (Mg_2SiO_4, Z_{eff}=11.1), SSO (Sr_2SiO_4, Z_{eff}=32.5) and BSO (Ba_2SiO_4, Z_{eff}=49.9). All TLDs are powder and are sealed in glass capsules of 2 mm in diameter and 12 mm in length. All TLDs are calibrated at a cobalt-60 standard gamma-ray field.

After washing with ethyl alcohol, TLDs were annealed for 30 minutes at 500 ℃. Four samples of each TLD were packed in a polyethylene bag, and seven bags were made in total. Six bags were set in the four experimental channels and at the front and rear surfaces of the assembly. The positions of TLDs were -1, 58, 210, 362, 514 and 609 mm from the front surface of the assembly. The rest of the bags was kept without irradiation for the background estimation.

The irradiation was carried out for 16 minutes with d^+ beam current of 1.5 mA, and the total neutron yield was 2.31×10^{14}. About 15 minutes after the irradiation, TLDs were taken out from the experimental assembly and kept in a dark place. One week later from the irradiation, thermoluminescences (TL) were read out by a TLD reader (KYOKKO 2500).

Data Processing

Average values and standard deviations of TL were calculated for each group of four TLDs which were the same kind and irradiated at the same position. Averaged TL for unirradiated TLDs, which were considered as background, was subtracted from that for irradiated TLDs. The obtained TL was converted to the unit of exposure dose of ^{60}Co equivalence.

Since TLDs were sensitive to neutrons as well as gamma-rays, neutron contribution

on each TLD has to be subtracted from the total TL response. The subtraction was done as follows.

The neutron contribution can be calculated by energy-integration of the products of neutron response function of each TLD and neutron flux. The used response function of each TLD as a function of energy were calculated with a code developed by Hashikura, et al [43]. However, in comparison with experimental values of the response functions, significant discrepancies between the experiment and the calculation were observed for MSO in a high energy region. Hence the calculated response function of MSO in an energy range higher than 4 MeV was normalized by the experimental values. The used neutron response functions of each TLD are shown in Fig. 3.4.1. The neutron energy spectra at the six measurement points were calculated by the Monte Carlo transport code MCNP. And then, neutron contribution of each TLD was calculated in a unit of equivalent exposure dose of ^{60}Co by integrating the products of the neutron response function and the spectrum. The obtained neutron contributions were subtracted from the total responses to obtain pure gamma-ray responses. Proportions of the neutron response to the total response are presented in Table 3.4.1.

All kinds of TLDs had been calibrated in a ^{60}Co standard field, and obtained gamma-ray response of each TLD was converted to absorbed dose. Since the atomic number of copper was 29, absorbed dose of copper, i.e., gamma-ray heating rate, was derived by interpolation of absorbed dose for MSO and SSO as shown in Fig. 3.4.2. As it is seen in the figure, absorbed doses of three kinds of TLDs at each position are not different so much. Thus errors associated with the interpolation process are considered as small.

Corrections

The following three corrections were made to the obtained gamma-ray heating rate of copper.

(i) Correction for Target Gamma-Ray

Contribution of target gamma-rays, which were emitted from the target assembly with neutron interactions, was estimated by a MCNP calculation. In the calculation, experimental assembly made of copper was modeled and source spectrum of the target gamma-rays described in the section 2.2 was used. Gamma-ray spectra at each measurement position were calculated and gamma-ray heating rates due to the target gamma-rays were derived by integration of the product of gamma-ray spectra and kerma factors of copper. The obtained gamma-ray heating rates due to target gamma-ray were subtracted from the total gamma-ray heating rates.

(ii) Correction for gamma-rays associated with decay of ^{62}Cu

As for gamma-rays emitted from activated nuclei by neutron reactions with copper, annihilation gamma-rays of 0.511 MeV emitted by ^{62}Cu nuclei produced by ^{63}Cu(n,2n) reactions

dominantly contribute to gamma-ray heating rate. Because the abundance of ^{63}Cu (69.2 %), cross section of ^{63}Cu(n,2n) reaction at 14 MeV (570 mb) and emission probability of annihilation gamma-ray (195.6 %) are large, and half life of ^{62}Cu (9.76 minutes) is almost the same as the duration of irradiation. Contribution of the annihilation gamma-rays to the measured gamma-ray heating rates was estimated as follows.

Gamma-ray production cross section data of ^{63}Cu and ^{65}Cu in JENDL-3.1 [1] was replaced as that secondary gamma-rays were generated by only the ^{63}Cu(n,2n) reaction and one gamma-ray of 0.511 MeV was emitted after the reaction. The changed cross section of copper was processed to yield continuous energy cross section data for MCNP. Modeling the experimental assembly and source D-T neutrons, a neutron-photon transport calculation was performed with MCNP and gamma-ray spectra formed by only annihilation gamma-rays from decays of ^{62}Cu were obtained. In the calculation, spatial distribution of generation of the annihilation gamma-rays and the transport effect of the gamma-rays were precisely simulated. Gamma-ray heating rates due to the annihilation gamma-rays were calculated multiplying kerma factors. The probability of 195.6 % of gamma-ray emission and the probability of 0.9 for decay of ^{62}Cu during the period between start of the irradiation and withdrawal of TLDs, were taken into account. The estimated gamma-ray heating rates due to annihilation gamma-rays from ^{62}Cu were subtracted from the total gamma-ray heating rates.

(iii) Correction for beta-rays associated with decay of ^{62}Cu

Copper-62 disintegrates accompanying positron emission. The maximum energy of positrons, 2.9 MeV, is enough to affect the measured gamma-ray heating rates. The following two approximations were assumed for correction of positron contribution. (i) The size of TLDs is so small that the electron equilibrium may stand up with the surrounding material. (ii) Range of the positron is short and all the positron energy is deposited at the position where the positron is emitted. Reaction rates of ^{63}Cu(n,2n) at measurement points were estimated by the MCNP calculation. Considering the mean energy of the positrons (1.28 MeV), the branching ratio to the beta-decay (97.8 %) and the probability of 0.9 for decay of ^{62}Cu during the period between start of the irradiation and withdrawal of TLDs, heating rate due to the positrons were calculated, and then they were subtracted from the measured gamma-ray heating rates.

Result of the three corrections is summarized in Table 3.4.2. The maximum correction is 25.9 % at the front surface of the experimental assembly, and the corrections are less than 1 % and can be negligible at positions more than 362 mm.

The corrected gamma-ray heating rates of copper are shown in Table 3.4.3 and Fig. 3.4.3.

Error Estimation

In the subtraction of neutron response and the three corrections, the following errors are adopted and added to the measured data according to the law of error propagation.

Neutron response function	30 %
Neutron Flux	10 %
Contribution of target gamma-ray	20 %
Gamma-ray contribution from decay of ^{62}Cu	20 %
Beta-ray contribution from decay of ^{62}Cu	30 %

Error sources in the measured gamma-ray heating rates are as follows.

Deviation of four TLDs	3 - 22 %
Neutron yield	2 %
Calibration of the TLD reader	7 %
Interpolation of atomic number	5 %

The error for deviation of four TLDs is considered as random error, and the other errors are systematic ones. The overall errors range between 11 and 25 % depending on measurement points.

4. Concluding Remarks

A benchmark experiment for the copper slab assembly was performed by bombarding D-T neutrons, and the precious experimental data were obtained. Since the present experimental assembly was thicker than the spherical shell of the OKTAVIAN and LLNL experiments, neutron and gamma-ray transport can be investigated more in detail with the present experiment.

Neutron spectra were measured in energy regions of MeV and keV. Neutron spectra, especially, below 0.1 MeV were not measured in the previous two experiments, while spectra in the energy region down to 3 keV were obtained in the present experiment. Neutron reaction rates of various energy sensitivities were measured. The obtained data are useful to examine neutron transport owing to their high accuracy and small perturbation to the neutron fields. As for gamma-rays, prompt gamma-ray spectra and heating rates were measured. Gamma-rays from neutron capture reactions, which were not included in the gamma-ray spectra measured in the previous two experiments, were also measured along with the prompt gamma-rays from threshold reactions. Decay gamma-ray spectra for short lived nuclei less than a few tens of minutes were also measured. Such spectra has not been measured so far in this kind of experiment.

These experimental data are very useful to verify cross section data of copper. Validity of newly evaluated nuclear data libraries, such as JENDL-3.2, ENDF/B-VI and FENDL, can be examined by analyzing the present experiment. The decay gamma-ray spectra is a very good experimental data to test codes and data bases for decay heat analyses.

Sample input data for two transport codes, DOT-3.5 [44] and MCNP-4, are attached in the Appendix.

Acknowledgment

The authors wish to express their thanks to Dr. M. Nakagawa for his useful discussions. They are grateful to Messrs. J. Kusano, C. Kutsukake, S. Tanaka and Y. Abe for their operations of the FNS accelerator.

4. Concluding Remarks

A benchmark experiment for the copper slab assembly was performed by bombarding D-T neutrons, and the precious experimental data were obtained. Since the present experimental assembly was thicker than the spherical shell of the OKTAVIAN and LLNL experiments, neutron and gamma-ray transport can be investigated more in detail with the present experiment.

Neutron spectra were measured in energy regions of MeV and keV. Neutron spectra, especially, below 0.1 MeV were not measured in the previous two experiments, while spectra in the energy region down to 3 keV were obtained in the present experiment. Neutron reaction rates of various energy sensitivities were measured. The obtained data are useful to examine neutron transport owing to their high accuracy and small perturbation to the neutron fields. As for gamma-rays, prompt gamma-ray spectra and heating rates were measured. Gamma-rays from neutron capture reactions, which were not included in the gamma-ray spectra measured in the previous two experiments, were also measured along with the prompt gamma-rays from threshold reactions. Decay gamma-ray spectra for short lived nuclei less than a few tens of minutes were also measured. Such spectra has not been measured so far in this kind of experiment.

These experimental data are very useful to verify cross section data of copper. Validity of newly evaluated nuclear data libraries, such as JENDL-3.2, ENDF/B-VI and FENDL, can be examined by analyzing the present experiment. The decay gamma-ray spectra is a very good experimental data to test codes and data bases for decay heat analyses.

Sample input data for two transport codes, DOT-3.5 [44] and MCNP-4, are attached in the Appendix.

Acknowledgment

The authors wish to express their thanks to Dr. M. Nakagawa for his useful discussions. They are grateful to Messrs. J. Kusano, C. Kutsukake, S. Tanaka and Y. Abe for their operations of the FNS accelerator.

References

1) Shibata K., et al.: "Japanese Evaluated Nuclear Data Library, Version-3 -- JENDL-3 --," JAERI 1319, Japan Atomic Energy Research Institute (1990).
2) Ganesan S. and Muir D. W.: "FENDL Multigroup Libraries," IAEA-NDS-129 (1992).
3) Hansen L. F., Wong. C., Komoto T. T., Rohl B. A. and Howerton R. J.: Nucl. Technol., 51, pp. 278 (1973).
4) Goldberg E., et al.: Nucl. Sci. Eng., 105, pp. 319-340 (1990).
5) "ENDF/B Summary Documentation," ENDF-201, National Nuclear Data Center, Brookhaven National Laboratory (Sep. 1987).
6) "ENDL, Lawrence Livermore National Laboratory (LLNL) Evaluated Nuclear Data Library," UCRL-50400, Vol. 15, Parts A to E, Lawrence Livermore National Laboratory (1975-1978).
7) Ichihara C., Hayashi S. A., Kobayashi K. and Kimura I.: "The Measurement of Leakage Neutron Spectra from Various Sphere Piles with 14 MeV Neutrons," Proc. Int. Conf. on Nucl. Data for Sci. and Technol., Mito, Japan, pp. 319-322 (1988).
8) Ichihara C., et al.: "Measurement of Leakage Neutron Spectra from Various Sphere Piles for Fusion Reactor Materials with 14 MeV Neutrons," Proc. Second Specialists' Meeting on Nucl. Data for Fusion Reactors, JAERI-M 91-062, pp. 255-267, Japan Atomic Energy Research Institute (1991).
9) Yamamoto J., Kanaoka T., Murata I., Takahashi A. and Sumita K.: "Gamma-Ray Emission Spectra from Spheres with 14 MeV Neutron Source," Proc. of the 1988 Seminar on Nucl. Data, JAERI-M 89-026, pp. 232-242, Japan Atomic Energy Research Institute (1989).
10) Yamamoto J.: "Integral experiment on Gamma-Ray Production at OKTAVIAN," Proc. Second Specialists' Meeting on Nucl. Data for Fusion Reactors, JAERI-M 91-062, pp. 118-125, Japan Atomic Energy Research Institute (1991).
11) Maekawa F., et al. (Ed.): "Benchmark Problems for Fusion Neutronics," JAERI-M, Japan Atomic Energy Research Institute. To be published.
12) JENDL Compilation Group (Nuclear Data Center, JAERI): JENDL-3T, private communication (1987).
13) ENDF/B Summary Documentation, BNL-NCS-17541 (ENDF-201), 2nd Edition (1975).
14) Nakamura T., Maekawa H., Ikeda Y. and Oyama Y.: "A DT Neutron Source for Fusion Neutronics Experiments at the JAERI," Proc. Int. Ion Eng. Congress - ISIAT '83 & IAPT '83, Kyoto, Japan, Vol. 1, pp. 567-570 (1983).

15) Maekawa H., et al.: "Fusion Blanket Benchmark Experiments on a 60 cm-thick Lithium-Oxide Cylindrical Assembly," JAERI-M 86-182, Japan Atomic Energy Research Institute (1986).
16) Maekawa H., et al.: Fusion Technol. 19, pp. 1949-1954 (1991).
17) Maekawa H., et al.: "Benchmark Experiments on a 60 cm-thick Graphite Cylindrical Assembly," JAERI-M 88-034, Japan Atomic Energy Research Institute (1988).
18) Oyama Y.: "Experiments of Nuclear Heating by Gamma-Rays at FNS," JAERI-M 91-062, pp.106-117, Japan Atomic Energy Research Institute (1991).
19) Yamaguchi S., et al.: Fusion Eng. Des., 10, pp.163-167 (1989).
20) Oishi K., Tomioka K., Ikeda Y. and Nakamura T.: "Experiment and Analysis of Neutron Spctra in a Concrete Assembly Bombarded by 14 MeV Neutrons," Proc. Int. Conf. on Nucl. Data for Sci. and Technol., Mito, Japan, pp. 237-240 (1988).
21) Oishi K., Ikeda Y., Maekawa H. and Nakamura T.: Nucl. Sci. Eng., 103, pp. 46-58 (1989).
22) Oishi K., Ikeda Y., Kosako K., Minami K. and Nakamura T.: Fusion Eng. Des., 17, pp.359-366 (1991).
23) Oishi K., Ikeda Y., Konno C. and Nakamura T.: "Measurement and Analysis of Neutron Spectra in a Large Cylindrical Iron Assembly Irradiated by 14 MeV Neutrons," Proc. 7th Int. Conf. on Radiation Shielding, Bournemouth, pp. 331-340 (1988).
24) Konno C., et al.: Fusion Eng. Des., 18, pp. 297-303 (1991).
25) Ikeda Y., Oishi K., Konno C. and Nakamura T.: ibid., pp. 309-315 (1991).
26) Maekawa H., Ikeda Y., Oyama Y., Yamaguchi S. and Nakamura T.: "Neutron Yield Monitors for the Fusion Neutronics Source (FNS) -- for 80° Beam Line --," JAERI-M 83-219, Japan Atomic Energy Research Institute (1983).
27) Yamaguchi S., Oyama Y. and Maekawa H.: "Calculation of Anisotropy Correction Factor for Determination of D-T Neutron Yield by Associated α-particle Method," JAERI-M 84-109, Japan Atomic Energy Research Institute (1984).
28) Nakagawa M. and Mori T.: "MORSE-DD; A Monte Corlo Code Using Multi-Group Double Differential Form Cross section," JAERI-M 84-126, Japan Atomic Energy Research Institute (1984).
29) Briesmeister J. F. (editor): "MCNP - A General Monte Carlo Code for Neutron and Photon Transport, Version 3B," RSIC/CCC-200 (1988).
30) Oyama Y., et al.: Nucl. Instrum. Meth., A256, pp. 333 (1987).
31) Kimbara S. and Kumahara T.: ibid., 70, pp. 173 (1969).
32) FORIST Spectrum Unfolding code: Radiation Shielding Information Center, Oak Ridge National Laboratory, PSR-92 (1975).

33) Nakashima H.: "Study on Shielding Design Methods for Fusion Reactors Using Benchmark Experiments," pp. 20-45, JAERI-M 92-025, Japan Atomic Energy Research Institute (1992, in Japanese).
34) Oyama Y., et al.: " Phase IIA and IIB Experiments of JAERI/USDOE Collaborative Program on Fusion Blanket Neutronics," JAERI-M 89-215, Japan Atomic Energy Research Institute (1989).
35) Oyama Y., et al.: " Phase IIC Experiments of JAERI/USDOE Collaborative Program on Fusion Blanket Neutronics," JAERI-M 92-182, Japan Atomic Energy Research Institute (1992).
36) Oyama Y., et al.: " Phase III Experiments of JAERI/USDOE Collaborative Program on Fusion Blanket Neutronics," JAERI-M, Japan Atomic Energy Research Institute. To be published.
37) Bennett E. F.: " A Continuous Mode Data Acquisition Technique for Proton Recoil Proportional Counter Neutron Spectrometers," ANL/FPP/TM-239, Argonne National Laboratory (1989).
38) Bennet E. F.: " Induction Filtering for Proportional Counter Amplifiers," ANL/FPP/TM-234, Argonne National Laboratory (1989).
39) Lederer C. M. and Shireley V.S.: Table of Isotopes, 7th edition (1978).
40) Maekawa F. and Oyama Y.: " Characteristics of a 40 mm Diameter NE213 Scintillation Counter for In-System Gamma-Ray Spectrum Measurement." JAERI-M 91-138, pp. 97-99, Japan Atomic Energy Research Institute (1991).
41) Saito K. and Moriuchi S.: Nucl. Instrum. Meth. 185, pp. 299 (1981).
42) Tanaka S. and Sasamoto N: J. Nucl. Sci. Technol., 22, pp. 109-119 (1985).
43) Hashikura H., Haikawa K., Tanaka S. and Kondo S.: "Calculation of Neutron Response of Thermoluminescent Dosimeters," J. Faculty of Eng., Univ. of Tokyo, 39, pp. 7 (1987).
44) Rhoades W. A. and Mynatt F. R.: "The DOT III Two-Dimensional Discrete Ordinate Transport Code," ORNL/TM-4280, Oak Ridge National Laboratory (1973).

Table 2.2.1 Neutron source energy spectrum of FNS new water cooled D-T target for 0 degree to the d^+ beam. The spectrum is calculated by MORSE-DD. The units of energy and spectrum are [eV] and [neutrons/energy-bin/D-T reaction], respectively.

Group	Upper Energy	Spectrum	Group	Upper energy	Spectrum
1	1.6487e+07	0.0	64	1.1943e+06	2.5765e-03
2	1.6231e+07	0.0	65	1.0540e+06	2.5872e-03
3	1.5980e+07	0.0	66	9.3013e+05	2.5709e-03
4	1.5732e+07	0.0	67	8.2084e+05	2.5211e-03
5	1.5488e+07	1.4419e-01	68	7.2438e+05	2.3040e-03
6	1.5248e+07	2.2296e-01	69	6.3927e+05	2.2042e-03
7	1.5012e+07	4.0901e-01	70	5.6415e+05	2.0605e-03
8	1.4779e+07	2.3565e-01	71	4.9786e+05	1.8238e-03
9	1.4550e+07	3.0897e-02	72	4.3936e+05	1.6473e-03
10	1.4324e+07	5.1474e-03	73	3.8774e+05	1.5803e-03
11	1.4102e+07	9.5007e-04	74	3.4217e+05	1.3867e-03
12	1.3883e+07	2.6083e-03	75	3.0197e+05	1.2232e-03
13	1.3668e+07	9.1020e-04	76	2.6649e+05	1.0785e-03
14	1.3456e+07	4.6458e-04	77	2.3517e+05	9.5392e-04
15	1.3248e+07	4.5938e-04	78	2.0754e+05	8.0965e-04
16	1.3042e+07	5.1771e-04	79	1.8315e+05	7.0593e-04
17	1.2840e+07	7.8183e-04	80	1.6163e+05	6.0762e-04
18	1.2641e+07	7.4899e-04	81	1.4264e+05	5.3824e-04
19	1.2445e+07	4.1363e-04	82	1.2588e+05	4.9933e-04
20	1.2252e+07	2.1025e-04	83	1.1109e+05	3.7225e-04
21	1.2062e+07	1.6563e-04	84	9.8035e+04	1.7906e-04
22	1.1875e+07	1.5985e-04	85	8.6515e+04	1.4874e-04
23	1.1691e+07	1.6798e-04	86	7.6349e+04	1.2632e-04
24	1.1510e+07	1.1227e-04	87	6.7378e+04	1.0531e-04
25	1.1331e+07	8.7841e-05	88	5.9461e+04	9.7450e-05
26	1.1156e+07	8.8737e-05	89	5.2474e+04	8.3190e-05
27	1.0983e+07	7.9567e-05	90	4.6308e+04	8.0602e-05
28	1.0812e+07	9.3708e-05	91	4.0867e+04	6.9230e-05
29	1.0645e+07	9.1407e-05	92	3.6065e+04	5.7202e-05
30	1.0480e+07	9.2862e-05	93	3.1827e+04	5.0292e-05
31	1.0317e+07	8.2287e-05	94	2.8087e+04	4.8831e-05
32	1.0157e+07	9.0768e-05	95	2.4787e+04	5.3362e-05
33	1.0000e+07	3.5649e-04	96	2.1874e+04	3.7185e-05
34	9.3940e+06	4.1280e-04	97	1.9304e+04	6.1572e-05
35	8.8249e+06	5.1007e-04	98	1.5034e+04	4.6320e-05
36	8.2902e+06	5.0750e-04	99	1.1709e+04	4.4237e-05
37	7.7879e+06	5.1710e-04	100	9.1186e+03	3.7633e-05
38	7.3161e+06	6.2956e-04	101	7.1016e+03	2.4899e-05
39	6.8728e+06	6.9228e-04	102	5.5307e+03	2.8404e-05
40	6.4564e+06	7.5872e-04	103	4.3073e+03	1.7624e-05
41	6.0652e+06	7.9293e-04	104	3.3546e+03	1.4791e-05
42	5.6978e+06	7.9827e-04	105	2.6125e+03	1.6544e-05
43	5.3525e+06	8.8451e-04	106	2.0346e+03	1.1820e-05
44	5.0282e+06	1.0018e-03	107	1.5846e+03	1.4320e-05
45	4.7236e+06	1.0563e-03	108	1.2341e+03	7.8013e-06
46	4.4374e+06	1.1937e-03	109	9.6110e+02	8.7622e-06
47	4.1686e+06	1.1711e-03	110	5.8293e+02	7.2049e-06
48	3.9160e+06	1.2741e-03	111	3.5357e+02	6.9372e-06
49	3.6787e+06	1.2861e-03	112	2.1445e+02	2.2612e-06
50	3.4559e+06	1.4053e-03	113	1.3007e+02	3.0541e-06
51	3.2465e+06	1.3518e-03	114	7.8891e+01	3.8068e-06
52	3.0498e+06	1.4558e-03	115	4.7850e+01	2.9754e-07
53	2.8650e+06	1.4329e-03	116	2.9023e+01	1.6817e-07
54	2.6914e+06	1.3760e-03	117	1.7603e+01	1.3922e-07
55	2.5284e+06	1.4312e-03	118	1.0677e+01	2.2450e-07
56	2.3752e+06	1.3820e-03	119	6.4758e+00	1.8398e-07
57	2.2313e+06	1.3489e-03	120	3.9278e+00	8.3975e-08
58	2.0961e+06	1.3270e-03	121	2.3823e+00	1.4264e-08
59	1.9691e+06	1.4298e-03	122	1.4449e+00	7.4848e-09
60	1.8498e+06	1.3898e-03	123	8.7640e-01	4.2225e-09
61	1.7377e+06	2.5945e-03	124	5.3156e-01	2.2732e-09
62	1.5335e+06	2.8528e-03	125	3.2241e-01	1.5142e-07
63	1.3533e+06	2.7699e-03	126	1.0010e-05	

Table 2.2.2 Gamma-ray source energy spectrum of FNS new water cooled D-T target. The spectrum is calculated by MCNP. The units of energy and spectrum are [MeV] and [gamma-rays/energy-bin/D-T reaction], respectively.

Group	Upper Energy	Spectrum	Group	Upper energy	Spectrum
1	1.4000e+01	0.0	21	1.3750e+00	1.0412e-02
2	1.2000e+01	1.8633e-04	22	1.2500e+00	1.0790e-02
3	1.0000e+01	2.4781e-04	23	1.1250e+00	7.3978e-03
4	9.0000e+00	2.6304e-04	24	1.0000e+00	5.8107e-03
5	8.0000e+00	1.0130e-03	25	9.0000e-01	6.8849e-03
6	7.5000e+00	9.4278e-04	26	8.0000e-01	8.5792e-03
7	7.0000e+00	1.2635e-03	27	7.0000e-01	6.3378e-03
8	6.5000e+00	1.5887e-03	28	6.0000e-01	2.4076e-03
9	6.0000e+00	2.2136e-03	29	5.2000e-01	2.8815e-03
10	5.5000e+00	2.6026e-03	30	5.0000e-01	5.9451e-03
11	5.0000e+00	3.3959e-03	31	4.0000e-01	8.5598e-03
12	4.5000e+00	4.2346e-03	32	3.0000e-01	1.2291e-02
13	4.0000e+00	5.0603e-03	33	2.0000e-01	5.8376e-03
14	3.5000e+00	6.1991e-03	34	1.5000e-01	4.5651e-03
15	3.0000e+00	6.8837e-03	35	1.0000e-01	1.3289e-03
16	2.5000e+00	3.0169e-03	36	8.0000e-02	9.3110e-04
17	2.2500e+00	5.4347e-03	37	6.0000e-02	1.9365e-04
18	2.0000e+00	5.5820e-03	38	4.5000e-02	2.8764e-04
19	1.7500e+00	9.1277e-03	39	3.0000e-02	5.0781e-05
20	1.5000e+00	2.9512e-03	40	2.0000e-02	0.0
			41	1.0000e-02	

Table 3.1.1.1 Systematic errors in various energy range. Errors expected in the range below 10 MeV is originating from the response error of 14.8 MeV neutrons.

No.	Energy range (MeV)	Efficiency	Energy Calibration	Neutron Source	Response Shape [fraction*1]	Total
0	>10	±2%	±3%	±2%	1	±4%
1	8.3 - 10.1	2	2	2	~ - 0.02	-20%*2
2	5.8 - 8.3	2	2	2	~ - 0.01	-11%*2
3	4.1 - 5.8	2	2	2	~ - 0.001	-3.4%*2
4	2.0 - 4.1	2	2	2	~ + 0.01	+3.5%*2
5	1.1 - 2.0	2	2	2	~ + 0.01	+3.5%*2

*1 Fraction is ratio of the error due to the response to the peak flux around 14 MeV.
*2 Example in the case of $\Phi_{peak}/\Phi(E_n) \sim 10$.

Table 3.1.1.2 Neutron spectra at -10, 76 and 228 mm from the surface of the experimental assembly measured by the NE213 spectrometer. The units are [n/lethargy/source neutron], [%] for flux and window, respectively.

Neutron Energy	-10 mm			76 mm			228 mm		
[MeV]	flux	error	window	flux	error	window	flux	error	window
0.811	7.087e-05	4.693e-04	53.86	9.466e-05	6.837e-05	53.86	6.170e-06	7.511e-05	53.86
0.853	1.091e-04	9.111e-05	52.99	9.002e-05	1.127e-05	52.99	1.594e-05	1.457e-05	52.99
0.896	1.168e-04	1.517e-05	52.07	8.849e-05	3.409e-06	52.16	1.739e-05	2.377e-06	52.16
0.942	1.171e-04	4.796e-06	50.92	8.701e-05	2.584e-06	51.34	1.706e-05	6.642e-07	51.34
0.990	1.157e-04	3.525e-06	49.62	8.518e-05	2.509e-06	50.47	1.646e-05	5.080e-07	50.47
1.041	1.136e-04	3.345e-06	48.18	8.296e-05	2.362e-06	49.57	1.583e-05	4.920e-07	49.57
1.095	1.116e-04	3.256e-06	46.54	8.028e-05	2.225e-06	48.64	1.520e-05	4.251e-07	48.64
1.151	1.100e-04	3.198e-06	44.80	7.730e-05	2.147e-06	47.59	1.449e-05	3.751e-07	47.59
1.210	1.092e-04	3.180e-06	43.33	7.412e-05	2.156e-06	46.51	1.361e-05	3.928e-07	46.51
1.272	1.092e-04	3.133e-06	42.24	7.089e-05	2.113e-06	45.40	1.253e-05	4.129e-07	45.40
1.337	1.091e-04	3.092e-06	41.59	6.768e-05	2.068e-06	44.21	1.130e-05	3.663e-07	44.21
1.406	1.077e-04	3.188e-06	41.03	6.442e-05	2.086e-06	42.95	1.003e-05	3.268e-07	42.95
1.478	1.033e-04	3.374e-06	40.60	6.091e-05	2.061e-06	41.72	8.889e-06	3.339e-07	41.72
1.553	9.464e-05	3.405e-06	40.16	5.705e-05	1.907e-06	40.57	7.915e-06	3.085e-07	40.57
1.633	8.142e-05	3.139e-06	39.53	5.281e-05	1.741e-06	39.53	7.103e-06	2.502e-07	39.53
1.717	6.474e-05	2.707e-06	38.56	4.842e-05	1.624e-06	38.56	6.392e-06	2.252e-07	38.56
1.805	4.714e-05	2.502e-06	37.69	4.432e-05	1.537e-06	37.69	5.756e-06	2.062e-07	37.69
1.897	3.175e-05	2.552e-06	36.86	4.097e-05	1.467e-06	36.86	5.207e-06	1.774e-07	36.86
1.995	2.127e-05	2.639e-06	36.00	3.849e-05	1.365e-06	36.00	4.759e-06	1.619e-07	36.00
2.097	1.718e-05	2.629e-06	35.14	3.677e-05	1.260e-06	35.14	4.396e-06	1.435e-07	35.14
2.204	1.923e-05	2.585e-06	34.31	3.553e-05	1.186e-06	34.31	4.093e-06	1.245e-07	34.31
2.317	2.533e-05	2.603e-06	33.55	3.426e-05	1.138e-06	33.55	3.825e-06	1.137e-07	33.55
2.436	3.219e-05	2.648e-06	32.80	3.262e-05	1.107e-06	32.80	3.566e-06	1.050e-07	32.80
2.561	3.682e-05	2.608e-06	32.04	3.044e-05	1.057e-06	32.04	3.292e-06	9.776e-08	32.04
2.692	3.791e-05	2.482e-06	31.25	2.792e-05	1.049e-06	31.25	2.990e-06	9.263e-08	31.25
2.830	3.613e-05	2.563e-06	30.49	2.546e-05	1.088e-06	30.49	2.675e-06	8.892e-08	30.49
2.975	3.306e-05	3.150e-06	29.74	2.341e-05	1.166e-06	29.74	2.389e-06	8.923e-08	29.74
3.128	2.996e-05	3.833e-06	29.02	2.187e-05	1.193e-06	29.02	2.174e-06	9.342e-08	29.02
3.288	2.733e-05	4.064e-06	28.30	2.072e-05	1.136e-06	28.30	2.036e-06	9.478e-08	28.30
3.457	2.528e-05	3.702e-06	27.58	2.165e-05	1.149e-06	27.58	1.974e-06	8.324e-08	27.58
3.634	2.384e-05	3.045e-06	26.82	2.084e-05	1.015e-06	26.82	1.920e-06	7.495e-08	26.82
3.821	2.316e-05	2.663e-06	26.06	1.996e-05	9.683e-07	26.06	1.882e-06	7.227e-08	26.06
4.016	2.302e-05	2.828e-06	25.27	1.895e-05	9.643e-07	25.27	1.814e-06	7.163e-08	25.27
4.222	2.256e-05	3.183e-06	24.55	1.782e-05	9.991e-07	24.55	1.697e-06	7.217e-08	24.55
4.439	2.038e-05	3.346e-06	23.94	1.647e-05	1.022e-06	23.94	1.533e-06	7.241e-08	23.94
4.666	1.541e-05	3.452e-06	23.33	1.474e-05	1.043e-06	23.33	1.345e-06	7.248e-08	23.33
4.906	8.156e-06	3.669e-06	22.72	1.260e-05	1.088e-06	22.72	1.158e-06	7.420e-08	22.72
5.157	9.432e-07	3.852e-06	22.18	1.037e-05	1.118e-06	22.18	9.975e-07	7.531e-08	22.18
5.422	-3.921e-06	-3.921e-06	21.67	8.761e-06	1.172e-06	21.67	8.847e-07	7.838e-08	21.67
5.700	-5.738e-06	-5.738e-06	21.10	8.347e-06	1.244e-06	21.10	8.328e-07	8.261e-08	21.10
5.992	-4.751e-06	-4.751e-06	20.56	8.760e-06	1.284e-06	20.56	8.274e-07	8.417e-08	20.56
6.299	-2.162e-06	-2.162e-06	20.02	8.875e-06	1.419e-06	20.02	8.209e-07	9.058e-08	20.02
6.622	-1.372e-06	-1.372e-06	19.48	8.193e-06	1.572e-06	19.48	7.793e-07	9.917e-08	19.48
6.961	-4.871e-06	-4.871e-06	18.97	7.502e-06	1.612e-06	18.97	7.406e-07	1.017e-07	18.97
7.318	-8.815e-06	-8.815e-06	18.49	7.692e-06	1.827e-06	18.49	7.631e-07	1.126e-07	18.49
7.694	-7.996e-06	-7.996e-06	18.04	8.398e-06	2.130e-06	18.04	7.943e-07	1.304e-07	18.04
8.088	-6.234e-06	-6.234e-06	17.62	8.235e-06	2.290e-06	17.62	7.356e-07	1.402e-07	17.62
8.503	-7.497e-06	-7.497e-06	17.22	6.862e-06	2.603e-06	17.22	7.267e-07	1.542e-07	17.22
8.939	-4.462e-06	-4.462e-06	16.78	5.830e-06	3.283e-06	16.78	9.052e-07	1.917e-07	16.78
9.397	5.224e-06	1.714e-05	16.36	6.490e-06	3.619e-06	16.36	9.865e-07	2.106e-07	16.36
9.879	1.144e-05	1.775e-05	15.93	8.739e-06	3.707e-06	15.93	8.622e-07	2.149e-07	15.93
10.390	9.148e-06	2.020e-05	15.47	1.025e-05	4.213e-06	15.47	8.051e-07	2.428e-07	15.47
10.920	1.145e-06	2.047e-05	15.07	8.029e-06	4.201e-06	15.07	8.853e-07	2.387e-07	15.07
11.480	1.652e-06	2.099e-05	14.76	5.808e-06	4.229e-06	14.76	1.216e-06	2.346e-07	14.76
12.070	4.600e-05	2.552e-05	14.54	1.318e-05	5.129e-06	14.54	2.009e-06	2.781e-07	14.54
12.680	1.913e-04	2.801e-05	14.42	3.758e-05	5.695e-06	14.42	3.643e-06	3.044e-07	14.42
13.340	5.896e-04	3.466e-05	14.40	1.055e-04	7.023e-06	14.40	7.365e-06	3.609e-07	14.40
14.020	1.224e-03	4.316e-05	14.40	2.290e-04	8.798e-06	14.40	1.258e-05	4.741e-07	14.40
14.740	1.406e-03	5.932e-05	14.40	2.824e-04	1.239e-05	14.40	1.285e-05	7.011e-07	14.40
15.490	7.990e-04	2.535e-05	14.40	1.729e-04	5.354e-06	14.40	6.930e-06	2.705e-07	14.40
16.290	2.274e-04	2.823e-05	14.40	5.460e-05	5.921e-06	14.40	2.293e-06	3.511e-07	14.40
17.120	1.068e-04	2.129e-05	14.40	2.658e-05	4.461e-06	14.40	1.127e-06	2.602e-07	14.40
18.000	9.212e-05	5.568e-06	14.40	2.165e-05	1.158e-06	14.40	8.115e-07	7.077e-08	14.40

Table 3.1.1.3 Neutron spectra at 380, 532 and 618 mm from the surface of the experimental assembly measured by the NE213 spectrometer. The units are [n/lethargy/source neutron], [%] for flux and window, respectively.

Neutron Energy	380 mm			532 mm			618 mm		
[MeV]	flux	error	window	flux	error	window	flux	error	window
0.811	1.488e-06	1.110e-05	53.86	1.548e-07	1.232e-06	53.86	4.928e-07	3.487e+00	53.86
0.853	2.438e-06	2.151e-06	52.99	2.655e-07	2.383e-07	52.99	4.270e-07	7.806e-01	52.99
0.896	2.525e-06	3.459e-07	52.16	2.749e-07	3.812e-08	52.16	4.028e-07	1.354e-01	50.39
0.942	2.427e-06	8.717e-08	51.34	2.626e-07	9.158e-09	51.34	3.868e-07	3.919e-02	47.72
0.990	2.298e-06	6.586e-08	50.47	2.465e-07	6.929e-09	50.47	3.718e-07	2.996e-02	44.98
1.041	2.155e-06	6.772e-08	49.57	2.286e-07	7.398e-09	49.57	3.574e-07	3.008e-02	42.07
1.095	2.000e-06	5.936e-08	48.64	2.090e-07	6.592e-09	48.64	3.436e-07	2.833e-02	39.06
1.151	1.829e-06	4.742e-08	47.59	1.874e-07	5.065e-09	47.59	3.293e-07	2.721e-02	37.69
1.210	1.646e-06	4.400e-08	46.51	1.653e-07	4.366e-09	46.51	3.144e-07	2.842e-02	36.41
1.272	1.463e-06	4.717e-08	45.40	1.447e-07	4.731e-09	45.40	2.985e-07	3.056e-02	35.38
1.337	1.292e-06	4.272e-08	44.21	1.269e-07	4.382e-09	44.21	2.813e-07	3.059e-02	34.71
1.406	1.140e-06	3.740e-08	42.95	1.120e-07	3.779e-09	42.95	2.632e-07	3.128e-02	34.32
1.478	1.004e-06	3.665e-08	41.72	9.821e-08	3.673e-09	41.72	2.435e-07	3.442e-02	34.32
1.553	8.773e-07	3.222e-08	40.57	8.420e-08	3.174e-09	40.57	2.222e-07	3.620e-02	34.80
1.633	7.591e-07	2.609e-08	39.53	7.032e-08	2.435e-09	39.53	2.000e-07	3.453e-02	35.55
1.717	6.533e-07	2.457e-08	38.56	5.782e-08	2.304e-09	38.56	1.778e-07	3.581e-02	36.07
1.805	5.646e-07	2.101e-08	37.69	4.786e-08	2.070e-09	37.69	1.580e-07	3.782e-02	36.41
1.897	4.937e-07	1.700e-08	36.86	4.063e-08	1.582e-09	36.86	1.429e-07	3.661e-02	36.46
1.995	4.380e-07	1.572e-08	36.00	3.576e-08	1.403e-09	36.00	1.345e-07	3.636e-02	36.00
2.097	3.946e-07	1.349e-08	35.14	3.291e-08	1.301e-09	35.14	1.329e-07	3.517e-02	35.04
2.204	3.621e-07	1.131e-08	34.31	3.173e-08	1.136e-09	34.31	1.366e-07	3.233e-02	33.92
2.317	3.388e-07	1.028e-08	33.55	3.151e-08	1.054e-09	33.55	1.424e-07	3.006e-02	32.77
2.436	3.201e-07	9.509e-09	32.80	3.129e-08	1.027e-09	32.80	1.463e-07	2.894e-02	31.76
2.561	3.012e-07	8.941e-09	32.04	3.036e-08	1.009e-09	32.04	1.452e-07	2.860e-02	31.01
2.692	2.787e-07	8.601e-09	31.25	2.866e-08	9.863e-10	31.25	1.387e-07	2.956e-02	30.31
2.830	2.533e-07	8.367e-09	30.49	2.670e-08	9.795e-10	30.49	1.287e-07	3.121e-02	29.84
2.975	2.281e-07	8.279e-09	29.74	2.491e-08	1.002e-09	29.74	1.177e-07	3.292e-02	29.49
3.128	2.065e-07	8.320e-09	29.02	2.334e-08	1.042e-09	29.02	1.080e-07	3.454e-02	29.02
3.288	1.906e-07	8.366e-09	28.30	2.199e-08	1.065e-09	28.26	1.010e-07	3.590e-02	28.30
3.457	1.727e-07	6.121e-09	27.58	1.897e-08	6.196e-10	27.54	9.808e-08	3.619e-02	27.58
3.634	1.627e-07	5.524e-09	26.82	1.772e-08	5.286e-10	26.79	9.863e-08	3.580e-02	26.82
3.821	1.505e-07	5.289e-09	26.06	1.586e-08	4.814e-10	26.03	1.006e-07	3.493e-02	26.06
4.016	1.368e-07	5.172e-09	25.27	1.337e-08	4.799e-10	25.24	1.013e-07	3.401e-02	25.27
4.222	1.231e-07	5.135e-09	24.55	1.085e-08	4.924e-10	24.55	9.991e-08	3.380e-02	24.55
4.439	1.113e-07	5.097e-09	23.94	9.020e-09	4.935e-10	23.94	9.744e-08	3.435e-02	23.94
4.666	1.022e-07	5.124e-09	23.33	8.181e-09	4.969e-10	23.33	9.569e-08	3.422e-02	23.33
4.906	9.392e-08	5.230e-09	22.72	7.824e-09	5.231e-10	22.72	9.488e-08	3.391e-02	22.72
5.157	8.399e-08	5.294e-09	22.18	7.162e-09	5.526e-10	22.18	9.275e-08	3.408e-02	22.18
5.422	7.259e-08	5.450e-09	21.67	6.062e-09	5.845e-10	21.67	8.756e-08	3.511e-02	21.67
5.700	6.292e-08	5.668e-09	21.10	5.086e-09	6.174e-10	21.10	8.062e-08	3.705e-02	21.10
5.992	5.714e-08	5.787e-09	20.56	4.643e-09	6.397e-10	20.56	7.452e-08	3.795e-02	20.56
6.299	5.498e-08	6.174e-09	20.02	4.532e-09	7.069e-10	20.02	6.913e-08	3.993e-02	20.02
6.622	5.564e-08	6.751e-09	19.48	4.616e-09	7.818e-10	19.48	6.198e-08	4.519e-02	19.48
6.961	5.787e-08	6.922e-09	18.97	5.186e-09	7.956e-10	18.97	5.227e-08	5.224e-02	18.97
7.318	5.816e-08	7.701e-09	18.49	5.880e-09	9.067e-10	18.49	4.182e-08	6.978e-02	18.49
7.694	5.559e-08	8.755e-09	18.04	5.466e-09	1.057e-09	18.04	3.339e-08	9.804e-02	18.04
8.088	5.250e-08	9.353e-09	17.62	3.899e-09	1.130e-09	17.62	3.088e-08	1.115e-01	17.62
8.503	5.245e-08	1.038e-08	17.22	2.998e-09	1.172e-09	17.22	3.567e-08	1.013e-01	17.22
8.939	5.944e-08	1.269e-08	16.78	4.048e-09	1.392e-09	16.78	4.130e-08	1.030e-01	16.78
9.397	6.176e-08	1.393e-08	16.36	5.858e-09	1.594e-09	16.36	4.284e-08	1.072e-01	16.36
9.879	5.027e-08	1.447e-08	15.93	7.178e-09	1.596e-09	15.93	4.495e-08	1.064e-01	15.93
10.390	5.396e-08	1.612e-08	15.47	8.399e-09	1.722e-09	15.47	6.110e-08	8.303e-02	15.47
10.920	8.604e-08	1.567e-08	15.07	1.067e-08	1.832e-09	15.07	8.792e-08	5.672e-02	15.07
11.480	1.178e-07	1.544e-08	14.76	1.286e-08	1.983e-09	14.76	9.528e-08	5.318e-02	14.76
12.070	1.615e-07	1.809e-08	14.54	1.411e-08	2.406e-09	14.54	8.520e-08	6.470e-02	14.54
12.680	3.074e-07	1.978e-08	14.42	2.231e-08	2.788e-09	14.42	8.623e-08	7.165e-02	14.42
13.340	6.116e-07	2.286e-08	14.40	4.155e-08	3.327e-09	14.40	1.074e-07	6.398e-02	14.40
14.020	8.431e-07	3.084e-08	14.40	6.065e-08	4.461e-09	14.40	1.342e-07	6.884e-02	14.40
14.740	6.887e-07	4.582e-08	14.40	5.418e-08	7.160e-09	14.40	1.297e-07	1.171e-01	14.40
15.490	3.412e-07	1.806e-08	14.40	2.564e-08	2.819e-09	14.40	5.561e-08	1.056e-01	14.40
16.290	1.430e-07	2.226e-08	14.40	7.601e-09	3.481e-09	14.40	-9.391e-09	1.000e+00	14.40
17.120	7.585e-08	1.690e-08	14.40	3.599e-09	2.600e-09	14.40	-1.069e-08	1.000e+00	14.40
18.000	3.157e-08	4.881e-09	14.40	1.694e-09	7.310e-10	14.40	4.127e-10	3.408e+00	14.40

Table 3.1.2.1 Neutron Spectra at -10, 76 and 228 mm from the front surface of the assembly measured by proton-recoil gas proportional counters.

-10 mm			76 mm			228 mm		
Neutron Energy [MeV]	Flux [n/leth/ source]	Error	Neutron Energy [MeV]	Flux [n/leth/ source]	Error	Neutron Energy [MeV]	Flux [n/leth/ source]	Error
2.770e-3	4.152e-7	2.240e-6	2.732e-3	-3.087e-6	4.030e-6	2.694e-3	-1.549e-6	2.310e-6
2.889e-3	2.627e-6	2.110e-6	2.849e-3	8.980e-6	3.820e-6	2.809e-3	3.842e-6	2.220e-6
3.013e-3	3.204e-6	2.040e-6	2.971e-3	9.332e-6	3.680e-6	2.930e-3	5.496e-6	2.150e-6
3.143e-3	4.830e-7	1.960e-6	3.099e-3	-2.083e-6	3.550e-6	3.056e-3	4.080e-7	2.080e-6
3.280e-3	1.617e-6	1.920e-6	3.233e-3	-1.415e-6	3.460e-6	3.188e-3	3.648e-6	2.010e-6
3.423e-3	1.539e-6	1.890e-6	3.374e-3	7.455e-6	3.430e-6	3.327e-3	4.389e-6	1.970e-6
3.573e-3	3.209e-6	1.810e-6	3.522e-3	4.607e-6	3.340e-6	3.472e-3	-2.416e-7	1.930e-6
3.730e-3	9.721e-7	1.810e-6	3.676e-3	5.464e-6	3.240e-6	3.624e-3	1.042e-6	1.920e-6
3.894e-3	3.132e-7	1.740e-6	3.838e-3	-2.154e-6	3.190e-6	3.784e-3	5.132e-6	1.870e-6
4.067e-3	-4.931e-7	1.750e-6	4.008e-3	1.722e-6	3.170e-6	3.951e-3	6.025e-6	1.850e-6
4.247e-3	1.064e-6	1.740e-6	4.186e-3	1.762e-6	3.170e-6	4.126e-3	2.560e-6	1.810e-6
4.437e-3	4.130e-6	1.700e-6	4.373e-3	4.413e-6	3.130e-6	4.310e-3	3.887e-6	1.780e-6
4.635e-3	3.350e-6	1.690e-6	4.568e-3	4.425e-6	3.120e-6	4.502e-3	6.235e-6	1.760e-6
4.843e-3	1.473e-6	1.630e-6	4.773e-3	2.383e-6	3.050e-6	4.704e-3	3.019e-6	1.750e-6
5.061e-3	1.904e-6	1.640e-6	4.988e-3	2.773e-6	3.050e-6	4.915e-3	3.042e-6	1.730e-6
5.290e-3	1.866e-6	1.600e-6	5.213e-3	3.920e-6	3.050e-6	5.136e-3	3.126e-6	1.730e-6
5.529e-3	1.727e-6	1.610e-6	5.448e-3	4.143e-6	3.020e-6	5.369e-3	5.879e-6	1.710e-6
5.780e-3	4.495e-6	1.590e-6	5.695e-3	1.035e-5	3.010e-6	5.612e-3	5.631e-6	1.700e-6
6.043e-3	4.089e-6	1.560e-6	5.954e-3	9.465e-6	2.970e-6	5.867e-3	8.062e-6	1.690e-6
6.319e-3	6.043e-7	1.560e-6	6.226e-3	1.067e-5	2.950e-6	6.134e-3	9.431e-6	1.670e-6
6.608e-3	3.410e-6	1.530e-6	6.510e-3	9.633e-6	2.900e-6	6.414e-3	1.125e-5	1.650e-6
6.911e-3	5.389e-6	1.530e-6	6.808e-3	7.588e-6	2.910e-6	6.707e-3	1.438e-5	1.620e-6
7.228e-3	5.718e-6	1.500e-6	7.121e-3	5.108e-6	2.880e-6	7.015e-3	1.311e-5	1.600e-6
7.560e-3	4.528e-6	1.470e-6	7.448e-3	1.291e-5	2.890e-6	7.337e-3	8.480e-6	1.580e-6
7.909e-3	2.920e-6	1.500e-6	7.791e-3	1.284e-5	2.890e-6	7.675e-3	8.445e-6	1.590e-6
8.274e-3	8.687e-7	1.490e-6	8.150e-3	8.360e-6	2.920e-6	8.029e-3	9.875e-6	1.610e-6
8.657e-3	2.627e-6	1.530e-6	8.527e-3	8.575e-6	2.950e-6	8.400e-3	1.243e-5	1.610e-6
9.058e-3	3.237e-6	1.540e-6	8.922e-3	8.235e-6	2.980e-6	8.788e-3	9.652e-6	1.620e-6
9.478e-3	4.870e-6	1.550e-6	9.336e-3	6.987e-6	3.030e-6	9.196e-3	1.144e-5	1.630e-6
9.918e-3	3.541e-6	1.570e-6	9.769e-3	9.705e-6	3.070e-6	9.623e-3	9.309e-6	1.640e-6
1.038e-2	2.926e-6	1.580e-6	1.022e-2	1.191e-5	3.100e-6	1.007e-2	1.092e-5	1.660e-6
1.086e-2	5.704e-6	1.600e-6	1.070e-2	1.988e-5	3.120e-6	1.054e-2	1.222e-5	1.670e-6
1.137e-2	4.030e-6	1.620e-6	1.120e-2	1.685e-5	3.140e-6	1.103e-2	1.659e-5	1.680e-6
1.190e-2	4.473e-6	1.610e-6	1.172e-2	1.116e-5	3.170e-6	1.154e-2	1.657e-5	1.680e-6
1.246e-2	4.302e-6	1.630e-6	1.227e-2	1.830e-5	3.200e-6	1.209e-2	1.468e-5	1.690e-6
1.304e-2	1.463e-6	1.660e-6	1.285e-2	1.792e-5	3.230e-6	1.265e-2	1.203e-5	1.700e-6
1.365e-2	2.338e-6	1.670e-6	1.345e-2	1.313e-5	3.250e-6	1.324e-2	1.238e-5	1.710e-6
1.429e-2	3.897e-6	1.700e-6	1.408e-2	1.465e-5	3.280e-6	1.386e-2	1.447e-5	1.720e-6
1.497e-2	4.078e-6	1.710e-6	1.474e-2	1.799e-5	3.320e-6	1.452e-2	1.295e-5	1.740e-6
1.567e-2	1.148e-6	1.750e-6	1.543e-2	1.708e-5	3.340e-6	1.520e-2	1.528e-5	1.740e-6
1.641e-2	2.509e-6	1.770e-6	1.616e-2	1.411e-5	3.360e-6	1.591e-2	1.621e-5	1.760e-6
1.718e-2	6.714e-6	1.800e-6	1.692e-2	1.475e-5	3.410e-6	1.666e-2	1.263e-5	1.760e-6
1.799e-2	6.727e-6	1.820e-6	1.772e-2	1.461e-5	3.450e-6	1.745e-2	1.542e-5	1.780e-6
1.884e-2	3.122e-6	1.830e-6	1.855e-2	1.897e-5	3.480e-6	1.827e-2	1.236e-5	1.800e-6
1.973e-2	4.283e-6	1.860e-6	1.943e-2	1.620e-5	3.540e-6	1.913e-2	1.247e-5	1.820e-6
2.066e-2	2.957e-6	1.890e-6	2.035e-2	1.275e-5	3.580e-6	2.004e-2	1.457e-5	1.840e-6
2.164e-2	3.980e-6	1.920e-6	2.131e-2	2.014e-5	3.620e-6	2.098e-2	1.566e-5	1.860e-6
2.266e-2	6.700e-6	1.960e-6	2.232e-2	2.072e-5	3.670e-6	2.198e-2	1.781e-5	1.860e-6
2.374e-2	3.549e-6	1.970e-6	2.337e-2	2.146e-5	3.710e-6	2.302e-2	1.665e-5	1.890e-6
2.486e-2	-2.433e-7	2.030e-6	2.448e-2	1.492e-5	3.770e-6	2.411e-2	1.157e-5	1.910e-6
2.604e-2	3.013e-6	2.070e-6	2.564e-2	8.155e-6	3.830e-6	2.525e-2	1.323e-5	1.920e-6
2.728e-2	5.499e-6	2.110e-6	2.686e-2	1.687e-5	3.910e-6	2.645e-2	1.676e-5	1.950e-6
2.857e-2	6.020e-6	2.150e-6	2.813e-2	2.191e-5	3.950e-6	2.770e-2	1.791e-5	1.980e-6
2.993e-2	2.106e-6	2.190e-6	2.947e-2	1.732e-5	4.030e-6	2.901e-2	1.376e-5	1.990e-6
3.135e-2	5.977e-6	2.220e-6	3.087e-2	1.716e-5	4.080e-6	3.039e-2	1.638e-5	2.020e-6
3.284e-2	9.333e-6	2.270e-6	3.233e-2	3.163e-5	4.150e-6	3.184e-2	1.886e-5	2.050e-6
3.440e-2	6.282e-6	2.300e-6	3.387e-2	2.342e-5	4.200e-6	3.335e-2	1.862e-5	2.060e-6
3.604e-2	6.767e-6	2.340e-6	3.548e-2	1.952e-5	4.260e-6	3.494e-2	2.051e-5	2.090e-6
3.775e-2	6.144e-6	2.380e-6	3.717e-2	2.528e-5	4.340e-6	3.660e-2	2.028e-5	2.110e-6
3.955e-2	6.350e-6	2.430e-6	3.894e-2	4.098e-5	4.390e-6	3.834e-2	2.287e-5	2.140e-6
4.143e-2	9.615e-6	2.450e-6	4.079e-2	2.737e-5	4.440e-6	4.017e-2	2.541e-5	2.160e-6
4.341e-2	1.105e-5	2.520e-6	4.274e-2	3.103e-5	4.500e-6	4.208e-2	2.613e-5	2.180e-6

Table 3.1.2.1 Continued

-10 mm			76 mm			228 mm		
4.548e-2	1.304e-5	2.520e-6	4.478e-2	3.990e-5	4.570e-6	4.409e-2	2.958e-5	2.180e-6
4.764e-2	1.502e-5	2.550e-6	4.691e-2	3.950e-5	4.590e-6	4.619e-2	3.261e-5	2.200e-6
4.992e-2	1.390e-5	2.590e-6	4.915e-2	3.634e-5	4.660e-6	4.839e-2	2.818e-5	2.210e-6
5.230e-2	1.074e-5	2.630e-6	5.149e-2	3.402e-5	4.730e-6	5.070e-2	2.945e-5	2.220e-6
5.479e-2	1.178e-5	2.670e-6	5.395e-2	3.713e-5	4.810e-6	5.312e-2	2.836e-5	2.240e-6
5.741e-2	9.690e-6	2.710e-6	5.652e-2	4.361e-5	4.860e-6	5.565e-2	2.877e-5	2.250e-6
6.015e-2	1.166e-5	2.760e-6	5.922e-2	3.954e-5	4.890e-6	5.831e-2	3.290e-5	2.270e-6
6.302e-2	1.642e-5	2.800e-6	6.205e-2	4.902e-5	4.990e-6	6.109e-2	2.938e-5	2.280e-6
6.603e-2	1.730e-5	2.830e-6	6.501e-2	4.884e-5	5.040e-6	6.401e-2	3.381e-5	2.290e-6
6.918e-2	1.544e-5	2.870e-6	6.812e-2	4.932e-5	5.090e-6	6.707e-2	4.005e-5	2.310e-6
7.249e-2	1.146e-5	2.930e-6	7.137e-2	4.151e-5	5.170e-6	7.027e-2	2.744e-5	2.320e-6
7.596e-2	1.164e-5	2.990e-6	7.478e-2	4.631e-5	5.230e-6	7.363e-2	2.516e-5	2.350e-6
7.959e-2	1.797e-5	3.040e-6	7.836e-2	4.287e-5	5.350e-6	7.715e-2	3.331e-5	2.380e-6
8.339e-2	1.968e-5	3.090e-6	8.210e-2	4.812e-5	5.410e-6	8.083e-2	3.442e-5	2.390e-6
8.738e-2	1.374e-5	3.150e-6	8.603e-2	6.731e-5	5.500e-6	8.470e-2	3.784e-5	2.420e-6
9.156e-2	1.220e-5	3.200e-6	9.014e-2	6.822e-5	5.530e-6	8.875e-2	3.637e-5	2.420e-6
9.594e-2	1.459e-5	3.270e-6	9.445e-2	6.444e-5	5.590e-6	9.300e-2	3.682e-5	2.450e-6
1.005e-1	2.298e-5	3.330e-6	9.897e-2	6.181e-5	5.650e-6	9.744e-2	3.946e-5	2.460e-6
1.053e-1	1.833e-5	3.410e-6	1.037e-1	5.578e-5	5.750e-6	1.021e-1	4.343e-5	2.470e-6
1.104e-1	2.154e-5	3.450e-6	1.087e-1	7.380e-5	5.820e-6	1.070e-1	4.252e-5	2.470e-6
1.157e-1	2.832e-5	3.580e-6	1.139e-1	8.529e-5	5.960e-6	1.121e-1	4.437e-5	2.510e-6
1.212e-1	2.218e-5	3.710e-6	1.193e-1	6.492e-5	6.110e-6	1.175e-1	4.396e-5	2.560e-6
1.270e-1	1.858e-5	3.850e-6	1.250e-1	6.154e-5	6.310e-6	1.231e-1	4.205e-5	2.610e-6
1.331e-1	2.193e-5	3.990e-6	1.310e-1	8.263e-5	6.520e-6	1.290e-1	4.367e-5	2.670e-6
1.395e-1	2.848e-5	4.150e-6	1.373e-1	8.321e-5	6.740e-6	1.352e-1	4.754e-5	2.730e-6
1.461e-1	2.253e-5	4.350e-6	1.439e-1	6.707e-5	6.960e-6	1.416e-1	4.159e-5	2.790e-6
1.531e-1	2.748e-5	4.480e-6	1.505e-1	8.060e-5	7.600e-6	1.459e-1	4.213e-5	1.960e-6
1.602e-1	3.005e-5	5.140e-6	1.577e-1	6.121e-5	7.610e-6	1.529e-1	3.895e-5	1.920e-6
1.679e-1	2.525e-5	5.140e-6	1.653e-1	6.155e-5	7.540e-6	1.602e-1	3.982e-5	1.890e-6
1.759e-1	2.241e-5	5.140e-6	1.732e-1	7.874e-5	7.520e-6	1.679e-1	4.181e-5	1.860e-6
1.844e-1	3.129e-5	5.150e-6	1.815e-1	9.511e-5	7.420e-6	1.759e-1	4.251e-5	1.820e-6
1.932e-1	3.938e-5	5.150e-6	1.902e-1	8.380e-5	7.350e-6	1.844e-1	4.771e-5	1.790e-6
2.025e-1	3.518e-5	5.160e-6	1.993e-1	9.648e-5	7.260e-6	1.932e-1	4.327e-5	1.750e-6
2.122e-1	4.087e-5	5.150e-6	2.089e-1	8.437e-5	7.240e-6	2.025e-1	4.276e-5	1.730e-6
2.223e-1	4.646e-5	5.170e-6	2.189e-1	9.902e-5	7.130e-6	2.122e-1	4.515e-5	1.700e-6
2.330e-1	4.138e-5	5.140e-6	2.294e-1	9.533e-5	7.070e-6	2.223e-1	4.376e-5	1.670e-6
2.441e-1	4.252e-5	5.160e-6	2.404e-1	8.051e-5	7.030e-6	2.330e-1	4.086e-5	1.640e-6
2.559e-1	4.384e-5	5.220e-6	2.519e-1	8.847e-5	7.050e-6	2.441e-1	4.181e-5	1.620e-6
2.681e-1	4.892e-5	5.280e-6	2.640e-1	1.008e-4	7.090e-6	2.559e-1	4.354e-5	1.610e-6
2.810e-1	4.114e-5	5.380e-6	2.766e-1	9.583e-5	7.150e-6	2.681e-1	4.359e-5	1.610e-6
2.944e-1	4.402e-5	5.440e-6	2.899e-1	1.092e-4	7.170e-6	2.810e-1	4.623e-5	1.600e-6
3.086e-1	4.636e-5	5.560e-6	3.038e-1	9.598e-5	7.200e-6	2.944e-1	4.388e-5	1.590e-6
3.233e-1	5.444e-5	5.600e-6	3.183e-1	1.062e-4	7.230e-6	3.086e-1	4.311e-5	1.580e-6
3.388e-1	5.610e-5	5.700e-6	3.336e-1	1.052e-4	7.320e-6	3.233e-1	4.535e-5	1.580e-6
3.551e-1	6.632e-5	5.740e-6	3.496e-1	1.064e-4	7.290e-6	3.388e-1	4.306e-5	1.570e-6
3.721e-1	7.433e-5	5.780e-6	3.664e-1	1.195e-4	7.310e-6	3.551e-1	4.577e-5	1.550e-6
3.900e-1	7.430e-5	5.820e-6	3.839e-1	1.207e-4	7.310e-6	3.721e-1	4.770e-5	1.530e-6
4.087e-1	7.150e-5	5.870e-6	4.023e-1	1.130e-4	7.290e-6	3.900e-1	4.582e-5	1.510e-6
4.283e-1	6.169e-5	5.890e-6	4.216e-1	1.268e-4	7.240e-6	4.087e-1	4.507e-5	1.480e-6
4.488e-1	6.360e-5	5.980e-6	4.419e-1	1.308e-4	7.240e-6	4.283e-1	4.660e-5	1.460e-6
4.703e-1	6.306e-5	6.010e-6	4.630e-1	1.170e-4	7.160e-6	4.488e-1	4.661e-5	1.430e-6
4.929e-1	6.115e-5	6.100e-6	4.852e-1	1.138e-4	7.150e-6	4.703e-1	4.279e-5	1.390e-6
5.165e-1	5.997e-5	6.150e-6	5.085e-1	1.144e-4	7.090e-6	4.929e-1	4.119e-5	1.370e-6
5.413e-1	7.566e-5	6.280e-6	5.329e-1	1.399e-4	7.070e-6	5.165e-1	3.944e-5	1.340e-6
5.673e-1	7.111e-5	6.440e-6	5.585e-1	1.218e-4	7.080e-6	5.413e-1	4.169e-5	1.310e-6
5.945e-1	7.629e-5	6.620e-6	5.853e-1	1.135e-4	7.170e-6	5.673e-1	3.993e-5	1.290e-6
6.230e-1	1.014e-4	6.770e-6	6.133e-1	1.319e-4	7.220e-6	5.945e-1	3.568e-5	1.280e-6
6.529e-1	1.189e-4	6.830e-6	6.428e-1	1.273e-4	7.260e-6	6.230e-1	3.544e-5	1.260e-6
6.842e-1	1.419e-4	6.850e-6	6.736e-1	1.190e-4	7.280e-6	6.529e-1	3.457e-5	1.250e-6
7.170e-1	1.506e-4	6.800e-6	7.059e-1	1.190e-4	7.360e-6	6.842e-1	3.294e-5	1.210e-6
7.514e-1	1.140e-4	6.830e-6	7.398e-1	1.125e-4	7.360e-6	7.170e-1	2.999e-5	1.200e-6
7.875e-1	8.618e-5	6.810e-6	7.752e-1	1.175e-4	7.390e-6	7.514e-1	2.640e-5	1.170e-6
8.252e-1	7.836e-5	7.010e-6	8.124e-1	1.177e-4	7.420e-6	7.875e-1	2.733e-5	1.150e-6
8.648e-1	8.513e-5	7.080e-6	8.514e-1	1.150e-4	7.370e-6	8.252e-1	2.430e-5	1.130e-6
9.063e-1	1.180e-4	7.150e-6	8.923e-1	1.260e-4	7.310e-6	8.648e-1	2.369e-5	1.100e-6
9.498e-1	1.086e-4	7.160e-6	9.351e-1	1.100e-4	7.260e-6	9.063e-1	2.173e-5	1.070e-6
9.954e-1	8.744e-5	7.170e-6	9.799e-1	9.943e-5	7.150e-6	9.498e-1	1.935e-5	1.040e-6
1.043e+0	6.881e-5	7.230e-6	1.027e+0	1.009e-4	7.100e-6	9.954e-1	1.737e-5	1.010e-6
						1.043e+0	1.573e-5	9.780e-7

Table 3.1.2.2 Neutron Spectra at 380, 532 and 618 mm from the front surface of the assembly measured by proton-recoil gas proportional counters.

380 mm			532 mm			618 mm		
Neutron Energy [MeV]	Flux [n/leth/ source]	Error	Neutron Energy [MeV]	Flux [n/leth/ source]	Error	Neutron Energy [MeV]	Flux [n/leth/ source]	Error
2.770e-3	2.514e-6	9.810e-7	2.732e-3	7.983e-8	2.220e-7	2.809e-3	4.934e-8	5.180e-8
2.889e-3	1.901e-6	9.370e-7	2.849e-3	7.242e-7	2.140e-7	2.930e-3	1.899e-8	5.000e-8
3.013e-3	8.088e-7	9.050e-7	2.971e-3	5.016e-7	2.050e-7	3.056e-3	1.083e-7	4.850e-8
3.143e-3	1.115e-6	8.770e-7	3.099e-3	4.086e-7	1.990e-7	3.188e-3	1.692e-7	4.710e-8
3.280e-3	2.493e-6	8.550e-7	3.233e-3	6.345e-7	1.930e-7	3.327e-3	1.028e-7	4.590e-8
3.423e-3	1.501e-6	8.380e-7	3.374e-3	5.167e-7	1.900e-7	3.472e-3	2.363e-8	4.450e-8
3.573e-3	2.243e-6	8.130e-7	3.522e-3	3.682e-7	1.860e-7	3.624e-3	2.003e-7	4.380e-8
3.730e-3	2.486e-6	7.950e-7	3.676e-3	9.017e-7	1.820e-7	3.784e-3	1.134e-7	4.260e-8
3.894e-3	1.170e-6	7.870e-7	3.838e-3	7.379e-7	1.770e-7	3.951e-3	5.100e-8	4.210e-8
4.067e-3	2.759e-6	7.700e-7	4.008e-3	4.861e-7	1.740e-7	4.126e-3	1.715e-7	4.170e-8
4.247e-3	2.639e-6	7.590e-7	4.186e-3	9.600e-7	1.710e-7	4.310e-3	1.253e-7	4.090e-8
4.437e-3	1.865e-6	7.450e-7	4.373e-3	1.229e-6	1.690e-7	4.502e-3	1.356e-7	4.010e-8
4.635e-3	2.369e-6	7.400e-7	4.568e-3	9.496e-7	1.650e-7	4.704e-3	1.620e-7	3.960e-8
4.843e-3	2.550e-6	7.320e-7	4.773e-3	7.090e-7	1.630e-7	4.915e-3	1.144e-7	3.910e-8
5.061e-3	2.390e-6	7.230e-7	4.988e-3	7.498e-7	1.610e-7	5.136e-3	1.621e-7	3.860e-8
5.290e-3	3.143e-6	7.170e-7	5.213e-3	1.030e-6	1.590e-7	5.369e-3	2.105e-7	3.820e-8
5.529e-3	3.087e-6	7.120e-7	5.448e-3	1.112e-6	1.580e-7	5.612e-3	2.683e-7	3.750e-8
5.780e-3	3.535e-6	7.040e-7	5.695e-3	1.296e-6	1.550e-7	5.867e-3	3.280e-7	3.700e-8
6.043e-3	4.628e-6	6.940e-7	5.954e-3	1.641e-6	1.520e-7	6.134e-3	4.291e-7	3.600e-8
6.319e-3	6.089e-6	6.860e-7	6.226e-3	2.217e-6	1.500e-7	6.414e-3	5.618e-7	3.510e-8
6.608e-3	7.145e-6	6.730e-7	6.510e-3	2.292e-6	1.460e-7	6.707e-3	6.726e-7	3.350e-8
6.911e-3	7.003e-6	6.600e-7	6.808e-3	2.214e-6	1.420e-7	7.015e-3	5.718e-7	3.220e-8
7.228e-3	5.480e-6	6.510e-7	7.121e-3	1.884e-6	1.390e-7	7.337e-3	4.414e-7	3.100e-8
7.560e-3	4.946e-6	6.450e-7	7.448e-3	1.699e-6	1.380e-7	7.675e-3	3.778e-7	3.050e-8
7.909e-3	4.540e-6	6.480e-7	7.791e-3	1.696e-6	1.360e-7	8.029e-3	3.054e-7	3.010e-8
8.274e-3	4.955e-6	6.480e-7	8.150e-3	1.490e-6	1.370e-7	8.400e-3	2.525e-7	3.000e-8
8.657e-3	5.954e-6	6.520e-7	8.527e-3	1.382e-6	1.370e-7	8.788e-3	2.061e-7	3.010e-8
9.058e-3	5.018e-6	6.550e-7	8.922e-3	1.343e-6	1.380e-7	9.196e-3	1.632e-7	3.020e-8
9.478e-3	4.520e-6	6.600e-7	9.336e-3	1.676e-6	1.380e-7	9.623e-3	1.870e-7	3.050e-8
9.918e-3	5.004e-6	6.630e-7	9.769e-3	1.666e-6	1.380e-7	1.007e-2	2.137e-7	3.070e-8
1.038e-2	6.571e-6	6.650e-7	1.022e-2	1.535e-6	1.390e-7	1.054e-2	3.246e-7	3.060e-8
1.086e-2	7.729e-6	6.650e-7	1.070e-2	1.758e-6	1.380e-7	1.103e-2	3.759e-7	3.050e-8
1.137e-2	7.563e-6	6.650e-7	1.120e-2	2.034e-6	1.390e-7	1.154e-2	3.922e-7	3.010e-8
1.190e-2	6.418e-6	6.640e-7	1.172e-2	2.102e-6	1.390e-7	1.209e-2	3.550e-7	3.000e-8
1.246e-2	6.988e-6	6.650e-7	1.227e-2	2.149e-6	1.380e-7	1.265e-2	2.374e-7	2.970e-8
1.304e-2	5.596e-6	6.690e-7	1.285e-2	1.741e-6	1.370e-7	1.324e-2	2.460e-7	2.980e-8
1.365e-2	5.654e-6	6.710e-7	1.345e-2	1.659e-6	1.370e-7	1.386e-2	2.497e-7	2.980e-8
1.429e-2	7.544e-6	6.740e-7	1.408e-2	1.790e-6	1.380e-7	1.452e-2	2.631e-7	2.990e-8
1.497e-2	6.883e-6	6.740e-7	1.474e-2	1.753e-6	1.370e-7	1.520e-2	2.826e-7	2.990e-8
1.567e-2	6.383e-6	6.750e-7	1.543e-2	1.933e-6	1.380e-7	1.591e-2	2.569e-7	2.990e-8
1.641e-2	6.376e-6	6.770e-7	1.616e-2	1.647e-6	1.380e-7	1.666e-2	1.919e-7	3.010e-8
1.718e-2	5.403e-6	6.840e-7	1.692e-2	1.458e-6	1.380e-7	1.745e-2	2.066e-7	3.010e-8
1.799e-2	5.519e-6	6.860e-7	1.772e-2	1.625e-6	1.390e-7	1.827e-2	2.836e-7	3.040e-8
1.884e-2	6.838e-6	6.900e-7	1.855e-2	1.666e-6	1.400e-7	1.913e-2	2.423e-7	3.040e-8
1.973e-2	7.297e-6	6.950e-7	1.943e-2	1.769e-6	1.400e-7	2.004e-2	2.413e-7	3.050e-8
2.066e-2	5.992e-6	6.960e-7	2.035e-2	1.747e-6	1.410e-7	2.098e-2	2.262e-7	3.060e-8
2.164e-2	6.216e-6	7.040e-7	2.131e-2	2.014e-6	1.410e-7	2.198e-2	2.443e-7	3.100e-8
2.266e-2	5.209e-6	7.100e-7	2.232e-2	1.830e-6	1.420e-7	2.302e-2	2.450e-7	3.120e-8
2.374e-2	8.278e-6	7.110e-7	2.337e-2	1.653e-6	1.420e-7	2.411e-2	2.142e-7	3.140e-8
2.486e-2	7.010e-6	7.150e-7	2.448e-2	1.521e-6	1.430e-7	2.525e-2	2.501e-7	3.170e-8
2.604e-2	5.085e-6	7.220e-7	2.564e-2	1.530e-6	1.440e-7	2.645e-2	2.404e-7	3.190e-8
2.728e-2	5.579e-6	7.290e-7	2.686e-2	1.561e-6	1.450e-7	2.770e-2	2.647e-7	3.220e-8
2.857e-2	6.945e-6	7.420e-7	2.813e-2	1.764e-6	1.460e-7	2.901e-2	2.699e-7	3.230e-8
2.993e-2	7.561e-6	7.450e-7	2.947e-2	2.019e-6	1.470e-7	3.039e-2	2.752e-7	3.260e-8
3.135e-2	7.790e-6	7.490e-7	3.087e-2	2.040e-6	1.470e-7	3.184e-2	1.868e-7	3.300e-8
3.284e-2	7.023e-6	7.550e-7	3.233e-2	2.072e-6	1.480e-7	3.335e-2	2.809e-7	3.330e-8
3.440e-2	8.196e-6	7.640e-7	3.387e-2	1.872e-6	1.480e-7	3.494e-2	3.290e-7	3.330e-8
3.604e-2	7.589e-6	7.680e-7	3.548e-2	2.240e-6	1.490e-7	3.660e-2	3.463e-7	3.370e-8
3.775e-2	1.027e-5	7.730e-7	3.717e-2	2.443e-6	1.490e-7	3.834e-2	3.425e-7	3.370e-8
3.955e-2	1.038e-5	7.750e-7	3.894e-2	2.344e-6	1.490e-7	4.017e-2	3.460e-7	3.400e-8
4.143e-2	8.711e-6	7.760e-7	4.079e-2	2.329e-6	1.500e-7	4.208e-2	4.298e-7	3.390e-8
4.341e-2	1.286e-5	7.760e-7	4.274e-2	2.925e-6	1.500e-7	4.409e-2	5.735e-7	3.360e-8

Table 3.1.2.2 Continued

380 mm			532 mm			618 mm		
4.548e-2	1.349e-5	7.760e-7	4.478e-2	3.264e-6	1.480e-7	4.619e-2	5.833e-7	3.330e-8
4.764e-2	1.099e-5	7.720e-7	4.691e-2	3.263e-6	1.470e-7	4.839e-2	5.416e-7	3.290e-8
4.992e-2	1.021e-5	7.760e-7	4.915e-2	2.839e-6	1.460e-7	5.070e-2	4.080e-7	3.260e-8
5.230e-2	1.062e-5	7.760e-7	5.149e-2	2.575e-6	1.440e-7	5.312e-2	3.472e-7	3.280e-8
5.479e-2	1.091e-5	7.800e-7	5.395e-2	2.412e-6	1.450e-7	5.565e-2	4.140e-7	3.260e-8
5.741e-2	1.101e-5	7.800e-7	5.652e-2	2.269e-6	1.450e-7	5.831e-2	4.168e-7	3.260e-8
6.015e-2	1.280e-5	7.790e-7	5.922e-2	2.761e-6	1.440e-7	6.109e-2	4.398e-7	3.260e-8
6.302e-2	1.228e-5	7.760e-7	6.205e-2	2.904e-6	1.440e-7	6.401e-2	4.899e-7	3.240e-8
6.603e-2	1.072e-5	7.810e-7	6.501e-2	2.844e-6	1.430e-7	6.707e-2	4.536e-7	3.220e-8
6.918e-2	1.059e-5	7.820e-7	6.812e-2	2.568e-6	1.430e-7	7.027e-2	3.747e-7	3.220e-8
7.249e-2	1.083e-5	7.850e-7	7.137e-2	2.218e-6	1.420e-7	7.363e-2	2.972e-7	3.230e-8
7.596e-2	1.054e-5	7.860e-7	7.478e-2	2.338e-6	1.420e-7	7.715e-2	3.542e-7	3.230e-8
7.959e-2	1.183e-5	7.860e-7	7.836e-2	2.610e-6	1.430e-7	8.083e-2	4.215e-7	3.250e-8
8.339e-2	1.126e-5	7.880e-7	8.210e-2	2.247e-6	1.420e-7	8.470e-2	4.111e-7	3.250e-8
8.738e-2	1.169e-5	7.910e-7	8.603e-2	2.671e-6	1.420e-7	8.875e-2	3.727e-7	3.250e-8
9.156e-2	1.307e-5	7.920e-7	9.014e-2	2.742e-6	1.420e-7	9.300e-2	4.179e-7	3.260e-8
9.594e-2	1.381e-5	7.900e-7	9.445e-2	2.658e-6	1.400e-7	9.744e-2	4.640e-7	3.240e-8
1.005e-1	1.164e-5	7.870e-7	9.897e-2	2.664e-6	1.400e-7	1.021e-1	4.287e-7	3.240e-8
1.053e-1	1.274e-5	7.890e-7	1.037e-1	2.677e-6	1.390e-7	1.070e-1	4.229e-7	3.220e-8
1.104e-1	1.509e-5	7.860e-7	1.087e-1	2.915e-6	1.380e-7	1.121e-1	5.141e-7	3.230e-8
1.157e-1	1.348e-5	7.920e-7	1.139e-1	2.875e-6	1.390e-7	1.175e-1	4.929e-7	3.250e-8
1.212e-1	1.245e-5	8.020e-7	1.193e-1	2.732e-6	1.390e-7	1.231e-1	4.016e-7	3.280e-8
1.270e-1	1.079e-5	8.200e-7	1.250e-1	2.566e-6	1.410e-7	1.290e-1	3.424e-7	3.350e-8
1.331e-1	1.302e-5	8.380e-7	1.310e-1	2.293e-6	1.420e-7	1.352e-1	4.204e-7	3.390e-8
1.395e-1	1.283e-5	8.480e-7	1.373e-1	2.625e-6	1.440e-7	1.416e-1	4.476e-7	3.450e-8
1.461e-1	1.441e-5	8.610e-7	1.439e-1	2.714e-6	1.460e-7	1.484e-1	4.163e-7	3.490e-8
1.531e-1	1.300e-5	8.730e-7	1.508e-1	2.512e-6	1.470e-7	1.505e-1	3.903e-7	3.010e-8
1.605e-1	1.306e-5	8.840e-7	1.580e-1	2.598e-6	1.490e-7	1.577e-1	3.729e-7	2.950e-8
1.681e-1	1.382e-5	8.990e-7	1.655e-1	2.323e-6	1.500e-7	1.653e-1	3.952e-7	2.880e-8
1.762e-1	1.423e-5	9.020e-7	1.735e-1	2.493e-6	1.520e-7	1.732e-1	3.890e-7	2.820e-8
1.846e-1	1.224e-5	9.230e-7	1.818e-1	2.459e-6	1.530e-7	1.815e-1	4.144e-7	2.740e-8
1.935e-1	1.083e-5	9.290e-7	1.905e-1	2.200e-6	1.540e-7	1.902e-1	4.485e-7	2.660e-8
1.962e-1	1.191e-5	5.810e-7	1.996e-1	2.194e-6	1.570e-7	1.993e-1	3.819e-7	2.580e-8
2.056e-1	1.136e-5	5.640e-7	2.056e-1	2.234e-6	1.060e-7	2.089e-1	3.875e-7	2.530e-8
2.155e-1	1.150e-5	5.540e-7	2.155e-1	2.166e-6	1.030e-7	2.189e-1	3.793e-7	2.450e-8
2.258e-1	1.086e-5	5.420e-7	2.258e-1	2.228e-6	1.010e-7	2.294e-1	4.116e-7	2.400e-8
2.366e-1	1.124e-5	5.280e-7	2.366e-1	1.936e-6	9.780e-8	2.404e-1	3.727e-7	2.330e-8
2.480e-1	1.073e-5	5.190e-7	2.480e-1	1.870e-6	9.570e-8	2.519e-1	3.552e-7	2.290e-8
2.599e-1	1.017e-5	5.110e-7	2.599e-1	1.897e-6	9.400e-8	2.640e-1	3.421e-7	2.260e-8
2.723e-1	1.096e-5	5.050e-7	2.723e-1	1.938e-6	9.240e-8	2.766e-1	3.337e-7	2.240e-8
2.854e-1	1.098e-5	5.010e-7	2.854e-1	1.995e-6	9.080e-8	2.899e-1	3.643e-7	2.200e-8
2.991e-1	1.070e-5	4.920e-7	2.991e-1	1.878e-6	8.880e-8	3.038e-1	3.109e-7	2.190e-8
3.134e-1	9.547e-6	4.860e-7	3.134e-1	1.753e-6	8.690e-8	3.183e-1	3.111e-7	2.150e-8
3.284e-1	9.522e-6	4.790e-7	3.284e-1	1.664e-6	8.510e-8	3.336e-1	3.038e-7	2.140e-8
3.442e-1	9.873e-6	4.730e-7	3.442e-1	1.720e-6	8.290e-8	3.496e-1	2.949e-7	2.110e-8
3.607e-1	1.049e-5	4.630e-7	3.607e-1	1.763e-6	8.110e-8	3.664e-1	3.360e-7	2.070e-8
3.780e-1	9.963e-6	4.530e-7	3.780e-1	1.602e-6	7.870e-8	3.839e-1	3.166e-7	2.040e-8
3.961e-1	9.749e-6	4.430e-7	3.961e-1	1.598e-6	7.620e-8	4.023e-1	3.276e-7	1.990e-8
4.151e-1	1.079e-5	4.280e-7	4.151e-1	1.540e-6	7.380e-8	4.216e-1	3.174e-7	1.940e-8
4.350e-1	9.511e-6	4.140e-7	4.350e-1	1.506e-6	7.070e-8	4.419e-1	2.923e-7	1.890e-8
4.559e-1	8.594e-6	3.990e-7	4.559e-1	1.474e-6	6.750e-8	4.630e-1	2.685e-7	1.830e-8
4.777e-1	8.200e-6	3.830e-7	4.777e-1	1.260e-6	6.470e-8	4.852e-1	2.507e-7	1.790e-8
5.006e-1	7.591e-6	3.730e-7	5.006e-1	1.023e-6	6.210e-8	5.085e-1	2.150e-7	1.740e-8
5.247e-1	6.764e-6	3.580e-7	5.247e-1	1.065e-6	5.980e-8	5.329e-1	2.499e-7	1.710e-8
5.498e-1	7.526e-6	3.500e-7	5.498e-1	1.037e-6	5.790e-8	5.585e-1	2.172e-7	1.690e-8
5.762e-1	6.819e-6	3.410e-7	5.762e-1	9.512e-7	5.600e-8	5.853e-1	2.155e-7	1.690e-8
6.038e-1	5.977e-6	3.310e-7	6.038e-1	7.280e-7	5.480e-8	6.133e-1	1.538e-7	1.680e-8
6.328e-1	5.473e-6	3.220e-7	6.328e-1	7.488e-7	5.330e-8	6.428e-1	1.607e-7	1.690e-8
6.631e-1	5.142e-6	3.170e-7	6.631e-1	8.411e-7	5.130e-8	6.736e-1	2.404e-7	1.670e-8
6.950e-1	4.641e-6	3.060e-7	6.950e-1	7.313e-7	4.920e-8	7.059e-1	2.080e-7	1.630e-8
7.283e-1	4.226e-6	2.990e-7	7.283e-1	5.126e-7	4.690e-8	7.398e-1	1.516e-7	1.600e-8
7.632e-1	4.020e-6	2.890e-7	7.632e-1	4.800e-7	4.500e-8	7.752e-1	1.761e-7	1.560e-8
7.998e-1	4.095e-6	2.780e-7	7.998e-1	5.738e-7	4.310e-8	8.124e-1	1.660e-7	1.520e-8
8.382e-1	3.376e-6	2.690e-7	8.382e-1	4.422e-7	4.050e-8	8.514e-1	1.163e-7	1.510e-8
8.784e-1	2.778e-6	2.550e-7	8.784e-1	2.708e-7	3.920e-8	8.923e-1	1.263e-7	1.470e-8
9.206e-1	2.996e-6	2.460e-7	9.206e-1	3.452e-7	3.680e-8	9.351e-1	1.328e-7	1.460e-8
9.647e-1	2.172e-6	2.350e-7	9.647e-1	2.881e-7	3.590e-8	9.799e-1	1.048e-7	1.430e-8
1.011e+0	1.776e-6	2.220e-7	1.011e+0	1.538e-7	3.320e-8	1.027e+0	7.817e-8	1.400e-8

Table 3.2.1 Dosimetry Reactions.

	Reactions	Half-Life	Abundance (%)	γ-ray Energy (keV)	γ-ray Branching (%)	Threshold Energy (MeV)
1.	$^{27}Al(n,\alpha)^{24}Na$	15.02 h	100.0	1368.6	100.0	5
2.	$^{n}Ti(n,x)^{46}Sc$	83.83 d	100.0	889.3	99.98	4
3.	$^{n}Ti(n,x)^{47}Sc$	3.341 d	100.0	159.4	68.0	1.5
4.	$^{n}Ti(n,x)^{48}Sc$	1.821 d	100.0	983.5	100.0	5
5.	$^{55}Mn(n,\gamma)^{56}Mn$	2.579 h	100.0	846.8	98.9	--------
6.	$^{54}Fe(n,p)^{54}Mn$	312.2 d	5.8	834.8	99.98	2
7.	$^{56}Fe(n,p)^{56}Mn$	2.579 h	91.72	846.8	98.9	5
8.	$^{58}Ni(n,p)^{58}Co$	70.92 d	68.26	810.8	99.5	2
9.	$^{58}Ni(n,2n)^{57}Ni$	1.503 d	68.27	1377.6	77.9	12.5
10.	$^{59}Co(n,\alpha)^{56}Mn$	2.579 h	100.0	846.8	98.9	6
11.	$^{59}Co(n,2n)^{58}Co$	70.92 d	100.0	810.8	99.5	10
12.	$^{64}Zn(n,p)^{64}Cu$	12.70 h	48.6	511.0	74.2	1.5
13.	$^{90}Zr(n,2n)^{89}Zr$	3.268 d	51.45	909.2	99.01	12
14.	$^{93}Nb(n,2n)^{92m}Nb$	10.15 d	100.0	934.5	99.0	9
15.	$^{115}In(n,n')^{115m}In$	4.486 h	95.7	336.3	45.8	0.34
16.	$^{197}Au(n,\gamma)^{198}Au$	2.694 d	100.0	411.8	95.5	--------
17.	$^{197}Au(n,2n)^{196}Au$	6.183 d	100.0	355.6	87.0	8.5

Table 3.2.2 Measured reaction rates in the copper assembly. The unit of the reaction rate is [reactions / atom / source neutron].

Reaction	Distance from Source [mm] 199.5		301.1		403.7		556.1		708.5		810.1	
	Reaction Rate	Error [%]	Reaction Rate	Error [%]	Reaction Rate	Error [%]	Reaction Rate	Error [%]	Reaction Rate	Error [%]	Reaction Rate	Error [%]
$^{27}Al(n,\alpha)^{24}Na$	2.387e-29	3.11	3.356e-30	3.23	4.859e-31	3.34	3.142e-32	4.23	2.312e-33	6.08	2.403e-34	4.94
$Ti(n,x)^{47}Sc$	5.555e-30	2.94	7.653e-31	2.92	1.100e-31	3.73	7.847e-33	6.11	5.179e-34	17.34		
$Ti(n,x)^{48}Sc$	1.258e-29	3.11	1.684e-30	3.21	2.261e-31	4.22	1.596e-32	6.04	9.157e-34	14.15		
$^{56}Fe(n,p)^{56}Mn$	2.173e-29	2.91	2.974e-30	2.97	4.440e-31	3.01	2.929e-32	3.34	2.178e-33	4.95	1.004e-33	10.80
$^{59}Co(n,\alpha)^{56}Mn$	6.559e-30	2.94	8.687e-31	3.25	1.233e-31	3.45	8.508e-33	4.00	6.255e-34	8.31	2.454e-34	35.34
$^{58}Ni(n,2n)^{57}Ni$	1.041e-29	3.10	1.286e-30	3.29	1.716e-31	3.92	9.998e-33	6.65	5.497e-34	11.27		
$Cu(n,x)^{64}Cu$	5.797e-29	3.42	1.297e-29	3.43	5.016e-30	3.50	1.742e-30	3.86	5.470e-31	3.83	1.941e-30	39.10
$^{64}Zn(n,p)^{64}Cu$	3.212e-29	3.30	6.078e-30	3.39	9.800e-31	3.48	7.489e-32	4.24	6.852e-33	4.85	5.412e-33	4.85
$^{90}Zr(n,2n)^{89}Zr$	1.739e-28	3.10	2.192e-29	3.17	2.968e-30	3.17	1.876e-31	3.48	1.119e-32	4.37	2.632e-33	5.11
$^{93}Nb(n,2n)^{92m}Nb$	9.797e-29	3.05	1.293e-29	3.14	1.799e-30	3.10	1.144e-31	3.59	8.385e-33	5.18	3.764e-33	5.32
$^{115}In(n,n')^{115m}In$	3.367e-29	2.87	1.703e-29	2.91	3.882e-30	3.25	3.822e-31	3.48	4.197e-32	5.04	2.270e-32	3.56
$^{197}Au(n,\gamma)^{198}Au$	8.188e-29	4.70	1.980e-28	4.36	2.114e-28	4.33	1.324e-28	4.51	5.981e-29	4.51	2.577e-29	4.85

Table 3.3.1.1 Measured Gamma-ray Spectra at 76 mm from the front surface of the experimental assembly. The unit of flux is [Gamma-rays / cm^2 / Lethargy / Source Neutron]. The errors contain statistical ones only. The window functions of energy resolution are given in FWHM.

Gamma-Ray Energy [MeV]	Flux	Error [%]	Window [%]	Gamma-Ray Energy [MeV]	Flux	Error [%]	Window [%]
0.251	3.559e-05	19.66	30.92	1.820	2.890e-05	5.10	18.36
0.263	4.217e-05	13.82	30.52	1.906	2.828e-05	5.02	18.36
0.275	4.608e-05	8.17	30.26	1.995	2.790e-05	4.92	18.23
0.288	4.693e-05	4.77	29.98	2.089	2.692e-05	4.83	18.30
0.302	4.551e-05	5.15	29.69	2.188	2.520e-05	4.95	18.48
0.316	4.334e-05	5.59	29.36	2.291	2.337e-05	5.04	18.80
0.331	4.171e-05	5.30	29.20	2.399	2.172e-05	5.06	19.20
0.347	4.108e-05	5.22	28.87	2.512	2.036e-05	5.13	19.53
0.363	4.119e-05	5.23	28.58	2.630	1.953e-05	5.14	19.82
0.380	4.160e-05	5.13	28.31	2.754	1.912e-05	5.00	20.13
0.398	4.216e-05	5.10	27.97	2.884	1.888e-05	4.91	20.49
0.417	4.313e-05	5.12	27.46	3.020	1.861e-05	4.91	20.95
0.437	4.501e-05	4.99	26.87	3.162	1.806e-05	4.85	21.77
0.457	4.788e-05	4.73	26.24	3.311	1.719e-05	4.74	22.88
0.479	5.078e-05	4.57	25.68	3.467	1.638e-05	4.97	23.72
0.501	5.203e-05	4.56	25.35	3.631	1.607e-05	5.26	24.29
0.525	5.054e-05	4.71	25.29	3.802	1.622e-05	4.86	24.98
0.550	4.697e-05	5.00	25.46	3.981	1.646e-05	4.54	25.30
0.575	4.326e-05	5.14	25.72	4.169	1.633e-05	4.89	25.30
0.603	4.104e-05	5.28	25.88	4.365	1.561e-05	4.76	25.45
0.631	4.071e-05	5.28	25.87	4.571	1.454e-05	5.27	25.74
0.661	4.164e-05	5.05	25.76	4.786	1.370e-05	6.51	25.74
0.692	4.281e-05	4.86	25.54	5.012	1.348e-05	5.31	25.74
0.724	4.329e-05	4.84	25.22	5.248	1.347e-05	5.72	25.74
0.759	4.297e-05	4.91	24.81	5.495	1.261e-05	8.14	25.74
0.794	4.295e-05	5.02	24.17	5.754	1.049e-05	8.28	25.74
0.832	4.486e-05	5.02	23.26	6.026	8.193e-06	10.78	25.74
0.871	4.950e-05	4.81	22.15	6.310	7.279e-06	12.64	25.74
0.912	5.551e-05	4.71	20.98	6.607	7.937e-06	9.28	25.74
0.955	5.969e-05	4.62	19.95	6.918	8.799e-06	8.70	25.74
1.000	5.996e-05	4.74	19.18	7.244	8.728e-06	7.80	25.74
1.047	5.783e-05	4.98	18.66	7.586	7.977e-06	6.86	25.74
1.097	5.642e-05	5.05	18.34	7.943	7.308e-06	7.18	25.74
1.148	5.618e-05	5.04	18.09	8.318	6.843e-06	7.29	25.74
1.202	5.506e-05	4.98	17.86	8.710	6.262e-06	7.67	25.74
1.259	5.230e-05	4.90	17.64	9.120	5.506e-06	8.19	25.74
1.318	4.968e-05	4.93	17.48	9.550	4.790e-06	8.56	25.74
1.380	4.788e-05	4.80	17.43	10.000	4.224e-06	9.14	25.74
1.445	4.480e-05	4.91	17.55	10.471	3.684e-06	10.27	25.74
1.514	3.976e-05	4.93	17.76	10.964	3.007e-06	11.55	25.74
1.585	3.502e-05	5.16	18.02	11.482	2.198e-06	12.55	25.74
1.660	3.201e-05	5.27	18.24	12.023	1.420e-06	14.57	25.74
1.738	3.015e-05	5.16	18.36	12.589	8.168e-07	21.19	25.74

Table 3.3.1.2 Measured Gamma-ray Spectra at 228 mm from the front surface of the experimental assembly. The unit of flux is [Gamma-rays / cm^2 / Lethargy / Source Neutron]. The errors contain statistical ones only. The window functions of energy resolution are given in FWHM.

Gamma-Ray Energy [MeV]	Flux	Error [%]	Window [%]	Gamma-Ray Energy [MeV]	Flux	Error [%]	Window [%]
0.251	5.106e-06	21.13	30.92	1.820	3.870e-06	5.20	20.85
0.263	6.088e-06	14.81	30.66	1.906	3.877e-06	5.10	20.74
0.275	6.705e-06	8.73	30.41	1.995	3.848e-06	5.00	20.61
0.288	6.879e-06	5.04	30.12	2.089	3.828e-06	4.94	20.52
0.302	6.697e-06	5.39	29.83	2.188	3.780e-06	5.01	20.49
0.316	6.348e-06	5.94	29.51	2.291	3.668e-06	5.02	20.57
0.331	6.015e-06	5.77	29.20	2.399	3.556e-06	4.98	20.78
0.347	5.800e-06	5.88	28.87	2.512	3.499e-06	4.99	21.14
0.363	5.748e-06	6.09	28.58	2.630	3.446e-06	4.94	21.72
0.380	5.907e-06	6.04	28.24	2.754	3.336e-06	4.93	22.54
0.398	6.379e-06	5.84	27.46	2.884	3.192e-06	5.00	23.36
0.417	7.327e-06	5.59	26.24	3.020	3.068e-06	5.08	24.12
0.437	8.853e-06	4.96	24.89	3.162	2.990e-06	4.98	24.81
0.457	1.075e-05	4.24	23.54	3.311	2.954e-06	4.92	25.27
0.479	1.231e-05	4.28	22.43	3.467	2.937e-06	5.23	25.49
0.501	1.263e-05	4.31	22.34	3.631	2.932e-06	5.57	25.64
0.525	1.137e-05	4.22	23.12	3.802	2.959e-06	5.36	25.74
0.550	9.183e-06	5.27	24.15	3.981	3.018e-06	5.37	25.74
0.575	7.164e-06	5.77	25.21	4.169	3.050e-06	5.69	25.74
0.603	6.009e-06	5.74	26.07	4.365	2.979e-06	5.59	25.74
0.631	5.708e-06	5.78	26.24	4.571	2.794e-06	6.95	25.74
0.661	5.830e-06	5.04	25.96	4.786	2.606e-06	8.60	25.74
0.692	5.939e-06	4.70	25.62	5.012	2.562e-06	7.01	25.74
0.724	5.848e-06	4.65	25.26	5.248	2.667e-06	7.58	25.74
0.759	5.622e-06	4.82	24.83	5.495	2.731e-06	9.60	25.74
0.794	5.457e-06	5.04	24.29	5.754	2.593e-06	8.85	25.74
0.832	5.571e-06	5.09	23.51	6.026	2.360e-06	9.99	25.74
0.871	6.081e-06	4.88	22.52	6.310	2.298e-06	10.22	25.74
0.912	6.816e-06	4.73	21.43	6.607	2.489e-06	7.73	25.74
0.955	7.331e-06	4.65	20.47	6.918	2.720e-06	7.26	25.74
1.000	7.345e-06	4.75	19.77	7.244	2.755e-06	6.25	25.74
1.047	7.078e-06	4.94	19.44	7.586	2.569e-06	5.50	25.74
1.097	6.861e-06	4.97	19.32	7.943	2.256e-06	6.02	25.74
1.148	6.623e-06	5.18	19.33	8.318	1.862e-06	6.66	25.74
1.202	6.220e-06	5.09	19.32	8.710	1.398e-06	7.98	25.74
1.259	5.840e-06	5.15	19.29	9.120	9.209e-07	10.96	25.74
1.318	5.662e-06	5.06	19.22	9.550	5.151e-07	17.98	25.74
1.380	5.586e-06	4.92	19.22	10.00	2.333e-07	40.17	25.74
1.445	5.435e-06	4.92	19.36	10.47	8.392e-08	117.08	25.74
1.514	5.085e-06	4.91	19.70	10.97	4.323e-08	212.61	25.74
1.585	4.550e-06	5.15	20.13	11.48	6.423e-08	112.58	25.74
1.660	4.068e-06	5.36	20.50	12.02	9.364e-08	56.43	25.74
1.738	3.867e-06	5.35	20.78	12.59	9.777e-08	46.49	25.74

Table 3.3.1.3 Measured Gamma-ray Spectra at 380 mm from the front surface of the experimental assembly. The unit of flux is [Gamma-rays / cm^2 / Lethargy / Source Neutron]. The errors contain statistical ones only. The window functions of energy resolution are given in FWHM.

Gamma-Ray Energy [MeV]	Flux	Error [%]	Window [%]	Gamma-Ray Energy [MeV]	Flux	Error [%]	Window [%]
0.251	1.053e-06	22.96	30.92	1.820	8.192e-07	5.15	24.90
0.263	1.247e-06	16.17	30.67	1.906	8.431e-07	5.03	24.35
0.275	1.368e-06	9.56	30.42	1.995	8.788e-07	4.89	23.54
0.288	1.405e-06	5.52	30.13	2.089	9.171e-07	4.83	22.74
0.302	1.381e-06	5.88	29.84	2.188	9.467e-07	4.84	22.23
0.316	1.332e-06	6.41	29.52	2.291	9.571e-07	4.85	22.19
0.331	1.284e-06	6.20	29.20	2.399	9.420e-07	4.86	22.67
0.347	1.248e-06	6.41	28.87	2.512	9.038e-07	4.96	23.47
0.363	1.232e-06	6.82	28.58	2.630	8.569e-07	5.11	24.30
0.380	1.263e-06	6.87	28.33	2.754	8.231e-07	5.16	25.02
0.398	1.401e-06	6.68	27.44	2.884	8.146e-07	5.17	25.51
0.417	1.743e-06	6.33	25.87	3.020	8.249e-07	5.13	25.63
0.437	2.362e-06	5.05	24.14	3.162	8.410e-07	4.99	25.63
0.457	3.178e-06	3.87	22.37	3.311	8.546e-07	4.90	25.63
0.479	3.852e-06	4.10	20.76	3.467	8.617e-07	5.15	25.63
0.501	3.952e-06	4.05	20.66	3.631	8.574e-07	5.52	25.65
0.525	3.358e-06	3.76	21.86	3.802	8.435e-07	5.48	25.74
0.550	2.428e-06	5.50	23.27	3.981	8.349e-07	5.50	25.74
0.575	1.634e-06	6.42	24.75	4.169	8.500e-07	5.80	25.74
0.603	1.182e-06	6.61	26.08	4.365	8.890e-07	5.41	25.74
0.631	1.022e-06	7.14	26.60	4.571	9.225e-07	5.74	25.74
0.661	1.008e-06	5.71	26.38	4.786	9.087e-07	6.90	25.74
0.692	1.017e-06	5.13	26.10	5.012	8.369e-07	6.44	25.74
0.724	1.008e-06	4.91	25.75	5.248	7.495e-07	6.96	25.74
0.759	9.913e-07	4.89	25.33	5.495	7.019e-07	9.81	25.74
0.794	9.922e-07	4.92	24.80	5.754	6.996e-07	8.89	25.74
0.832	1.022e-06	4.88	24.32	6.026	7.026e-07	6.92	25.74
0.871	1.076e-06	4.75	23.88	6.310	7.045e-07	6.33	24.78
0.912	1.129e-06	4.63	23.52	6.607	7.646e-07	5.24	22.99
0.955	1.149e-06	4.61	23.32	6.918	9.199e-07	4.38	20.74
1.000	1.124e-06	4.66	23.32	7.244	1.096e-06	4.13	18.31
1.047	1.067e-06	4.81	23.44	7.586	1.157e-06	4.15	16.27
1.097	1.010e-06	4.96	23.57	7.943	1.032e-06	4.19	17.08
1.148	9.759e-07	5.04	23.53	8.318	7.634e-07	4.58	18.86
1.202	9.702e-07	5.03	23.30	8.710	4.594e-07	6.54	21.12
1.259	9.851e-07	4.90	22.89	9.120	2.281e-07	11.21	23.55
1.318	1.006e-06	4.80	22.50	9.550	1.073e-07	22.15	25.58
1.380	1.014e-06	4.81	22.29	10.00	5.871e-08	36.06	25.74
1.445	9.974e-07	4.86	22.49	10.47	3.652e-08	39.05	25.74
1.514	9.547e-07	4.91	23.06	10.97	2.409e-08	22.95	25.74
1.585	8.969e-07	5.08	23.85	11.48	1.769e-08	61.05	25.74
1.660	8.447e-07	5.18	24.59	12.02	1.353e-08	113.60	25.74
1.738	8.171e-07	5.23	24.99	12.59	9.129e-09	147.33	25.74

Table 3.3.1.4 Measured Gamma-ray Spectra at 532 mm from the front surface of the experimental assembly. The unit of flux is [Gamma-rays / cm^2 / Lethargy / Source Neutron]. The errors contain statistical ones only. The window functions of energy resolution are given in FWHM.

Gamma-Ray Energy [MeV]	Flux	Error [%]	Window [%]	Gamma-Ray Energy [MeV]	Flux	Error [%]	Window [%]
0.251	1.966e-07	26.24	30.92	1.820	1.974e-07	5.12	25.40
0.263	2.350e-07	18.28	30.67	1.906	2.030e-07	5.05	25.02
0.275	2.600e-07	10.71	30.42	1.995	2.115e-07	4.95	24.50
0.288	2.689e-07	6.19	30.13	2.089	2.213e-07	4.86	23.92
0.302	2.649e-07	6.61	29.84	2.188	2.299e-07	4.84	23.46
0.316	2.552e-07	7.23	29.52	2.291	2.345e-07	4.83	23.32
0.331	2.463e-07	7.06	29.20	2.399	2.333e-07	4.85	23.53
0.347	2.420e-07	7.33	28.87	2.512	2.267e-07	4.95	24.02
0.363	2.448e-07	7.75	28.58	2.630	2.182e-07	5.09	24.60
0.380	2.606e-07	7.62	28.33	2.754	2.120e-07	5.16	25.14
0.398	3.044e-07	7.15	27.39	2.884	2.110e-07	5.18	25.51
0.417	4.010e-07	6.58	25.72	3.020	2.146e-07	5.14	25.61
0.437	5.699e-07	5.05	23.89	3.162	2.202e-07	5.01	25.64
0.457	7.879e-07	3.72	22.03	3.311	2.249e-07	4.91	25.64
0.479	9.617e-07	4.00	20.34	3.467	2.266e-07	5.13	25.64
0.501	9.761e-07	3.98	20.25	3.631	2.244e-07	5.51	25.65
0.525	8.089e-07	3.65	21.56	3.802	2.207e-07	5.52	25.74
0.550	5.648e-07	5.56	23.06	3.981	2.198e-07	5.50	25.74
0.575	3.652e-07	6.65	24.63	4.169	2.250e-07	5.64	25.74
0.603	2.526e-07	6.87	26.04	4.365	2.343e-07	5.34	25.74
0.631	2.089e-07	7.68	26.60	4.571	2.395e-07	5.75	25.74
0.661	2.009e-07	6.05	26.50	4.786	2.336e-07	6.83	25.74
0.692	2.025e-07	5.33	26.39	5.012	2.180e-07	6.35	25.74
0.724	2.016e-07	5.01	26.28	5.248	2.029e-07	6.62	25.74
0.759	1.974e-07	4.92	26.21	5.495	1.957e-07	8.87	25.74
0.794	1.928e-07	4.99	26.14	5.754	1.930e-07	8.24	25.74
0.832	1.902e-07	5.07	26.07	6.026	1.891e-07	6.38	25.66
0.871	1.902e-07	5.09	25.99	6.310	1.879e-07	5.61	24.65
0.912	1.921e-07	5.04	25.85	6.607	1.987e-07	5.21	22.67
0.955	1.948e-07	4.99	25.68	6.918	2.247e-07	5.05	19.83
1.000	1.978e-07	4.93	25.52	7.244	2.738e-07	4.48	16.46
1.047	2.002e-07	4.91	25.40	7.586	3.405e-07	3.69	13.36
1.097	2.012e-07	4.94	25.34	7.943	3.415e-07	3.04	12.25
1.148	2.003e-07	4.98	25.32	8.318	2.296e-07	3.19	14.23
1.202	1.982e-07	5.02	25.30	8.710	1.072e-07	5.01	17.07
1.259	1.969e-07	5.00	25.24	9.120	4.215e-08	7.40	20.44
1.318	1.980e-07	4.95	25.15	9.550	1.606e-08	11.74	23.61
1.380	2.010e-07	4.91	25.08	10.00	6.221e-09	18.90	25.74
1.445	2.030e-07	4.91	25.08	10.47	3.274e-09	28.61	25.74
1.514	2.021e-07	4.93	25.18	10.97	2.714e-09	33.48	25.74
1.585	1.987e-07	5.00	25.34	11.48	2.429e-09	32.98	25.74
1.660	1.957e-07	5.09	25.50	12.02	1.968e-09	31.01	25.74
1.738	1.949e-07	5.14	25.56	12.59	1.426e-09	32.47	25.74

Table 3.3.2.1 Time chart for measurement of decay gamma-ray spectra.

	start	stop	duration
BG #1	-27' 00"	-20' 00"	7' 00"
Irradiation	-20' 00"	0' 00"	20' 00"
Meas. #1	0' 00"	1' 00"	1' 00"
#2	1' 05"	2' 00"	0' 55"
#3	2' 05"	4' 00"	1' 55"
#4	4' 05"	6' 00"	1' 55"
#5	6' 05"	8' 00"	1' 55"
#6	8' 05"	13' 00"	4' 55"
#7	13' 05"	18' 00"	4' 55"
#8	18' 05"	23' 00"	4' 55"
#9	23' 05"	28' 00"	4' 55"
#10	28' 05"	33' 00"	4' 55"
#11	33' 05"	40' 00"	6' 55"
#12	40' 05"	56' 45"	40' 00"
BG #2	187' 00"	248' 00"	61' 00"

Table 3.3.2.6 Integrated decay gamma-ray spectra of four energy ranges. The unit is [Gamma-rays / cm^2 / sec].

Measuring Time [min.]		Energy Range of Integration [MeV]			
start	stop	0.4 - 0.65	0.65 - 1.0	1.0 - 1.4	1.4 - 3.0
0	1	7.23e+02	3.15e+01	3.28e+01	7.67e+01
1	2	7.02e+02	3.16e+01	3.15e+01	5.82e+01
2	4	6.15e+02	2.84e+01	2.28e+01	3.93e+01
4	6	5.47e+02	2.25e+01	1.81e+01	2.53e+01
6	8	4.72e+02	1.90e+01	1.70e+01	1.69e+01
8	13	3.66e+02	1.46e+01	1.18e+01	1.03e+01
13	18	2.61e+02	1.12e+01	7.92e+00	5.72e+00
18	23	1.81e+02	7.39e+00	5.81e+00	4.02e+00
23	28	1.27e+02	5.90e+00	3.86e+00	2.96e+00
28	33	9.03e+01	4.49e+00	2.86e+00	2.49e+00
33	40	5.99e+01	2.76e+00	2.27e+00	1.66e+00
40	57	2.87e+01	2.12e+00	1.20e+00	1.07e+00

Table 3.3.2.2 Measured decay gamma-ray spectra during 0 - 1, 1 - 2 and 2 - 4 minutes after the stop of the irradiation of 20 minutes by 10^{10} n/sec. The unit of the flux is [Gamma-rays / cm^2 / sec / Lethargy]. The errors contain statistical ones only.

	0 - 1 min.			1 - 2 min.			2 - 4 min.		
Eγ [MeV]	Flux	Error	Window	Flux	Error	Window	Flux	Error	Window
0.200	7.512E+02	6.02	31.29	7.264E+02	6.03	31.28	6.188E+02	6.46	31.34
0.209	8.191E+02	6.74	29.51	8.054E+02	6.71	29.49	6.781E+02	6.58	29.52
0.219	8.422E+02	7.43	27.78	8.317E+02	7.38	27.77	7.162E+02	6.58	27.73
0.229	8.335E+02	6.50	28.64	8.218E+02	6.45	28.64	7.418E+02	6.37	27.13
0.240	8.131E+02	5.90	26.93	8.094E+02	5.80	26.89	7.558E+02	6.31	25.37
0.251	7.972E+02	7.38	25.19	8.161E+02	7.20	25.10	7.494E+02	8.15	23.62
0.263	7.924E+02	8.62	24.98	8.295E+02	8.25	24.85	7.204E+02	11.39	23.43
0.275	7.963E+02	7.27	26.12	8.204E+02	6.95	25.99	6.840E+02	9.97	24.65
0.288	7.996E+02	6.43	25.83	7.842E+02	6.52	25.70	6.613E+02	7.19	25.76
0.302	7.952E+02	8.10	26.93	7.520E+02	8.55	26.83	6.586E+02	10.04	26.91
0.316	7.909E+02	7.33	26.69	7.516E+02	7.59	26.71	6.671E+02	8.55	26.70
0.331	8.011E+02	6.26	26.53	7.758E+02	6.39	26.70	6.779E+02	6.44	26.56
0.347	8.190E+02	5.96	25.05	7.993E+02	6.02	25.28	6.883E+02	6.14	25.02
0.363	8.157E+02	5.87	24.76	8.096E+02	5.92	25.00	6.950E+02	5.92	24.74
0.380	7.789E+02	7.08	24.50	8.094E+02	6.70	24.74	6.903E+02	6.87	24.49
0.398	7.357E+02	8.88	25.66	8.074E+02	6.95	25.83	6.707E+02	8.28	25.62
0.417	7.390E+02	9.87	24.98	8.261E+02	6.25	25.09	6.587E+02	9.29	24.94
0.437	8.674E+02	7.57	23.72	9.267E+02	5.54	26.00	7.286E+02	7.52	23.75
0.457	1.248E+03	7.22	20.65	1.235E+03	6.12	22.89	1.013E+03	7.46	20.67
0.479	2.022E+03	7.06	17.48	1.892E+03	5.09	19.67	1.666E+03	7.20	17.47
0.501	3.076E+03	3.33	14.72	2.777E+03	2.70	16.89	2.615E+03	3.30	14.68
0.525	3.556E+03	3.64	14.17	3.206E+03	2.87	16.36	3.081E+03	3.51	14.10
0.550	2.592E+03	4.64	16.26	2.520E+03	3.55	16.21	2.242E+03	4.49	16.17
0.575	1.039E+03	4.66	19.04	1.194E+03	3.90	19.04	8.670E+02	4.60	18.96
0.603	2.200E+02	26.48	21.93	2.928E+02	15.88	21.97	1.648E+02	28.85	21.88
0.631	4.596E+01	65.28	24.44	4.221E+01	59.75	24.50	4.111E+01	60.33	24.42
0.661	3.642E+01	39.75	26.50	4.588E+01	31.71	26.50	4.677E+01	23.16	26.50
0.692	4.564E+01	28.01	26.42	6.694E+01	19.55	26.42	5.111E+01	19.08	25.81
0.724	5.716E+01	13.32	26.35	7.234E+01	10.47	26.35	5.254E+01	10.81	24.73
0.759	6.813E+01	9.76	25.56	7.223E+01	8.87	25.82	5.776E+01	8.55	23.37
0.794	7.826E+01	8.27	24.62	7.257E+01	8.53	25.17	6.611E+01	7.83	21.88
0.832	8.793E+01	7.44	23.71	7.483E+01	8.22	25.09	7.451E+01	7.13	20.38
0.871	9.463E+01	7.45	22.82	7.800E+01	8.22	24.25	7.967E+01	7.49	19.46
0.912	9.389E+01	7.76	22.75	8.089E+01	8.40	23.22	7.940E+01	7.68	18.85
0.955	8.691E+01	8.31	22.49	8.461E+01	8.20	22.57	7.669E+01	8.17	18.47
1.000	8.224E+01	8.73	22.23	9.023E+01	7.78	21.98	7.756E+01	7.78	18.19
1.047	8.616E+01	8.44	21.86	9.521E+01	7.78	20.80	8.224E+01	7.38	18.05
1.097	9.689E+01	7.64	21.44	9.798E+01	7.95	20.41	8.494E+01	7.20	18.08
1.148	1.087E+02	7.18	20.27	1.018E+02	7.67	20.26	8.114E+01	7.59	18.46
1.202	1.145E+02	7.57	20.23	1.052E+02	7.88	20.33	7.070E+01	7.71	20.06
1.259	1.076E+02	7.55	21.28	9.868E+01	8.11	21.43	5.710E+01	9.26	21.67
1.318	9.177E+01	8.30	22.45	8.259E+01	8.62	22.57	4.620E+01	9.18	23.22
1.380	8.029E+01	9.47	23.65	7.049E+01	9.98	23.70	4.235E+01	9.95	24.61
1.445	8.149E+01	8.81	23.42	6.991E+01	9.41	23.37	4.485E+01	8.62	24.25
1.514	9.219E+01	8.60	22.72	7.826E+01	8.80	22.65	5.032E+01	8.43	22.41
1.585	1.058E+02	7.65	20.73	9.367E+01	7.44	20.86	5.793E+01	7.61	20.28
1.660	1.215E+02	7.69	18.55	1.124E+02	6.68	19.12	6.850E+01	7.30	17.89
1.738	1.427E+02	7.64	16.36	1.224E+02	7.11	17.51	7.977E+01	7.46	15.90
1.820	1.620E+02	6.39	15.69	1.149E+02	7.14	17.44	8.585E+01	6.62	15.53
1.906	1.585E+02	7.11	17.35	9.790E+01	8.18	17.73	8.215E+01	7.37	15.82
1.995	1.314E+02	6.94	17.67	8.556E+01	8.62	18.10	7.086E+01	7.05	16.63
2.089	1.097E+02	8.03	18.26	8.080E+01	8.68	18.36	5.979E+01	8.07	17.69
2.188	1.040E+02	7.41	19.00	7.870E+01	8.26	18.50	5.312E+01	7.32	18.28
2.291	9.902E+01	6.94	19.75	7.544E+01	8.03	18.65	4.897E+01	7.12	18.83
2.399	8.918E+01	7.02	19.75	6.910E+01	7.96	20.05	4.408E+01	6.95	19.51
2.512	7.768E+01	7.47	21.42	5.922E+01	7.98	21.48	3.681E+01	7.24	20.84
2.630	6.463E+01	7.94	23.01	4.694E+01	8.94	22.95	2.789E+01	8.32	22.16
2.754	5.200E+01	8.68	24.45	3.434E+01	9.84	24.42	1.926E+01	10.06	23.56
2.884	4.394E+01	9.12	25.74	2.389E+01	11.29	25.74	1.261E+01	12.56	24.86
3.020	4.047E+01	8.61	25.74	1.700E+01	12.96	25.74	8.533E+00	14.55	25.74
3.162	3.844E+01	8.04	25.74	1.277E+01	15.20	25.74	6.529E+00	15.45	25.74
3.311	3.541E+01	7.89	25.74	9.398E+00	16.66	25.74	5.621E+00	15.28	25.74
3.467	3.027E+01	8.57	25.74	6.269E+00	18.09	25.74	4.955E+00	16.00	25.74
3.631	2.294E+01	10.07	25.74	3.876E+00	23.45	25.74	4.058E+00	18.22	25.74
3.802	1.466E+01	12.15	25.74	2.369E+00	33.76	25.74	2.863E+00	21.39	25.74
3.981	7.533E+00	14.61	25.74	1.382E+00	42.72	25.74	1.639E+00	25.64	25.74
4.169	2.985E+00	17.59	25.74	6.782E-01	48.94	25.74	7.260E-01	31.65	25.74

Table 3.3.2.3 Measured decay gamma-ray spectra during 4 - 6, 6 - 8 and 8 - 13 minutes after the stop of the irradiation of 20 minutes by 10^{10} n/sec. The unit of the flux is [Gamma-rays / cm^2 / sec / Lethargy]. The errors contain statistical ones only.

	4 - 6 min.			6 - 8 min.			8 - 13 min.		
Eγ [MeV]	Flux	Error	Window	Flux	Error	Window	Flux	Error	Window
0.200	5.278E+02	6.59	31.38	4.577E+02	6.53	31.38	3.752E+02	6.28	31.29
0.209	5.818E+02	6.64	29.57	4.946E+02	6.64	29.66	4.043E+02	6.49	29.53
0.219	6.179E+02	6.63	27.77	5.227E+02	6.68	27.88	4.197E+02	6.64	27.77
0.229	6.431E+02	6.49	27.11	5.442E+02	6.46	27.25	4.283E+02	6.42	27.25
0.240	6.584E+02	6.39	25.33	5.494E+02	6.50	25.49	4.320E+02	6.40	25.49
0.251	6.576E+02	8.26	23.55	5.316E+02	8.93	23.68	4.279E+02	8.50	23.71
0.263	6.382E+02	11.51	23.35	5.079E+02	12.42	23.36	4.170E+02	11.61	23.43
0.275	6.096E+02	9.91	24.57	5.079E+02	10.06	24.56	4.072E+02	9.74	24.63
0.288	5.850E+02	7.32	25.71	5.321E+02	7.06	25.67	4.029E+02	7.13	25.71
0.302	5.694E+02	10.60	26.88	5.460E+02	9.69	26.82	4.001E+02	10.08	26.86
0.316	5.630E+02	9.07	26.72	5.314E+02	8.39	26.63	3.966E+02	8.70	26.63
0.331	5.680E+02	6.72	26.58	5.127E+02	6.50	26.47	3.994E+02	6.49	26.42
0.347	5.847E+02	6.63	25.04	5.149E+02	6.55	24.88	4.118E+02	6.34	24.82
0.363	6.046E+02	6.78	23.70	5.297E+02	6.79	23.57	4.253E+02	6.67	23.46
0.380	6.151E+02	7.45	23.44	5.374E+02	7.56	23.32	4.291E+02	7.49	23.21
0.398	6.119E+02	7.70	24.55	5.312E+02	7.79	24.47	4.207E+02	7.67	24.39
0.417	6.096E+02	8.53	23.88	5.202E+02	8.56	23.93	4.101E+02	8.48	23.83
0.437	6.624E+02	7.75	22.71	5.510E+02	7.92	22.81	4.347E+02	7.91	22.72
0.457	8.835E+02	7.42	20.69	7.396E+02	7.66	20.75	5.783E+02	7.56	20.70
0.479	1.432E+03	7.17	17.48	1.236E+03	7.10	17.54	9.572E+02	7.13	17.48
0.501	2.281E+03	3.33	14.66	1.995E+03	3.25	14.73	1.550E+03	3.27	14.65
0.525	2.738E+03	3.47	14.03	2.390E+03	3.46	14.06	1.865E+03	3.39	13.99
0.550	2.023E+03	4.34	16.09	1.755E+03	4.32	16.11	1.362E+03	4.30	16.06
0.575	8.044E+02	4.34	18.89	6.888E+02	4.44	18.91	5.166E+02	4.36	18.86
0.603	1.629E+02	25.52	21.81	1.352E+02	27.10	21.83	8.697E+01	31.08	21.80
0.631	2.548E+01	83.83	24.37	2.574E+01	72.16	24.39	1.135E+01	124.67	24.37
0.661	1.647E+01	58.45	26.50	2.379E+01	37.16	26.50	1.553E+01	37.42	26.50
0.692	2.572E+01	33.32	26.42	2.985E+01	26.32	26.42	2.148E+01	24.39	25.58
0.724	3.801E+01	13.12	25.36	3.463E+01	13.00	25.74	2.622E+01	11.56	24.26
0.759	4.918E+01	8.94	24.03	3.915E+01	9.86	24.74	3.199E+01	8.14	22.68
0.794	5.952E+01	7.50	22.57	4.559E+01	8.42	23.53	3.878E+01	7.24	21.02
0.832	6.916E+01	6.71	21.16	5.385E+01	7.27	22.34	4.505E+01	6.27	19.40
0.871	7.379E+01	7.05	19.81	5.915E+01	7.17	21.17	4.653E+01	6.81	18.58
0.912	6.932E+01	7.44	19.44	5.665E+01	7.77	20.54	4.091E+01	7.69	18.03
0.955	6.070E+01	8.62	19.34	4.976E+01	8.83	20.13	3.529E+01	9.09	17.58
1.000	5.702E+01	8.51	19.33	4.790E+01	8.74	19.78	3.712E+01	8.22	17.26
1.047	5.838E+01	8.18	19.30	5.396E+01	7.89	19.42	4.086E+01	7.70	16.96
1.097	5.937E+01	8.01	19.27	6.095E+01	7.43	19.11	4.009E+01	8.19	16.81
1.148	5.968E+01	7.81	19.37	6.200E+01	7.20	19.06	3.916E+01	8.00	17.14
1.202	5.935E+01	7.93	19.70	5.656E+01	7.51	20.34	3.909E+01	7.71	17.85
1.259	5.431E+01	8.19	21.02	4.771E+01	8.61	21.74	3.422E+01	8.19	19.69
1.318	4.457E+01	8.44	22.34	3.861E+01	8.61	23.19	2.639E+01	8.05	20.48
1.380	3.608E+01	10.05	23.62	3.145E+01	10.04	24.56	2.221E+01	9.28	20.99
1.445	3.225E+01	10.05	24.77	2.744E+01	9.85	25.74	2.160E+01	8.03	20.94
1.514	3.199E+01	9.92	24.40	2.685E+01	9.29	24.61	2.093E+01	7.62	20.52
1.585	3.476E+01	8.70	22.69	2.919E+01	8.07	23.33	1.979E+01	7.72	18.85
1.660	4.190E+01	7.91	20.76	3.284E+01	7.12	22.00	1.964E+01	7.46	18.19
1.738	5.252E+01	6.70	18.88	3.515E+01	7.05	20.68	2.053E+01	7.37	17.71
1.820	6.011E+01	6.22	17.18	3.439E+01	7.49	19.47	2.091E+01	7.36	17.54
1.906	5.727E+01	7.03	18.52	3.169E+01	7.84	19.61	1.948E+01	7.84	17.79
1.995	4.555E+01	6.81	20.24	2.900E+01	7.67	20.90	1.649E+01	7.58	19.46
2.089	3.499E+01	8.15	21.08	2.576E+01	8.52	22.22	1.332E+01	8.92	21.16
2.188	3.086E+01	8.27	22.07	2.101E+01	9.02	23.53	1.076E+01	9.20	22.83
2.291	2.941E+01	7.49	23.77	1.635E+01	9.72	24.75	8.679E+00	9.60	24.41
2.399	2.647E+01	7.38	23.77	1.338E+01	10.33	25.74	6.991E+00	9.83	25.74
2.512	2.178E+01	8.20	23.77	1.155E+01	10.55	25.74	5.806E+00	10.62	25.74
2.630	1.674E+01	9.25	24.86	9.909E+00	10.99	25.74	4.973E+00	11.65	25.74
2.754	1.257E+01	10.63	25.74	8.355E+00	12.05	25.74	4.187E+00	12.82	25.74
2.884	9.738E+00	12.33	25.74	6.833E+00	13.64	25.74	3.354E+00	14.31	25.74
3.020	7.907E+00	13.43	25.74	5.149E+00	15.82	25.74	2.603E+00	15.95	25.74
3.162	6.478E+00	13.83	25.74	3.372E+00	19.53	25.74	2.009E+00	17.76	25.74
3.311	5.166E+00	14.72	25.74	1.811E+00	26.26	25.74	1.505E+00	20.17	25.74
3.467	3.909E+00	17.53	25.74	7.065E-01	41.78	25.74	1.013E+00	25.06	25.74
3.631	2.668E+00	22.21	25.74	9.901E-02	156.55	25.74	5.540E-01	35.33	25.74
3.802	1.517E+00	28.19	25.74	-1.254E-01	53.78	25.74	2.112E-01	61.77	25.74
3.981	6.601E-01	35.81	25.74	-1.388E-01	16.53	25.74	2.929E-02	240.91	25.74
4.169	1.995E-01	47.06	25.74	-8.324E-02	11.81	25.74	-2.426E-02	120.38	25.74

Table 3.3.2.4 Measured decay gamma-ray spectra during 13 - 18, 18 - 23 and 23 - 28 minutes after the stop of the irradiation of 20 minutes by 10^{10} n/sec. The unit of the flux is [Gamma-rays / cm^2 / sec / Lethargy]. The errors contain statistical ones only.

	13 - 18 min.			18 - 23 min.			23 - 28 min.		
Eγ [MeV]	Flux	Error	Window	Flux	Error	Window	Flux	Error	Window
0.200	2.558E+02	6.54	31.35	1.783E+02	6.43	31.35	1.231E+02	6.68	31.41
0.209	2.789E+02	6.69	29.57	1.950E+02	6.56	29.58	1.354E+02	6.74	29.60
0.219	2.912E+02	6.70	27.80	2.041E+02	6.70	27.83	1.464E+02	6.59	27.77
0.229	2.984E+02	6.39	27.20	2.086E+02	6.54	27.28	1.556E+02	6.42	27.09
0.240	3.047E+02	6.54	25.42	2.104E+02	6.42	25.57	1.582E+02	6.34	25.38
0.251	3.096E+02	8.29	23.60	2.089E+02	8.05	23.83	1.501E+02	7.88	23.72
0.263	3.103E+02	10.04	23.32	2.035E+02	11.22	23.60	1.352E+02	12.11	23.61
0.275	3.064E+02	8.05	23.18	1.970E+02	10.08	24.78	1.255E+02	11.67	24.86
0.288	2.996E+02	8.36	24.29	1.945E+02	6.77	25.83	1.281E+02	7.25	25.99
0.302	2.923E+02	10.13	25.47	1.989E+02	8.45	25.64	1.386E+02	8.40	25.73
0.316	2.868E+02	8.09	25.38	2.079E+02	7.71	25.38	1.489E+02	7.65	25.34
0.331	2.852E+02	8.03	25.39	2.157E+02	6.43	25.26	1.551E+02	6.36	25.04
0.347	2.865E+02	7.11	25.33	2.158E+02	6.11	23.83	1.561E+02	6.09	23.49
0.363	2.861E+02	6.08	25.05	2.067E+02	6.12	23.55	1.505E+02	6.05	23.20
0.380	2.803E+02	6.72	24.79	1.943E+02	7.58	24.59	1.405E+02	7.80	24.31
0.398	2.718E+02	8.49	25.87	1.877E+02	9.55	25.76	1.320E+02	9.92	25.52
0.417	2.738E+02	9.86	25.05	1.944E+02	9.92	24.94	1.313E+02	10.12	24.86
0.437	3.152E+02	7.66	23.65	2.302E+02	7.29	23.55	1.515E+02	7.55	23.62
0.457	4.441E+02	7.20	20.51	3.276E+02	6.86	20.40	2.200E+02	7.17	20.58
0.479	7.166E+02	7.26	17.28	5.165E+02	7.04	17.20	3.631E+02	6.83	17.45
0.501	1.104E+03	3.37	14.50	7.614E+02	3.38	14.45	5.510E+02	3.24	14.76
0.525	1.293E+03	3.56	13.95	8.629E+02	3.72	14.00	6.275E+02	3.57	14.37
0.550	9.447E+02	4.54	16.09	6.269E+02	4.74	16.17	4.487E+02	4.61	16.50
0.575	3.763E+02	4.40	18.94	2.597E+02	4.53	19.03	1.694E+02	5.05	19.26
0.603	7.966E+01	24.74	21.88	6.364E+01	22.26	21.95	2.562E+01	41.20	22.10
0.631	1.416E+01	71.73	24.41	1.284E+01	55.04	24.44	3.354E+00	158.82	24.54
0.661	1.032E+01	43.67	26.50	4.701E+00	77.89	26.50	9.032E+00	34.13	26.50
0.692	1.852E+01	22.20	25.38	8.789E+00	37.01	26.42	1.205E+01	22.94	26.42
0.724	2.748E+01	9.15	24.13	1.533E+01	12.78	26.35	1.238E+01	14.02	26.35
0.759	3.200E+01	6.84	22.83	1.905E+01	9.06	25.78	1.288E+01	12.00	26.28
0.794	3.274E+01	7.22	21.55	2.000E+01	8.33	25.09	1.420E+01	10.34	26.21
0.832	3.241E+01	7.06	20.44	2.016E+01	8.20	24.33	1.569E+01	9.16	26.14
0.871	3.091E+01	7.49	20.42	2.062E+01	8.10	23.48	1.645E+01	8.61	26.06
0.912	2.692E+01	8.61	20.44	2.124E+01	7.97	22.55	1.596E+01	8.59	25.99
0.955	2.298E+01	9.35	20.42	2.122E+01	7.96	22.13	1.444E+01	8.96	25.92
1.000	2.294E+01	8.82	20.33	2.009E+01	8.01	21.83	1.284E+01	9.25	25.85
1.047	2.501E+01	8.02	20.09	1.880E+01	8.24	21.63	1.209E+01	9.25	25.81
1.097	2.542E+01	8.00	19.81	1.873E+01	8.48	21.60	1.232E+01	9.01	25.78
1.148	2.540E+01	7.84	19.67	1.934E+01	8.41	22.42	1.284E+01	8.83	25.74
1.202	2.627E+01	7.85	19.77	1.884E+01	8.10	23.26	1.277E+01	8.99	25.74
1.259	2.480E+01	7.85	21.00	1.678E+01	8.65	24.12	1.165E+01	9.64	25.74
1.318	2.026E+01	8.18	22.24	1.415E+01	9.24	24.96	9.648E+00	11.05	25.74
1.380	1.653E+01	9.40	23.47	1.175E+01	9.98	25.74	7.469E+00	13.34	25.74
1.445	1.506E+01	8.70	24.66	9.924E+00	10.43	25.74	5.920E+00	15.24	25.74
1.514	1.372E+01	8.36	25.74	8.856E+00	9.99	25.74	5.332E+00	14.77	25.74
1.585	1.167E+01	7.72	25.74	8.396E+00	9.13	25.74	5.401E+00	12.69	25.74
1.660	1.002E+01	7.58	25.74	8.061E+00	8.37	25.74	5.577E+00	11.00	25.74
1.738	9.354E+00	7.52	25.74	7.460E+00	8.34	25.74	5.537E+00	10.25	25.74
1.820	9.118E+00	7.38	25.74	6.609E+00	8.85	25.74	5.293E+00	10.24	25.74
1.906	8.722E+00	7.45	25.74	5.803E+00	9.49	25.74	4.978E+00	10.54	25.74
1.995	8.094E+00	7.67	25.74	5.285E+00	10.01	25.74	4.658E+00	10.94	25.74
2.089	7.420E+00	7.91	25.74	5.025E+00	10.38	25.74	4.310E+00	11.47	25.74
2.188	6.793E+00	8.20	25.74	4.784E+00	10.61	25.74	3.879E+00	12.16	25.74
2.291	6.096E+00	8.62	25.74	4.378E+00	10.77	25.74	3.342E+00	13.02	25.74
2.399	5.163E+00	9.32	25.74	3.808E+00	11.29	25.74	2.745E+00	14.28	25.74
2.512	4.002E+00	10.81	25.74	3.118E+00	12.92	25.74	2.169E+00	16.72	25.74
2.630	2.809E+00	14.28	25.74	2.260E+00	17.12	25.74	1.659E+00	21.66	25.74
2.754	1.777E+00	21.19	25.74	1.212E+00	30.87	25.74	1.194E+00	29.50	25.74
2.884	9.723E-01	32.30	25.74	1.701E-01	202.66	25.74	7.454E-01	40.06	25.74
3.020	3.924E-01	52.60	25.74	-5.105E-01	54.14	25.74	3.322E-01	59.27	25.74
3.162	2.897E-02	343.24	25.74	-6.633E-01	27.32	25.74	1.409E-02	670.39	23.79
3.311	-1.477E-01	24.07	25.74	-4.794E-01	18.97	25.74	-1.660E-01	19.34	21.97
3.467	-1.988E-01	8.58	25.74	-2.579E-01	13.06	25.74	-2.142E-01	5.07	21.97
3.631	-1.879E-01	8.19	25.74	-1.257E-01	10.38	25.74	-1.749E-01	5.53	21.97
3.802	-1.538E-01	8.97	25.74	-6.209E-02	16.83	25.74	-1.035E-01	11.51	21.97
3.981	-1.102E-01	10.25	25.74	-3.091E-02	30.70	25.74	-4.343E-02	26.73	23.92
4.169	-6.406E-02	14.42	25.74	-1.324E-02	64.82	25.74	-1.159E-02	81.45	25.74

Table 3.3.2.5 Measured decay gamma-ray spectra during 28 - 33, 33 - 40 and 40 - 57 minutes after the stop of the irradiation of 20 minutes by 10^{10} n/sec. The unit of the flux is [Gamma-rays / cm^2 / sec / Lethargy]. The errors contain statistical ones only.

	28 - 33 min.			33 - 40 min.			40 - 57 min.		
Eγ [MeV]	Flux	Error	Window	Flux	Error	Window	Flux	Error	Window
0.200	9.144E+01	6.15	31.33	6.243E+01	5.89	31.21	3.030E+01	5.85	31.25
0.209	1.002E+02	7.50	29.53	6.432E+01	6.75	29.65	3.298E+01	6.96	29.55
0.219	1.035E+02	8.62	27.78	6.281E+01	8.13	28.01	3.338E+01	8.29	27.91
0.229	1.025E+02	7.31	28.59	6.059E+01	7.72	28.95	3.209E+01	7.42	28.81
0.240	9.910E+01	5.59	28.27	6.026E+01	7.02	27.18	3.035E+01	5.84	28.48
0.251	9.533E+01	6.46	26.60	6.271E+01	7.72	25.31	2.929E+01	6.65	26.78
0.263	9.295E+01	7.11	26.42	6.703E+01	7.47	24.75	2.930E+01	7.52	26.49
0.275	9.352E+01	6.46	26.27	7.117E+01	6.53	24.41	2.996E+01	6.71	27.54
0.288	9.726E+01	6.29	25.99	7.269E+01	8.00	24.12	3.056E+01	5.66	27.26
0.302	1.021E+02	7.41	24.45	7.014E+01	8.48	25.28	3.081E+01	6.42	26.97
0.316	1.054E+02	7.94	24.20	6.505E+01	7.70	25.29	3.094E+01	6.71	26.69
0.331	1.058E+02	7.00	24.13	6.143E+01	8.76	25.31	3.137E+01	6.14	26.49
0.347	1.044E+02	6.80	24.04	6.190E+01	7.58	25.19	3.215E+01	5.87	24.92
0.363	1.025E+02	7.07	23.75	6.515E+01	6.53	23.86	3.310E+01	6.34	23.56
0.380	1.002E+02	7.32	24.75	6.775E+01	7.06	23.61	3.414E+01	6.77	23.31
0.398	9.791E+01	9.28	25.83	6.782E+01	7.70	24.64	3.485E+01	7.18	23.16
0.417	9.977E+01	9.93	24.95	6.763E+01	8.69	23.85	3.512E+01	9.28	22.36
0.437	1.159E+02	7.27	23.56	7.516E+01	7.62	22.62	3.868E+01	9.07	21.14
0.457	1.627E+02	7.03	20.48	1.038E+02	7.07	20.64	5.408E+01	6.60	19.23
0.479	2.569E+02	7.11	17.39	1.665E+02	6.79	17.58	8.578E+01	7.22	16.24
0.501	3.829E+02	3.37	14.76	2.523E+02	3.33	14.93	1.217E+02	3.96	15.00
0.525	4.372E+02	3.74	14.50	2.909E+02	3.78	14.64	1.317E+02	4.00	15.03
0.550	3.170E+02	4.80	16.66	2.138E+02	4.62	16.75	9.425E+01	5.35	17.17
0.575	1.232E+02	5.22	19.45	8.578E+01	5.48	19.47	3.797E+01	6.80	19.87
0.603	2.066E+01	39.42	22.26	1.551E+01	38.42	22.24	7.051E+00	45.37	22.58
0.631	3.805E+00	110.78	24.63	2.129E+00	142.17	24.64	2.043E+00	81.90	24.87
0.661	7.553E+00	36.08	26.50	3.626E+00	58.68	26.50	3.834E+00	33.16	26.50
0.692	9.515E+00	25.21	26.42	4.774E+00	39.26	26.42	4.602E+00	24.98	26.42
0.724	9.523E+00	16.84	26.35	4.821E+00	26.59	26.35	4.367E+00	19.06	26.35
0.759	9.767E+00	15.12	26.28	4.922E+00	24.35	26.28	4.330E+00	18.18	26.28
0.794	1.077E+01	13.09	26.21	5.675E+00	20.13	26.21	4.910E+00	15.51	26.21
0.832	1.188E+01	11.69	26.14	7.011E+00	16.02	26.14	5.705E+00	13.20	26.14
0.871	1.227E+01	11.12	26.06	8.348E+00	13.28	26.06	6.064E+00	12.15	26.06
0.912	1.174E+01	11.16	25.99	8.964E+00	12.00	25.99	5.715E+00	12.31	25.99
0.955	1.074E+01	11.49	25.92	8.537E+00	11.95	25.92	4.922E+00	13.40	25.92
1.000	9.917E+00	11.53	25.85	7.473E+00	12.52	25.85	4.155E+00	14.56	25.85
1.047	9.544E+00	11.34	25.81	6.645E+00	13.16	25.81	3.747E+00	15.18	25.81
1.097	9.478E+00	11.32	25.78	6.657E+00	13.04	25.78	3.750E+00	15.13	25.78
1.148	9.395E+00	11.60	25.74	7.284E+00	12.27	25.74	3.906E+00	14.97	25.74
1.202	9.012E+00	12.22	25.74	7.693E+00	11.82	25.74	3.836E+00	15.46	25.74
1.259	8.155E+00	13.30	25.74	7.254E+00	12.31	25.74	3.445E+00	16.77	25.74
1.318	6.924E+00	14.92	25.74	6.074E+00	14.00	25.74	3.021E+00	18.24	25.74
1.380	5.781E+00	16.61	25.74	4.750E+00	16.75	25.74	2.831E+00	18.51	25.74
1.445	5.228E+00	16.76	25.74	3.808E+00	18.88	25.74	2.788E+00	17.21	25.74
1.514	5.248E+00	14.88	25.74	3.410E+00	18.05	25.74	2.640E+00	15.50	25.74
1.585	5.306E+00	12.81	25.74	3.429E+00	14.95	25.74	2.347E+00	14.06	25.74
1.660	5.003E+00	11.74	25.74	3.591E+00	12.39	25.74	2.095E+00	12.94	25.74
1.738	4.521E+00	11.55	25.74	3.610E+00	11.40	25.74	1.991E+00	12.16	25.74
1.820	4.247E+00	11.66	25.74	3.359E+00	11.48	25.74	1.930E+00	11.99	25.74
1.906	4.221E+00	11.57	25.74	2.949E+00	12.22	25.74	1.770E+00	12.63	25.74
1.995	4.164E+00	11.68	25.74	2.574E+00	13.24	25.74	1.516E+00	14.13	25.74
2.089	3.843E+00	12.43	25.74	2.289E+00	14.55	25.74	1.277E+00	16.13	25.74
2.188	3.243E+00	13.82	25.74	1.999E+00	16.34	25.74	1.118E+00	18.13	25.74
2.291	2.523E+00	15.86	25.74	1.618E+00	19.47	25.74	9.978E-01	20.46	25.74
2.399	1.887E+00	19.09	25.74	1.168E+00	25.49	25.74	8.286E-01	23.97	25.74
2.512	1.413E+00	24.36	25.74	7.335E-01	37.38	25.74	5.846E-01	29.62	25.74
2.630	1.034E+00	33.97	25.74	3.877E-01	59.28	25.74	3.375E-01	39.75	25.74
2.754	6.760E-01	52.42	25.74	1.716E-01	101.18	25.74	1.787E-01	75.49	25.74
2.884	3.362E-01	91.79	25.74	8.871E-02	200.29	25.74	1.244E-01	134.06	25.74
3.020	7.526E-02	282.36	25.74	8.559E-02	254.69	25.74	1.195E-01	142.33	25.74
3.162	-5.688E-02	281.80	25.74	7.719E-02	271.91	25.74	1.198E-01	120.49	25.74
3.311	-8.700E-02	207.02	25.74	1.741E-02	853.37	25.74	1.261E-01	89.86	25.74
3.467	-9.028E-02	180.10	25.74	-7.189E-02	91.78	25.74	1.418E-01	68.14	25.74
3.631	-1.031E-01	102.09	25.74	-1.420E-01	12.70	25.74	1.460E-01	62.39	25.74
3.802	-1.065E-01	46.26	25.74	-1.626E-01	26.21	25.74	1.207E-01	66.83	25.74
3.981	-8.291E-02	20.66	25.74	-1.339E-01	32.69	25.74	7.598E-02	79.89	25.74
4.169	-4.441E-02	18.40	25.74	-8.080E-02	36.28	25.74	3.568E-02	101.04	25.74

Table 3.4.1 Contribution of neutron response to total one for TLDs of MSO, SSO and BSO.

Position	MSO	SSO	BSO
-1 mm	41.8 %	23.1 %	19.6 %
58	31.1	15.7	10.0
210	24.3	12.8	8.1
362	13.2	7.2	5.5
514	6.8	3.3	2.3
608	2.7	1.4	0.8

Table 3.4.2 Proportion of three corrections to the total gamma-ray heating.

Position	Target-γ	γ from ^{62}Cu	β from ^{62}Cu	Total
-1 mm	15.4 %	2.5 %	8.0 %	25.9 %
58	4.0	4.2	4.1	12.3
210	0.2	1.6	1.8	3.6
362	0.0	0.2	0.5	0.7
514	0.0	0.0	0.1	0.1
608	0.0	0.0	0.0	0.0

Table 3.4.3 Measured gamma-ray heating rates of copper in the copper assembly.

Position	Gamma-Ray Heating Rate [Gy / Source Neutron]	Error [%]
-1 mm	1.20×10^{-15}	24.5
58	8.35×10^{-16}	22.2
210	1.12×10^{-16}	13.2
362	2.70×10^{-17}	14.5
514	7.48×10^{-18}	11.1
608	2.28×10^{-18}	20.7

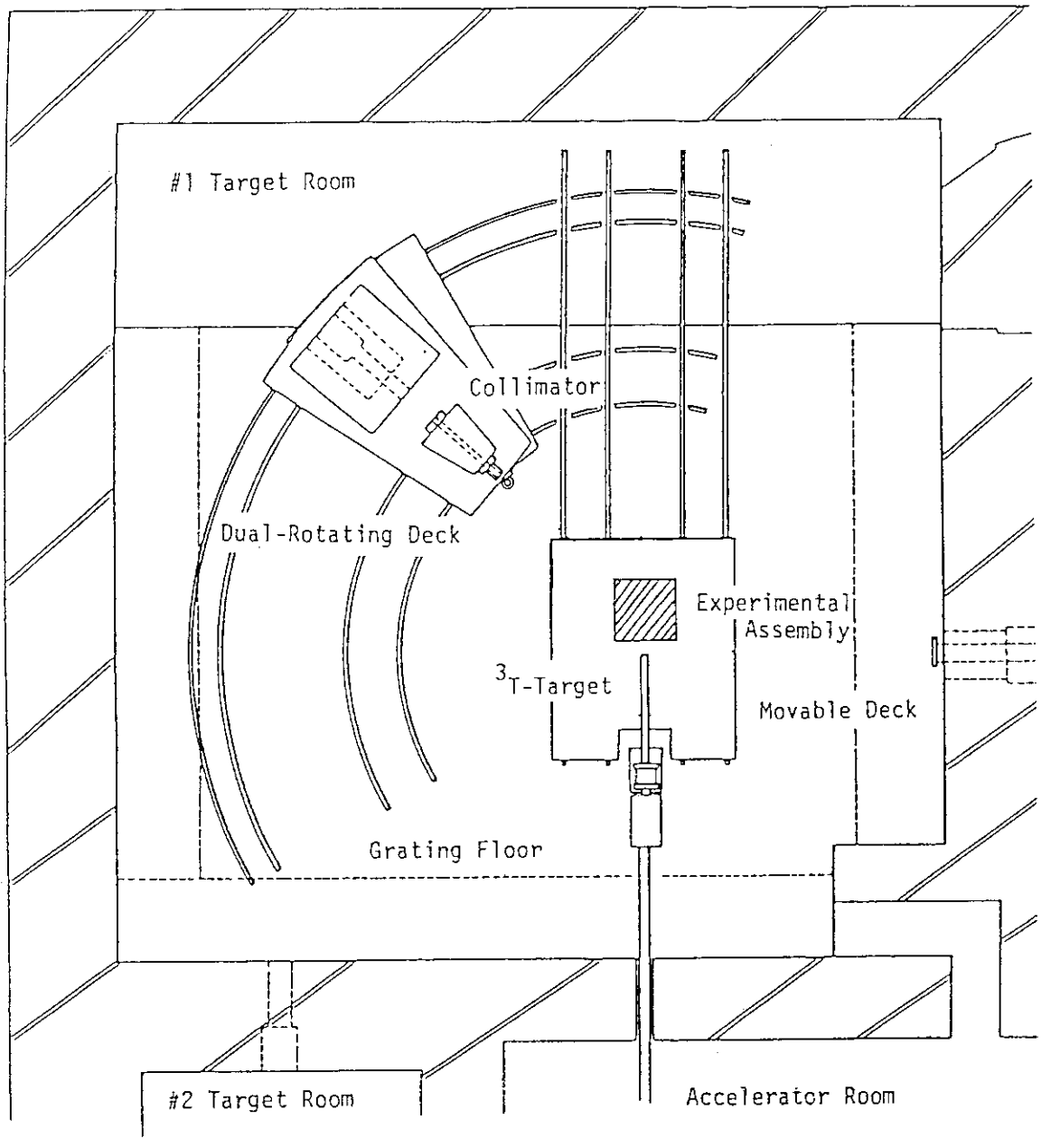

Fig. 2.1.1 Layout of the FNS first target room.

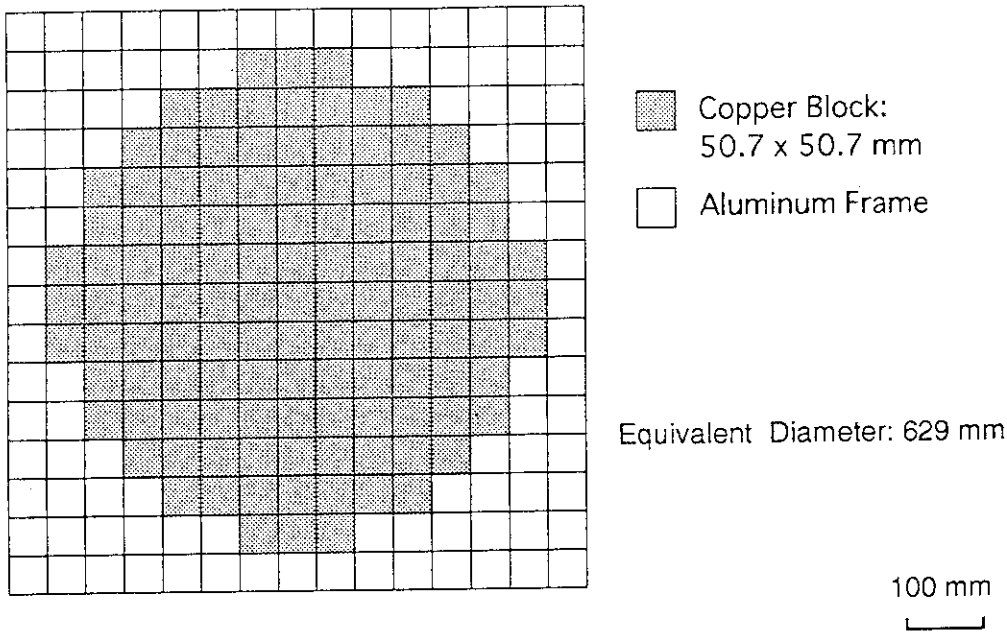

Fig. 2.1.2 Front view of the experimental assembly.

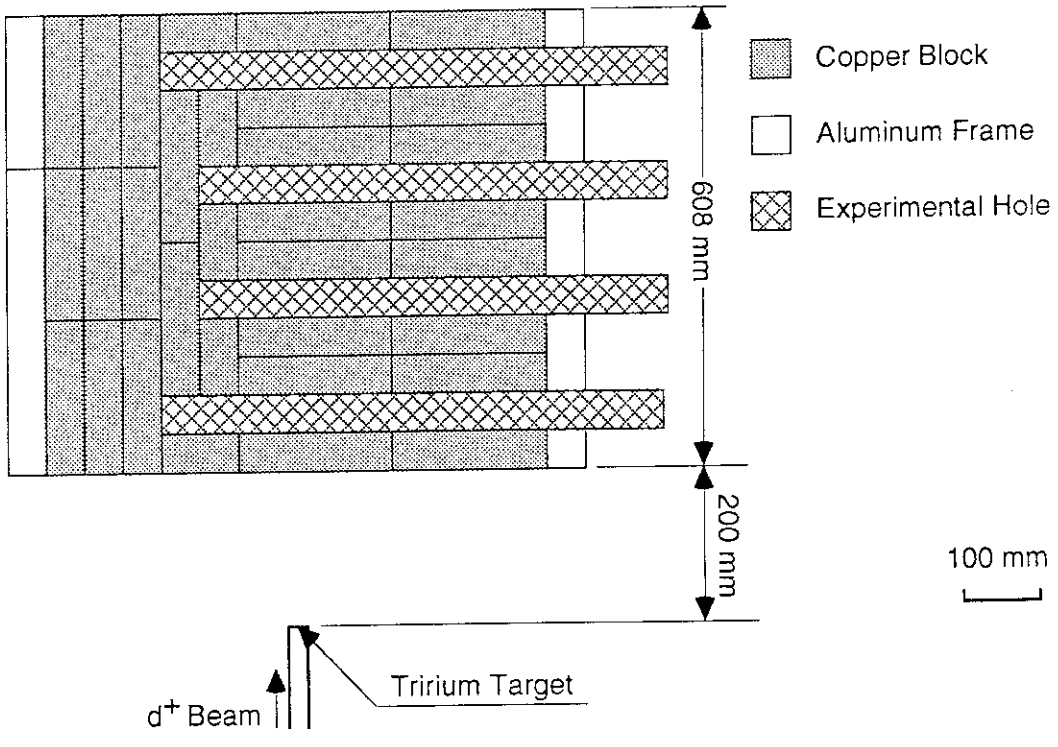

Fig. 2.1.3 Equatorial view of the experimental assembly.

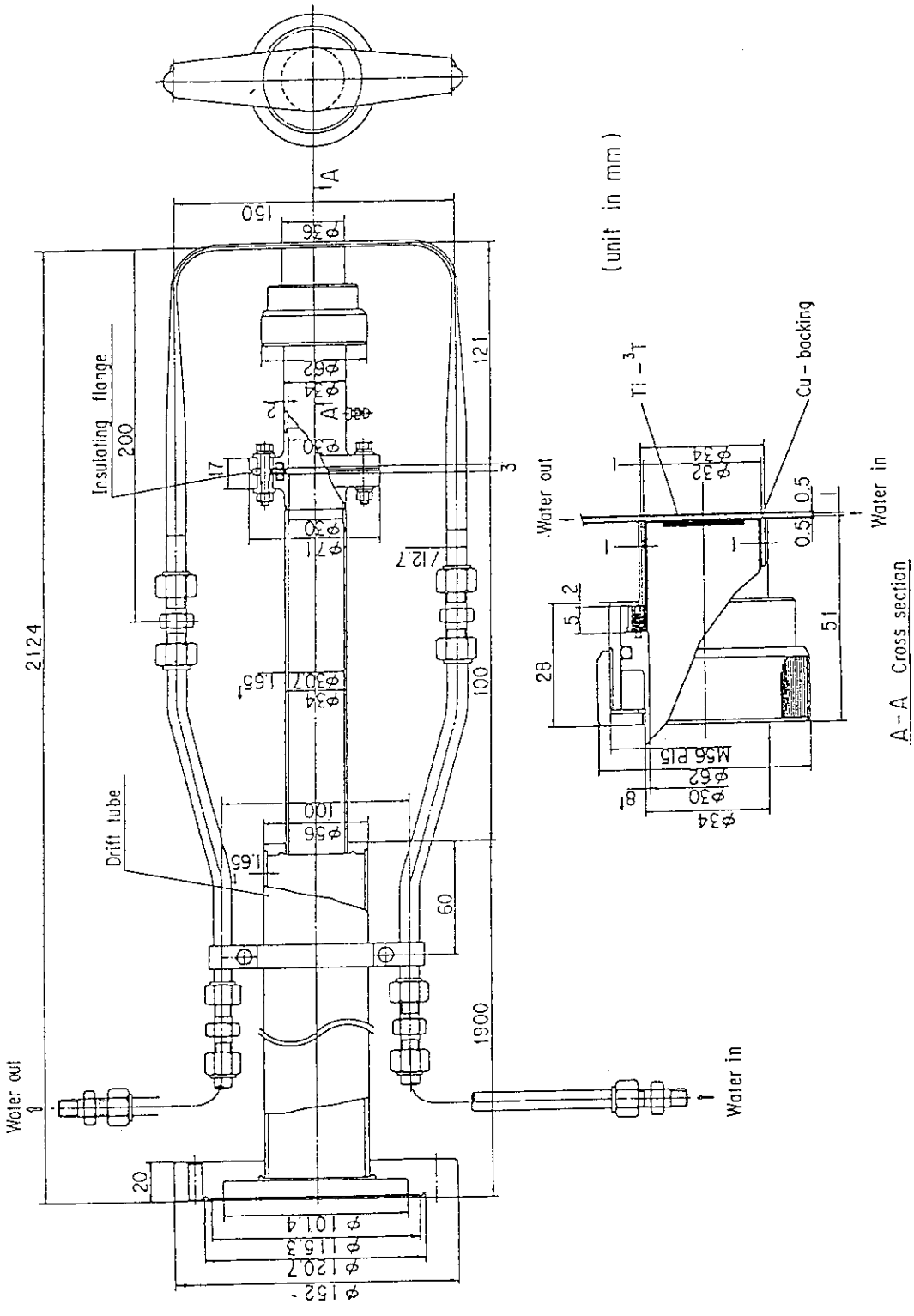

Fig. 2.2.1 Structure of the FNS fast water cooled tritium target for the 80° beam line.

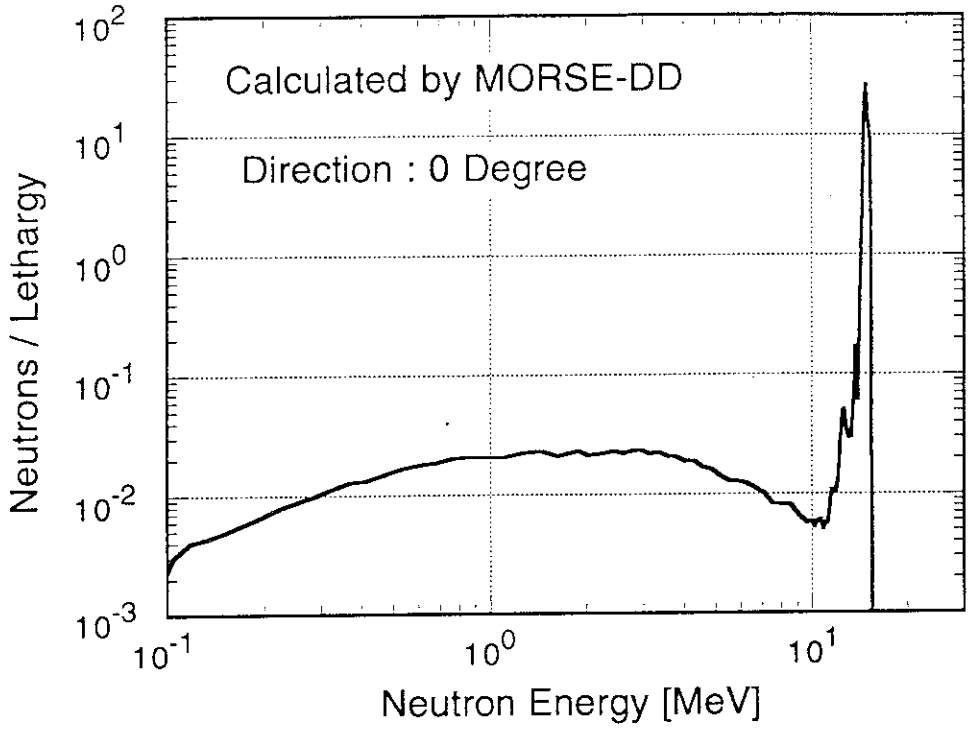

Fig. 2.2.2 Source neutron spectrum of the FNS fast water cooled target calculated with MORSE-DD.

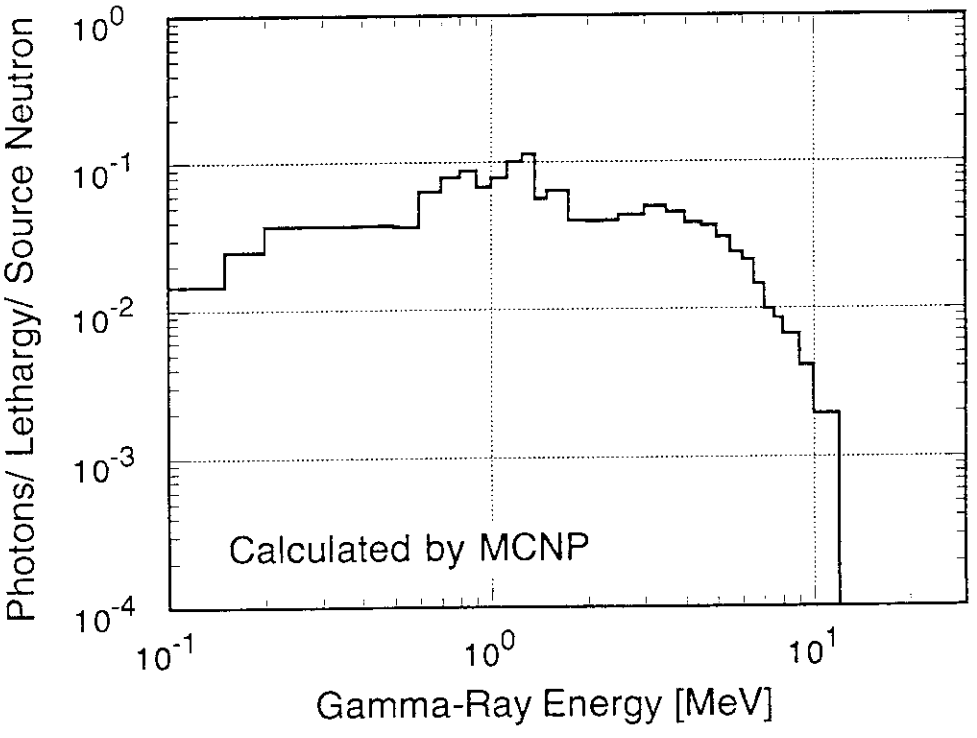

Fig. 2.2.3 Source gamma-ray spectrum of the FNS fast water cooled target calculated with MCNP.

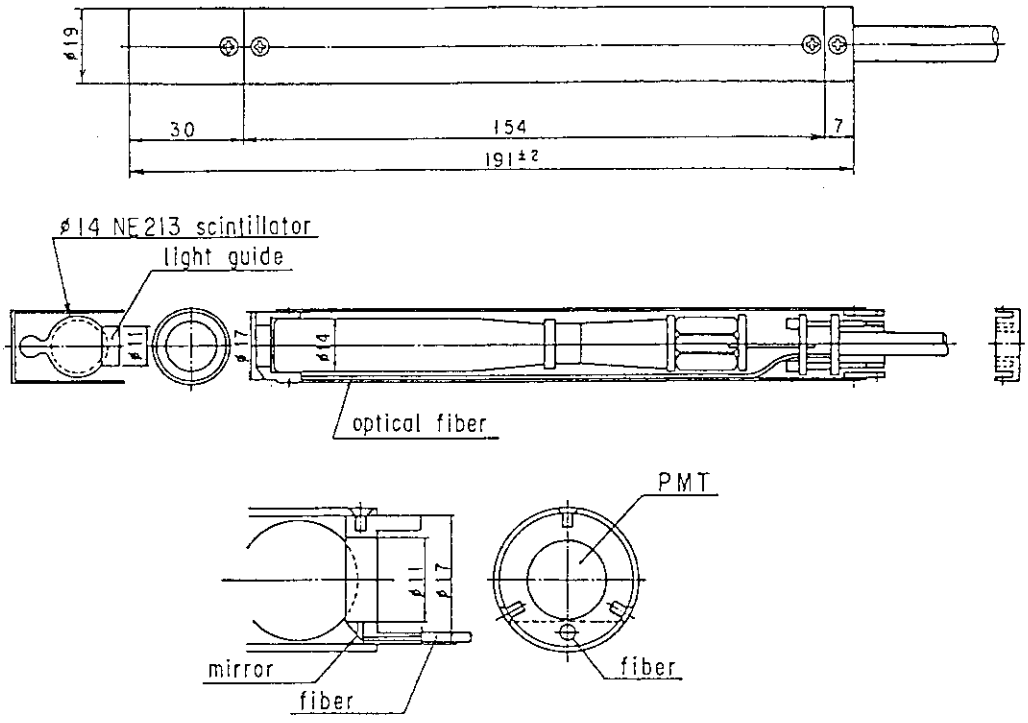

Fig. 3.1.1.1 Sectional view of small sphere NE213 scintillation detector assembly.

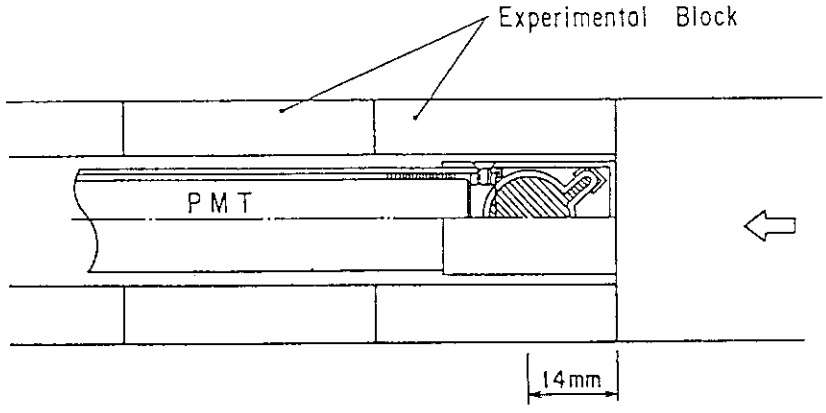

Fig. 3.1.1.2 Arrangement in measurement using the experimental drawer.

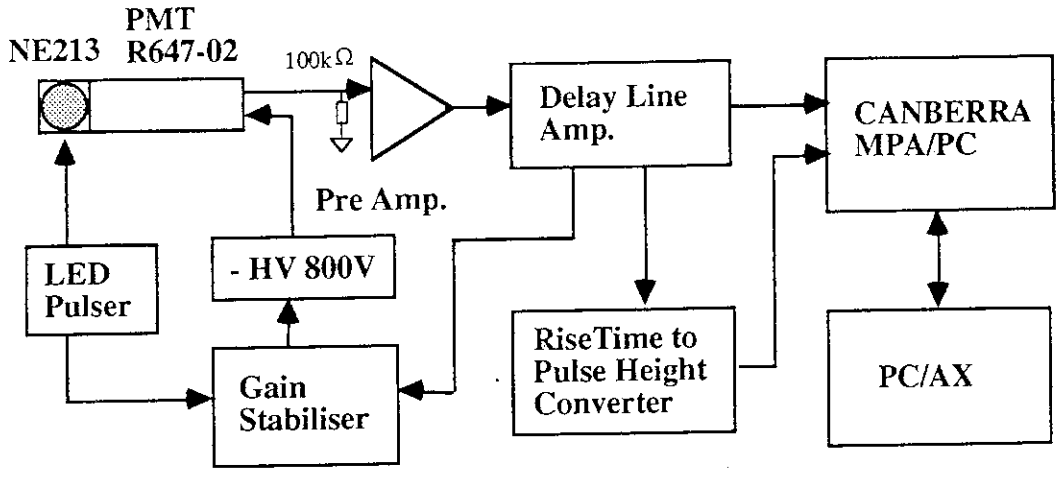

Fig. 3.1.1.3 Schematic diagram of electronic circuit.

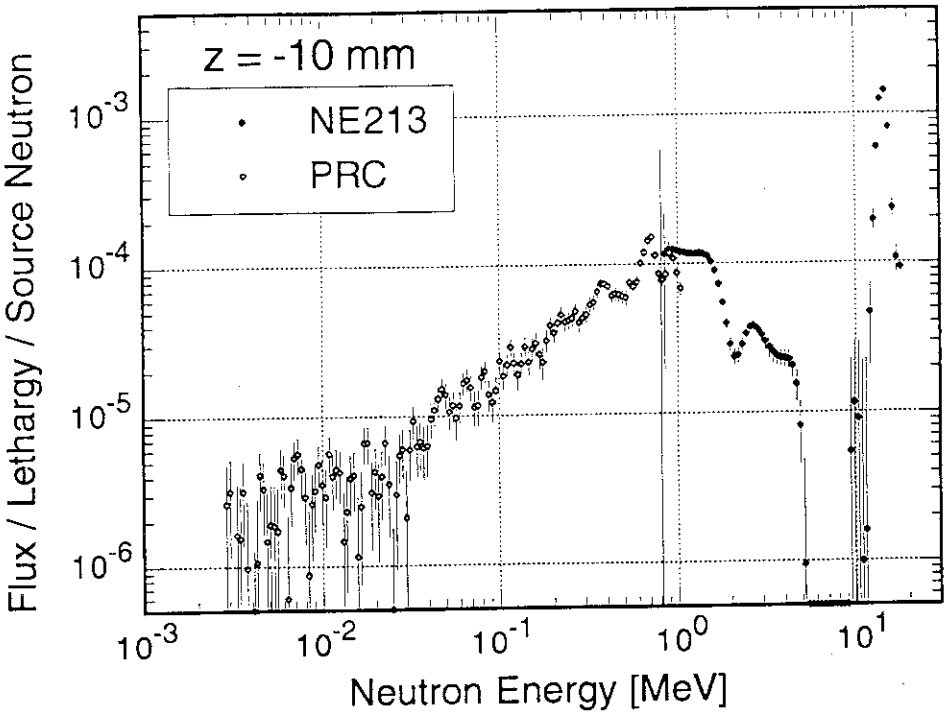

Fig. 3.1.1.4 Neutron spectra at the front surface of the copper assembly measured by NE213 counter and proton-recoil gas proportional counters (PRC) .

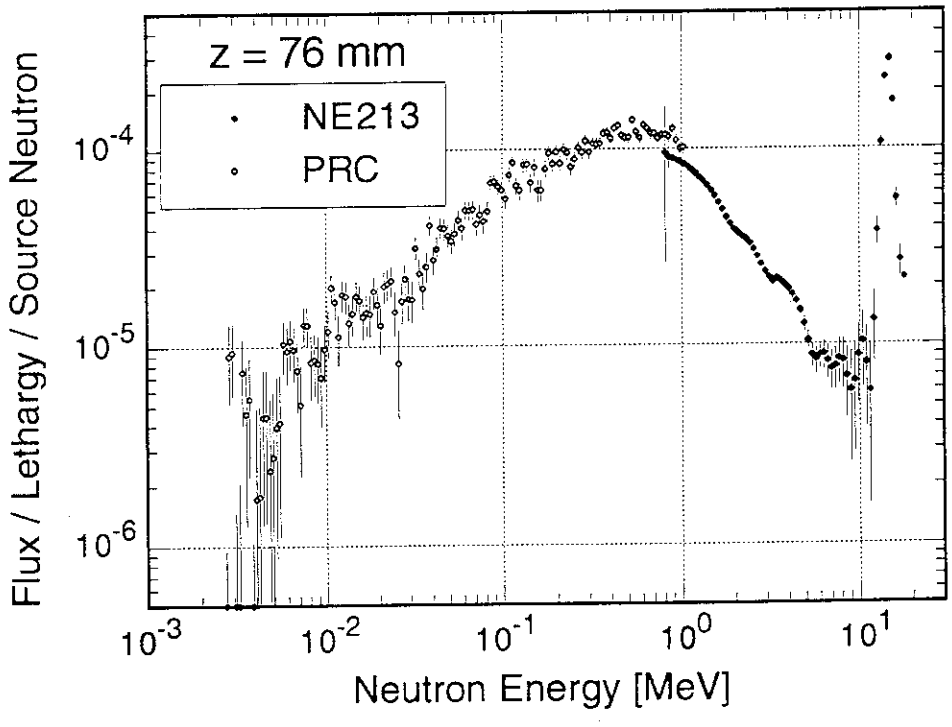

Fig. 3.1.1.5 Neutron spectra at 76 mm depth in the copper assembly measured by NE213 counter and proton-recoil gas proportional counters (PRC) .

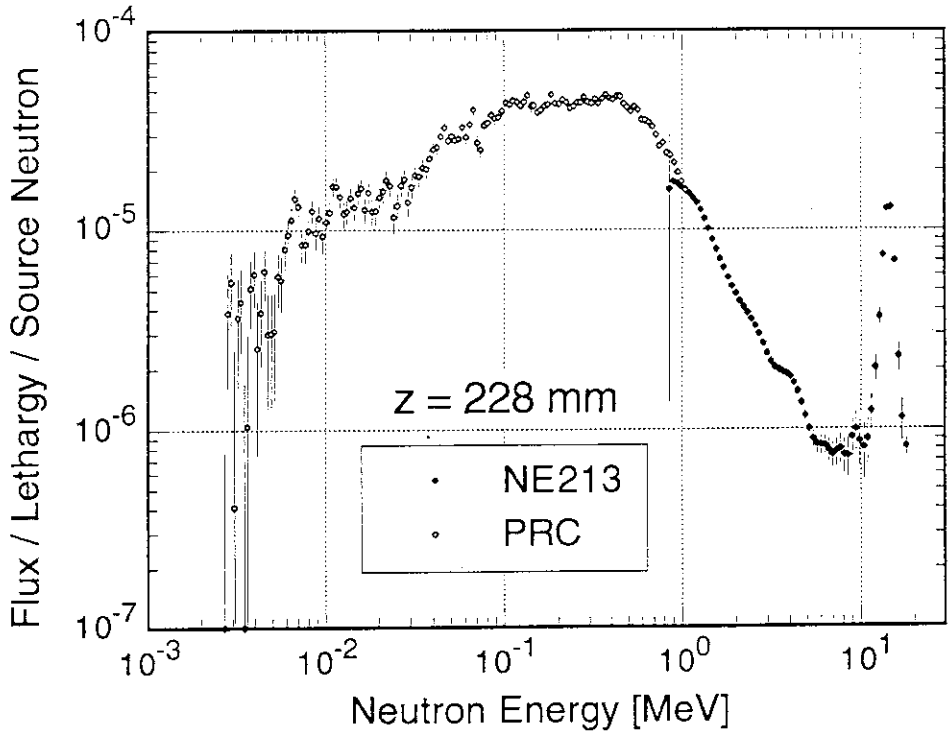

Fig. 3.1.1.6 Neutron spectra at 228 mm depth in the copper assembly measured by NE213 counter and proton-recoil gas proportional counters (PRC) .

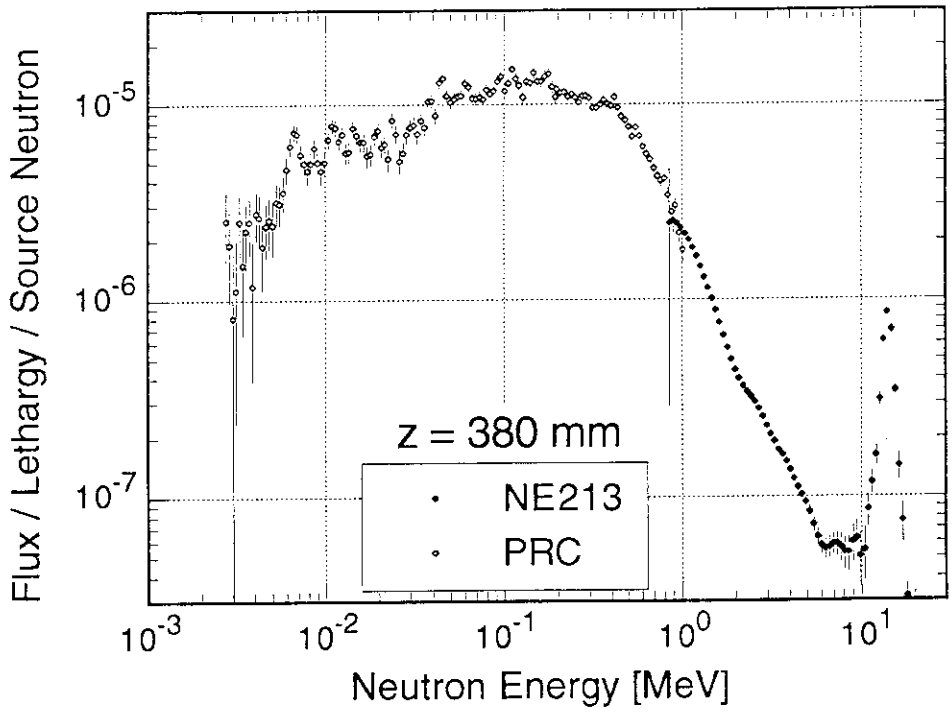

Fig. 3.1.1.7 Neutron spectra at 380 mm depth in the copper assembly measured by NE213 counter and proton-recoil gas proportional counters (PRC) .

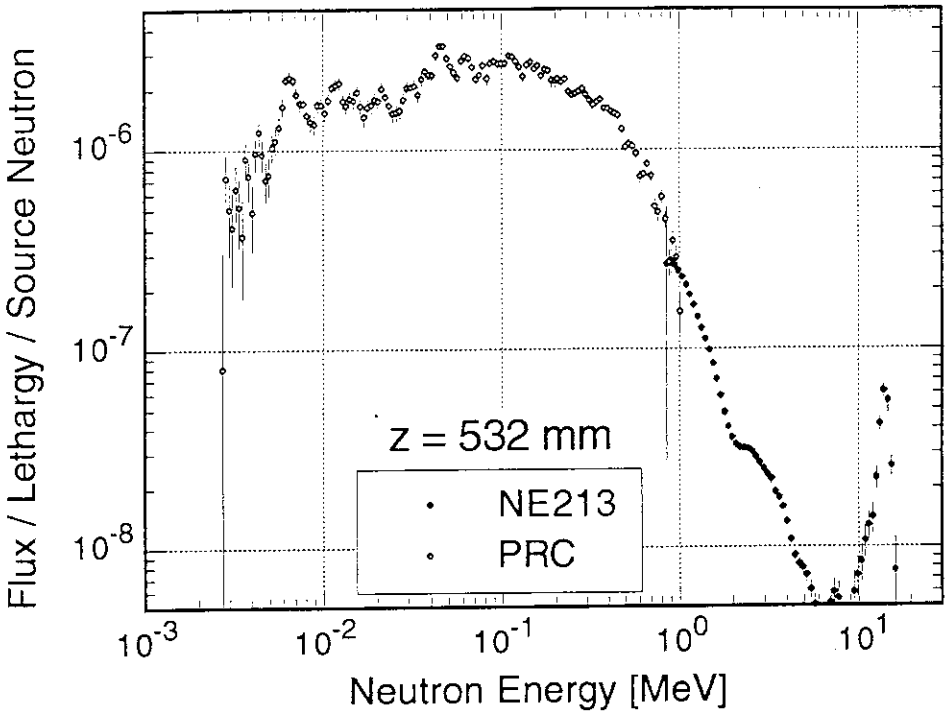

Fig. 3.1.1.8 Neutron spectra at 532 mm depth in the copper assembly measured by NE213 counter and propton-recoil gas proportional counters (PRC) .

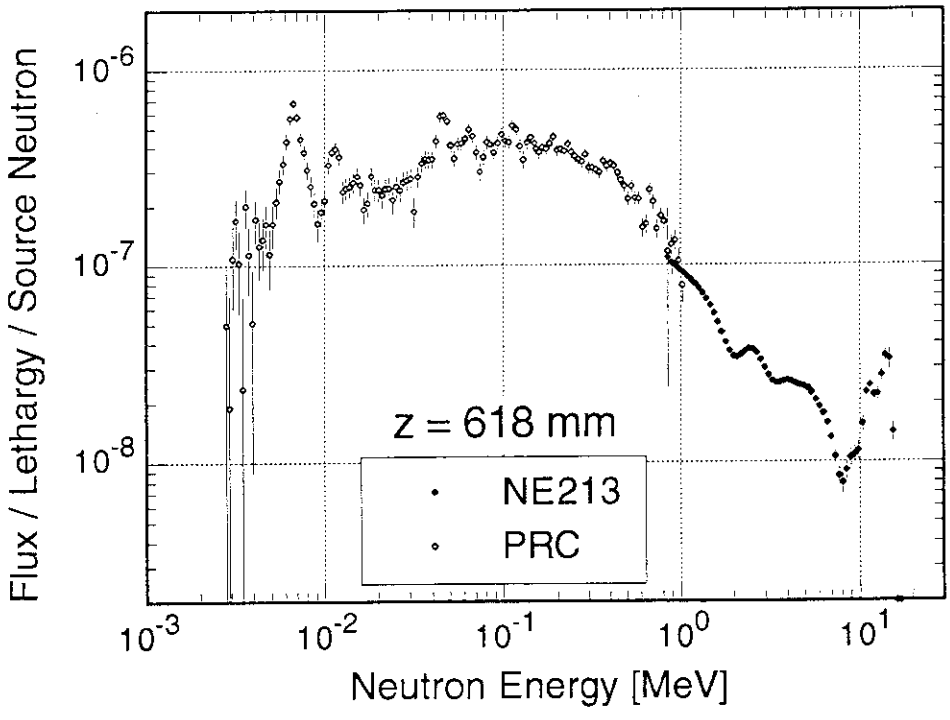

Fig. 3.1.1.9 Neutron spectra at the rear surface of the copper assembly measured by NE213 counter and proton-recoil gas proportional counters (PRC) .

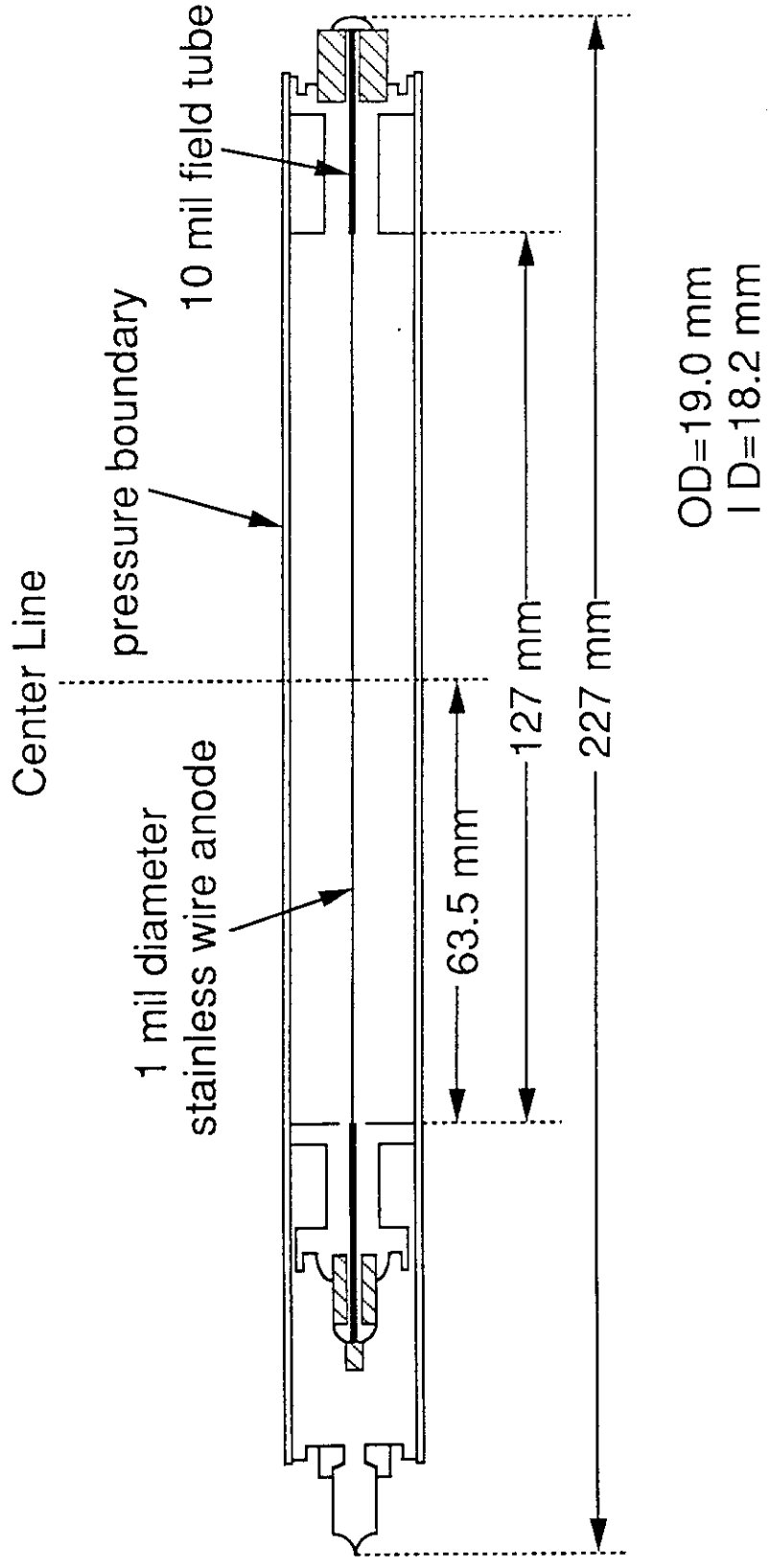

Fig. 3.1.2.1 Sectional view of the proton-recoil gas proportional counters (PRC).

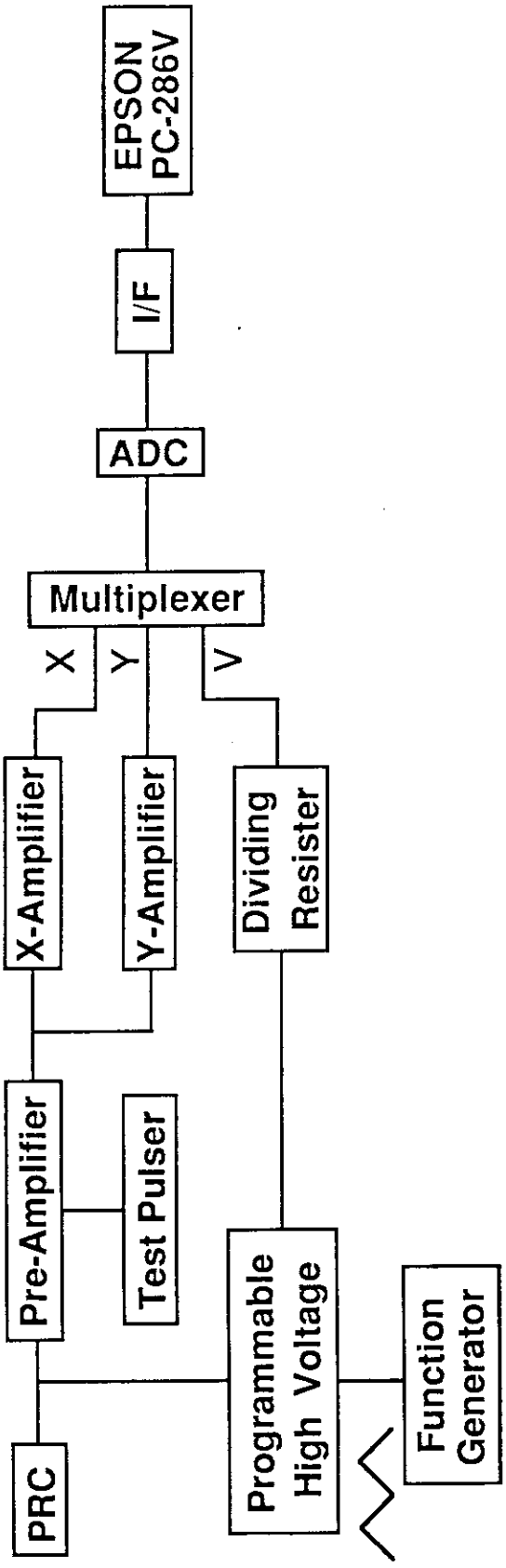

Fig. 3.1.2.2 Block diagram of the data acquisition system.

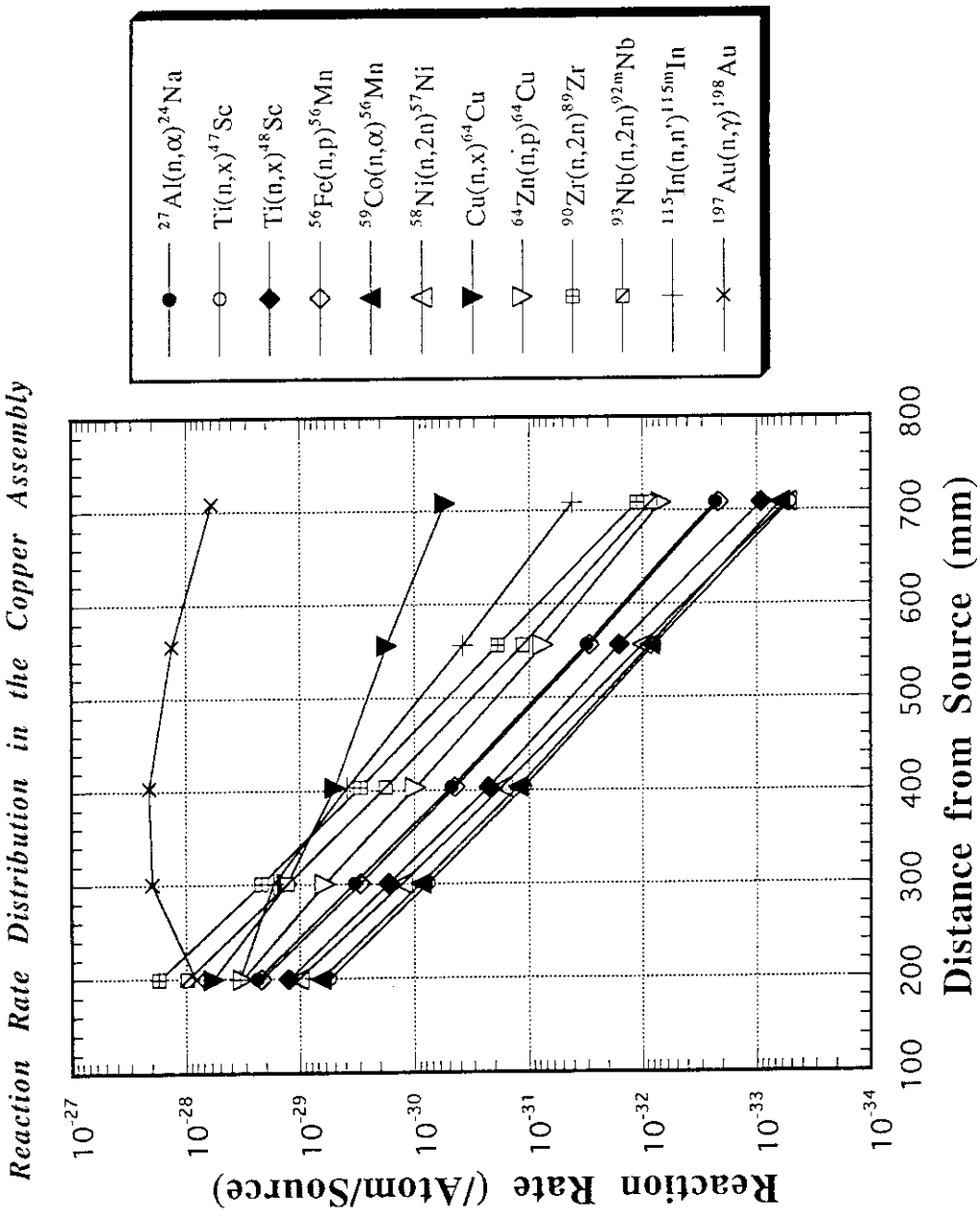

Fig. 3.2.1 Reaction rate distributions in the copper assembly mesured with the foil activation technique.

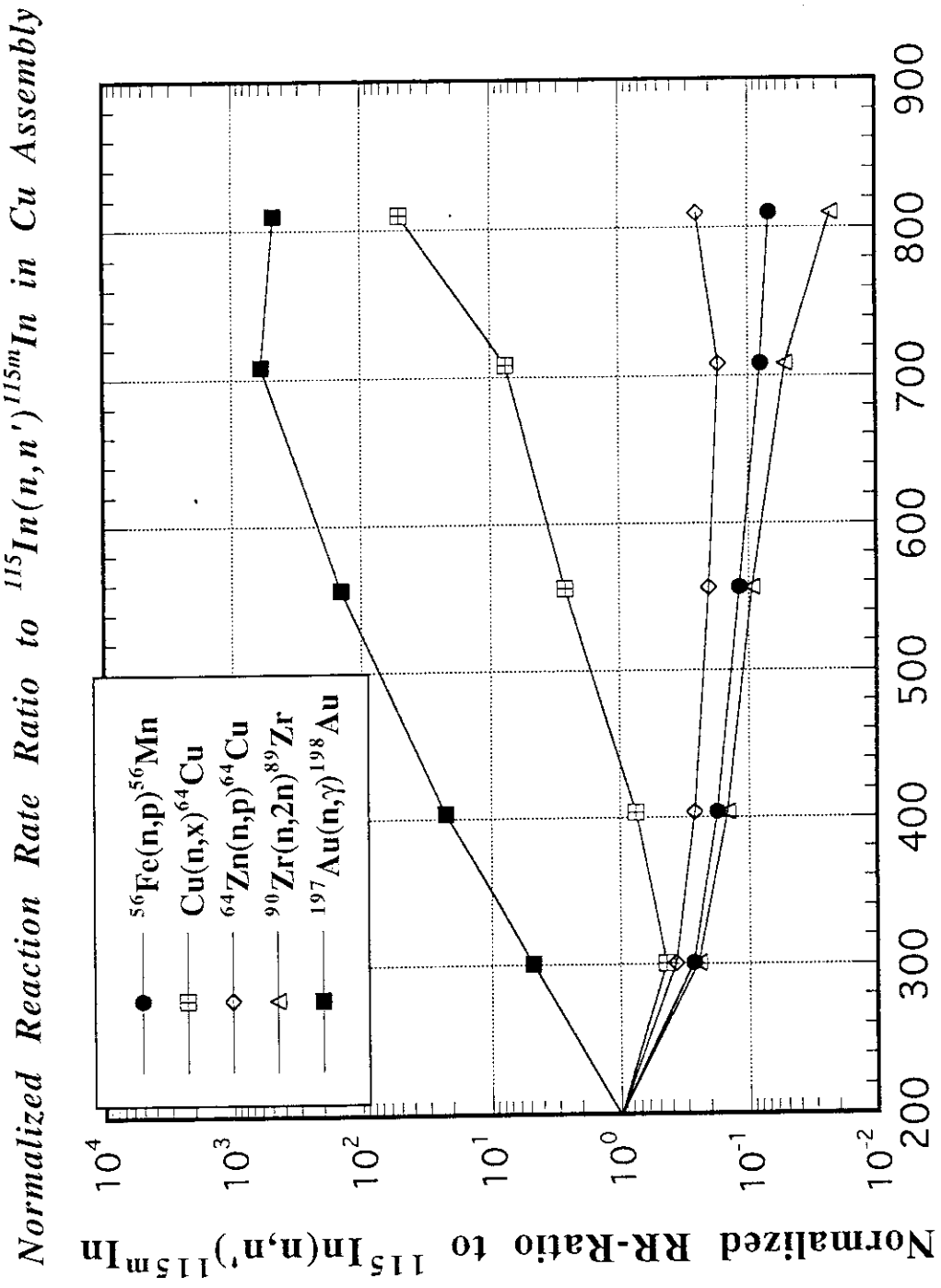

Fig. 3.2.2 Ratios of reaction rate to $^{115}In(n,n')^{115m}In$ reaction. All of the ratios are normalized at the position of the front surface (200 mm from the source) to be unity.

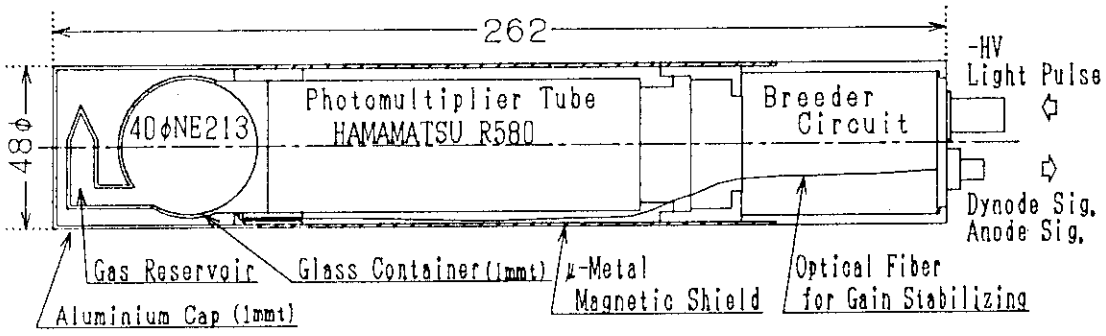

Fig. 3.3.1.1 Sectional view of the 40 mm diameter NE213 gamma-ray spectrometer

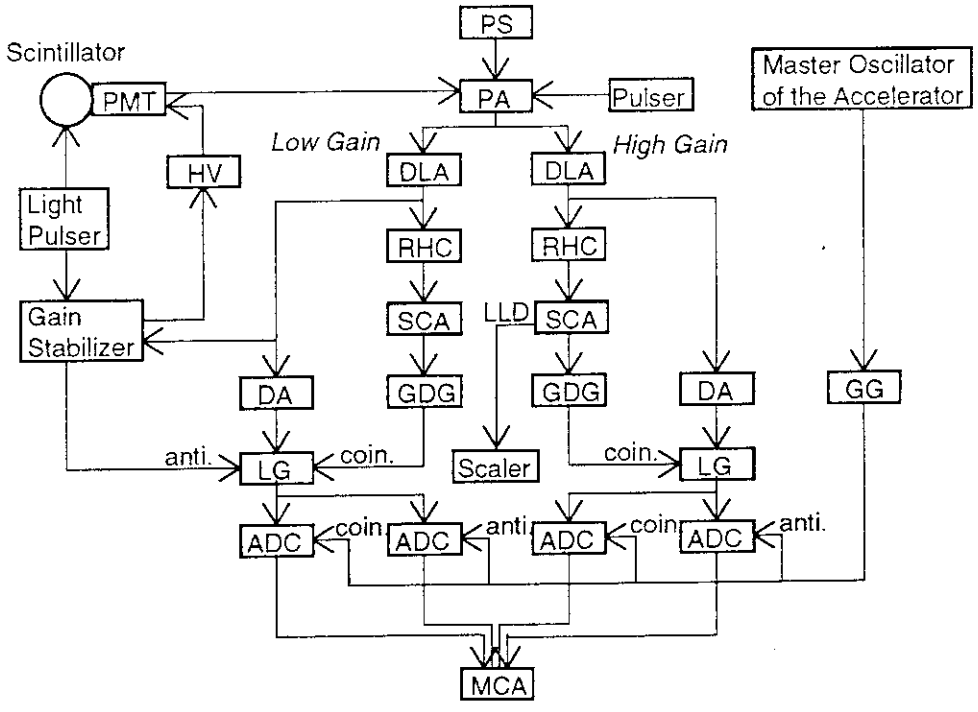

PMT	: Photomultiplier Tube	Hamamatsu	R580
HV	: High Voltage Power Supply	ORTEC	456H
PS	: Power Supply	ORTEC	114
PA	: Preamplifier	ORTEC	113
Pulser	: Research Pulser	ORTEC	448
DLA	: Delay Line Amplifier	ORTEC	460
RHC	: Risetime to Height Convertor	OKEN	723-1
SCA	: Single Channel Analyzer	CANBERRA	2035A
GDG	: Gate & Delay Generator	ORTEC	416A
Scaler	: Timer & Scaler	JAERI	178RA
DA	: Delay Amplifier	CANBERRA	1457
LG	: Linear Gate & Slow Coincidence	OKEN	721-1
GG	: Dual Gate Generator	Le Croy	222
ADC	: Analog to Digital Convertor	CANBERRA	6075
MCA	: Multichannel Analyzer	CANBERRA	MPA/LBB

Fig. 3.3.1.2 Electric circuit used in the prompt gamma-ray spectrum measurement.

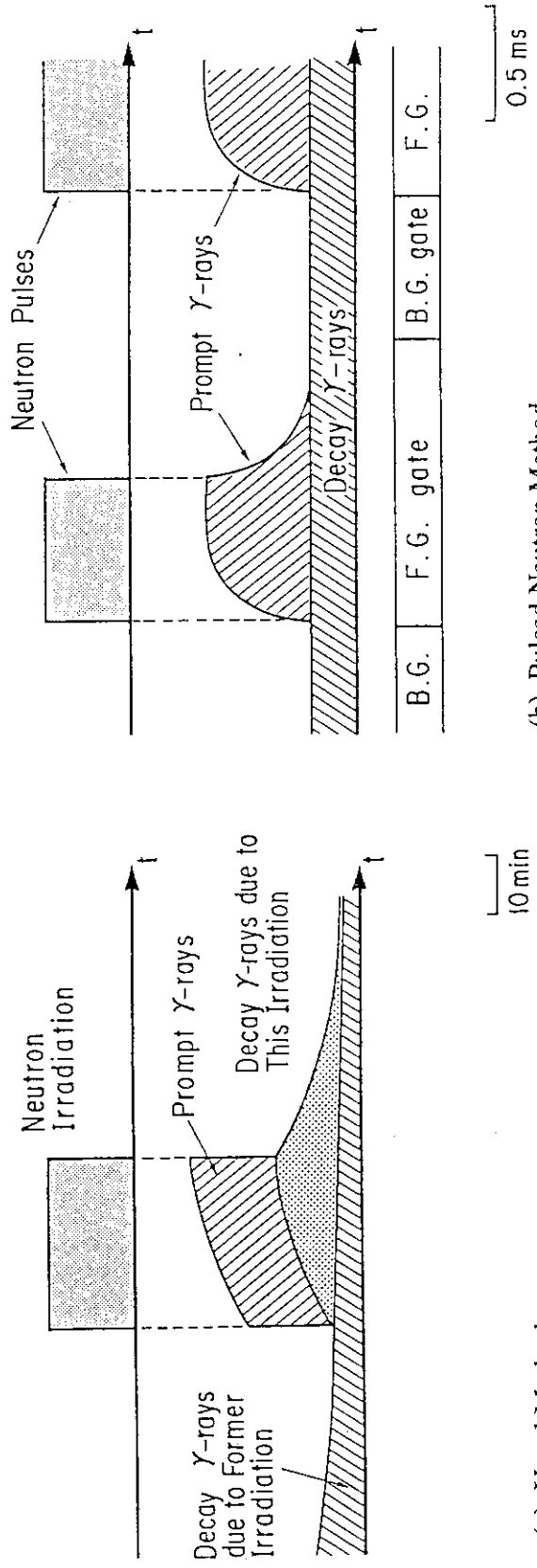

Fig. 3.3.1.3 Figure for explanation of rejection of decay gamma-rays. Amount of decay gamma-rays can not be determined accurately with (a) usual method but with (b) pulsed neutron method.

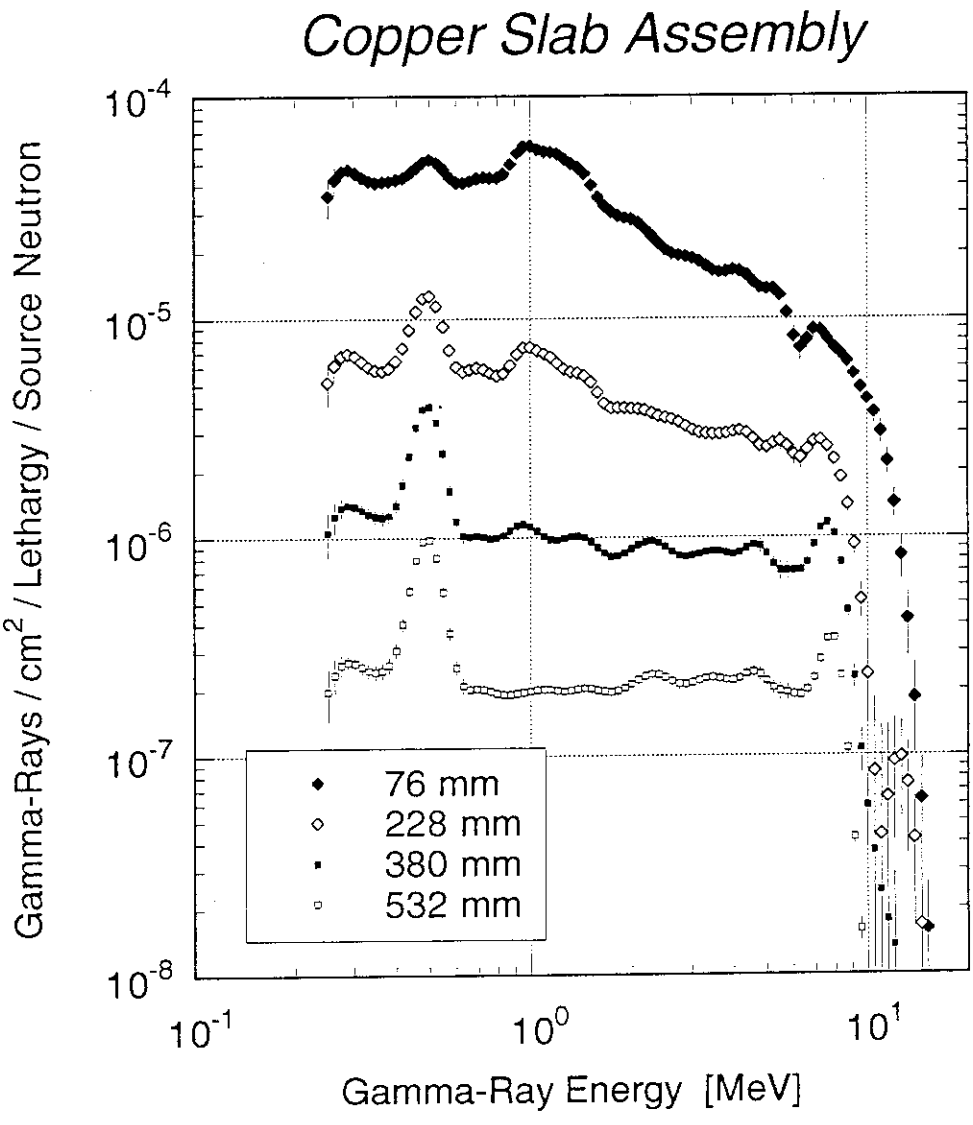

Fig. 3.3.1.4 Prompt gamma-ray spectra at 76, 228, 380 and 532 mm from the front surface of the copper assembly measured by the 40 mm diameter NE213 gamma-ray spectrometer.

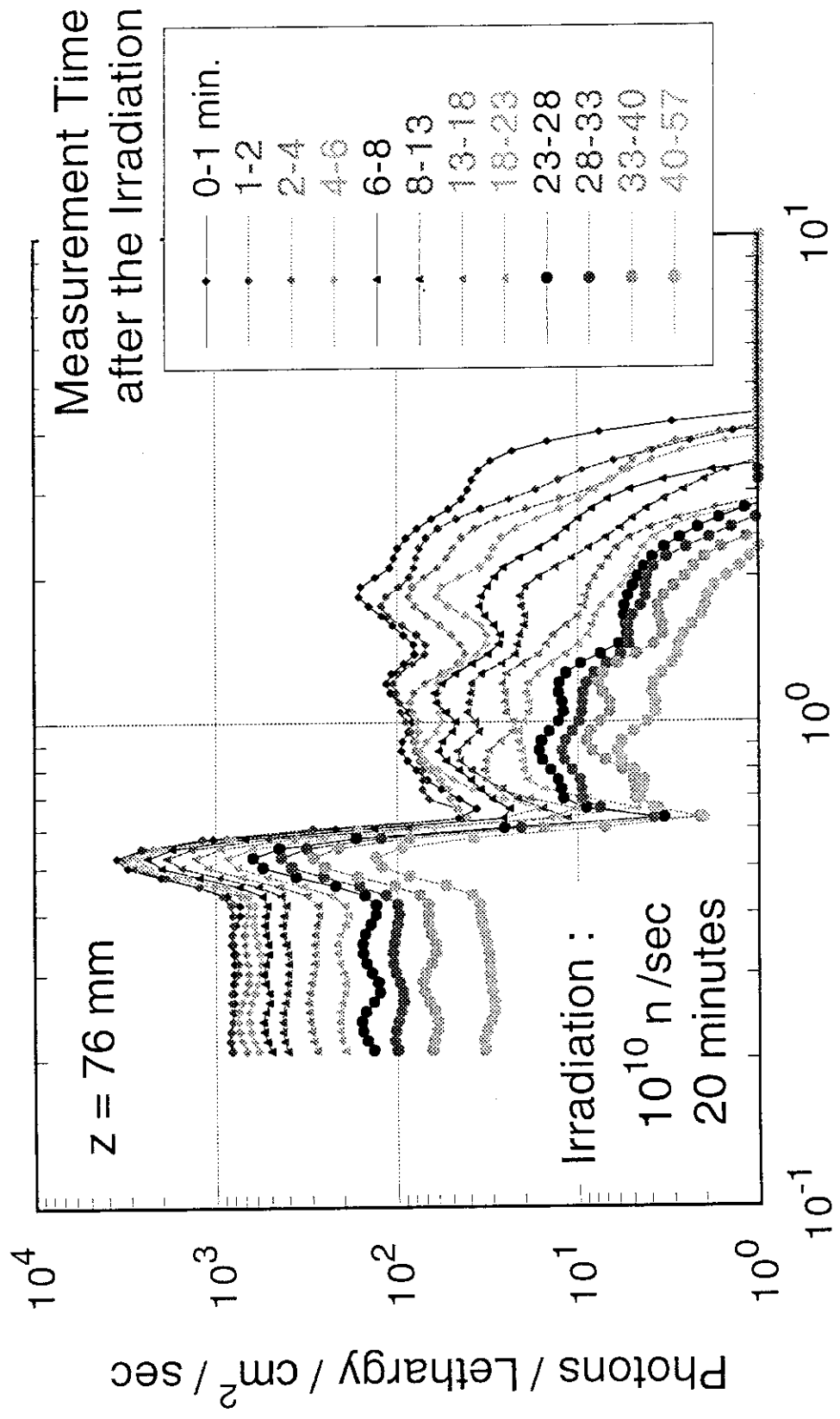

Fig. 3.3.2.1 Decay gamma-ray spectra at 76 mm from the front surface of the copper assembly. The spectra were measured as a function of cooling time after stop of the irradiation of neutron generation rate of 10^{10} n／sec for 20 minutes.

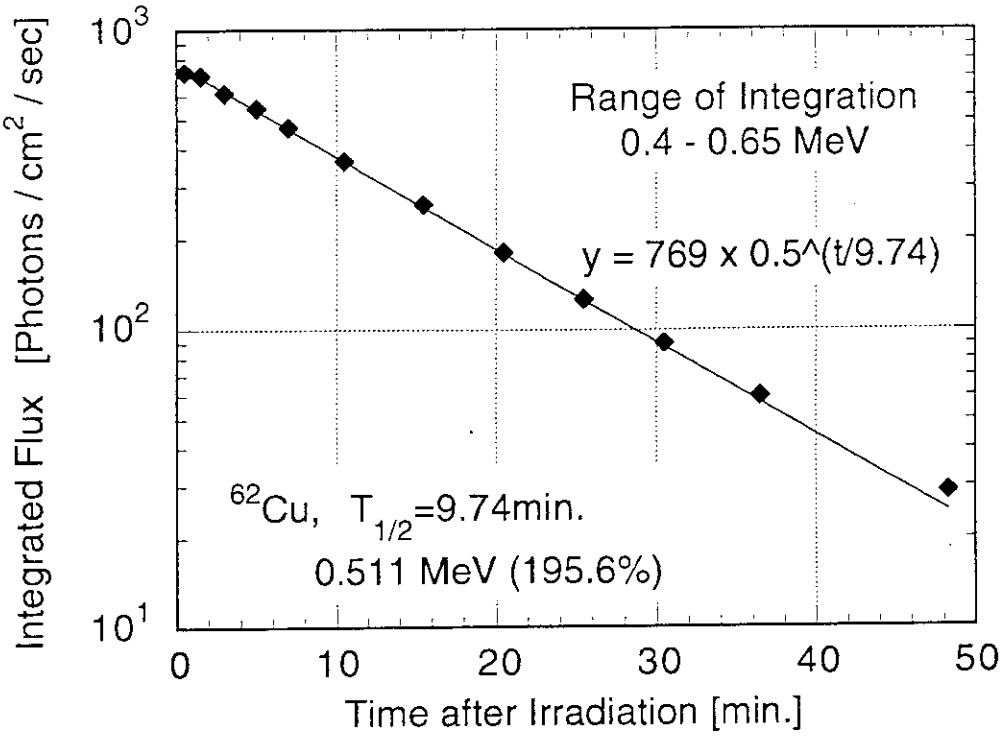

Fig. 3.3.2.2 Integrated decay gamma-ray spectra between 0.4 and 0.65 MeV as a function of cooling time.

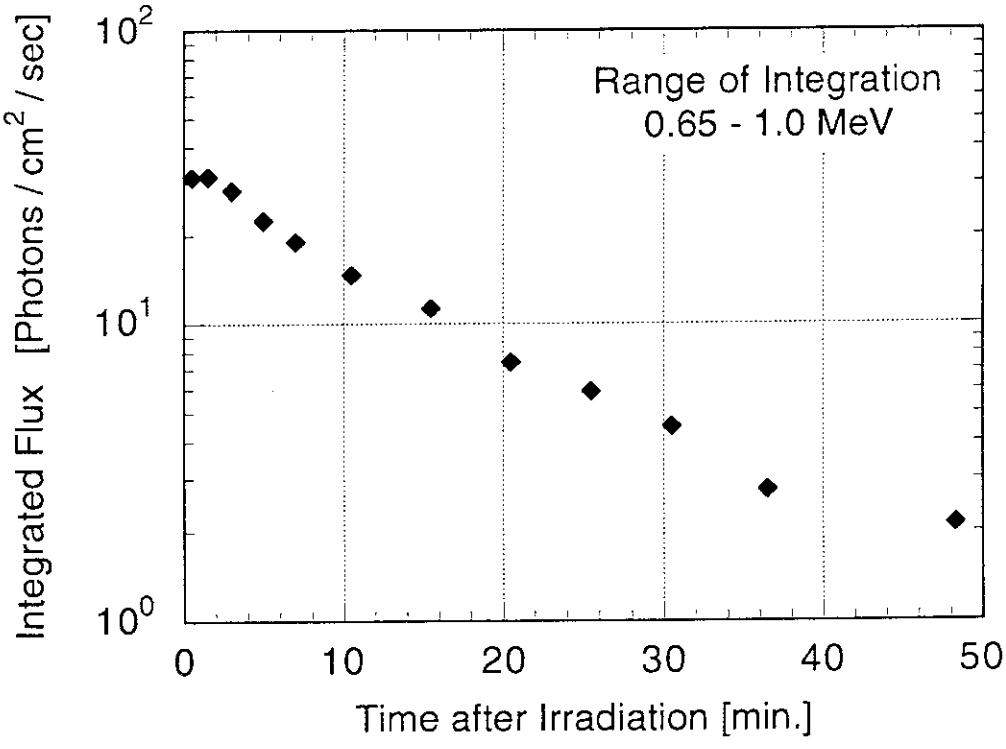

Fig. 3.3.2.3 Integrated decay gamma-ray spectra between 0.65 and 1.0 MeV as a function of cooling time.

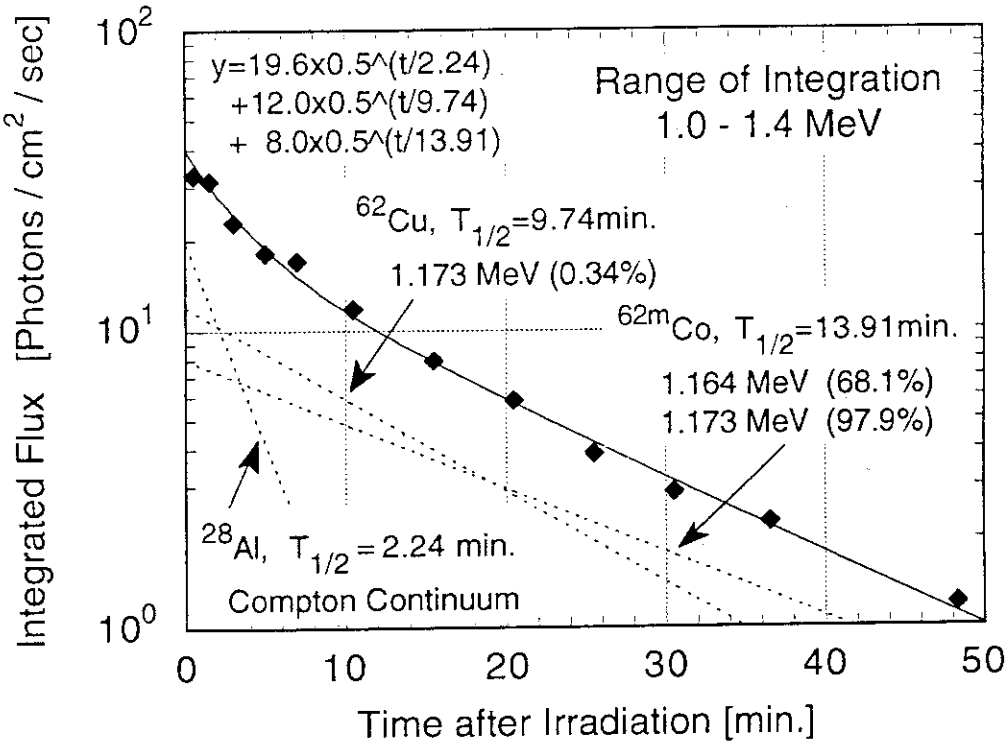

Fig. 3.3.2.4 Integrated decay gamma-ray spectra between 1.0 and 1.4 MeV as a function of cooling time.

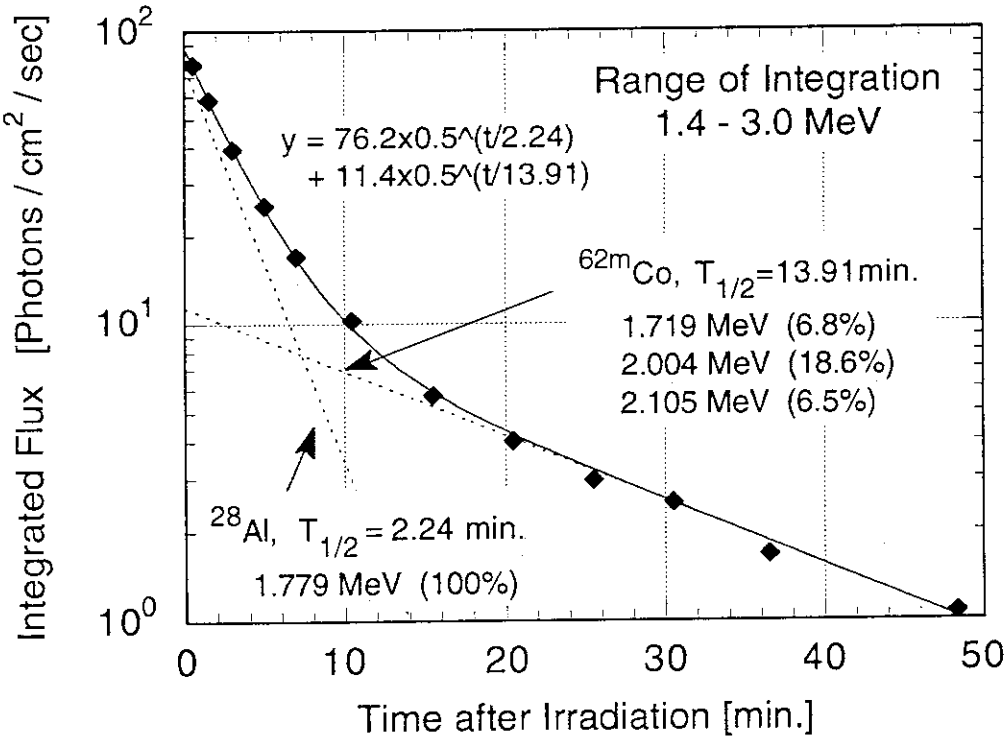

Fig. 3.3.2.5 Integrated decay gamma-ray spectra between 1.4 and 3.0 MeV as a function of cooling time.

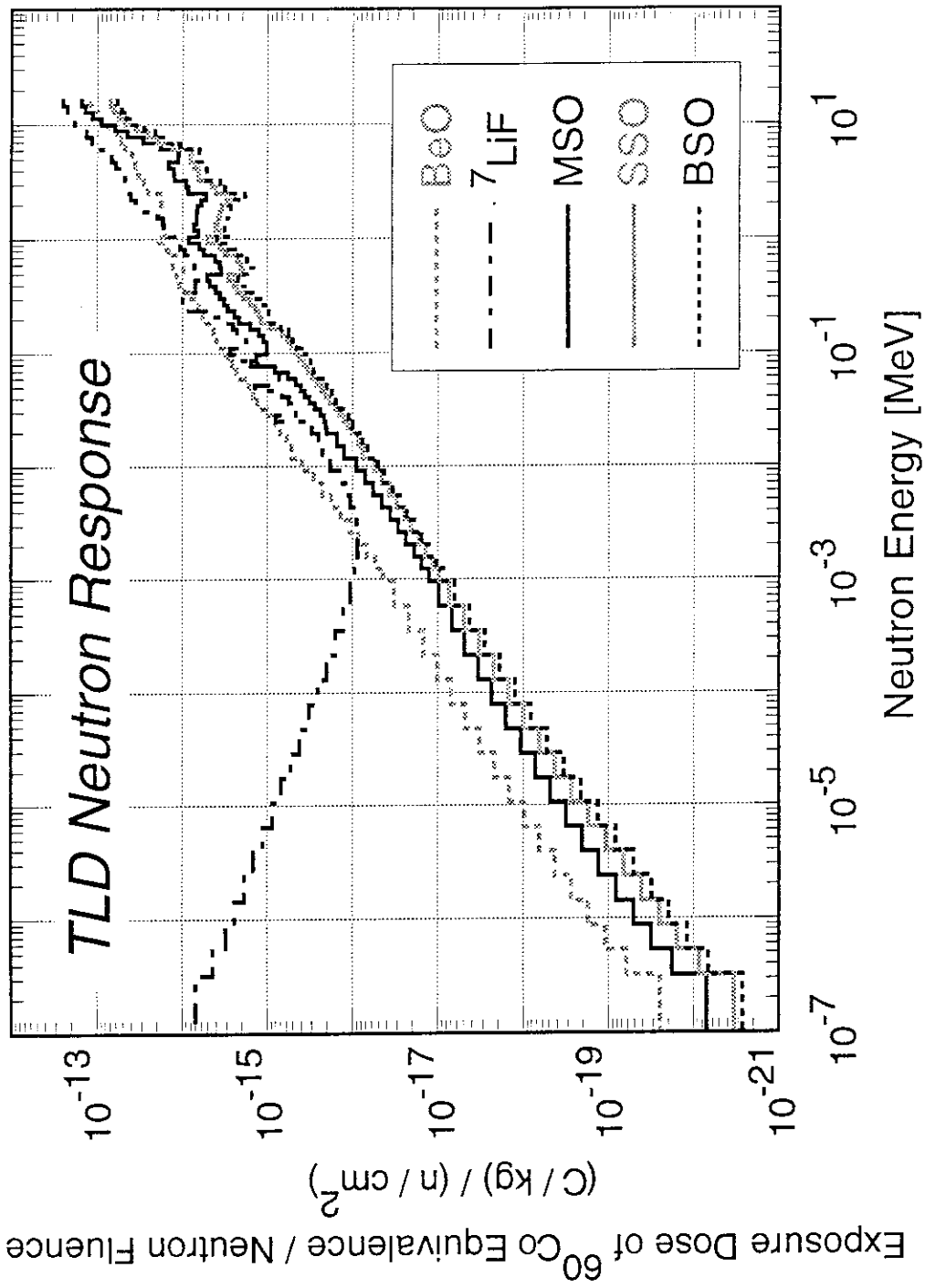

Fig. 3.4.1 Energy dependent neutron responses of five kinds of TLDs; BeO, ^{7}LiF, Mg_2SiO_4 (MSO), Sr_2SiO_4 (SSO) and Ba_2SiO_4 (BSO).

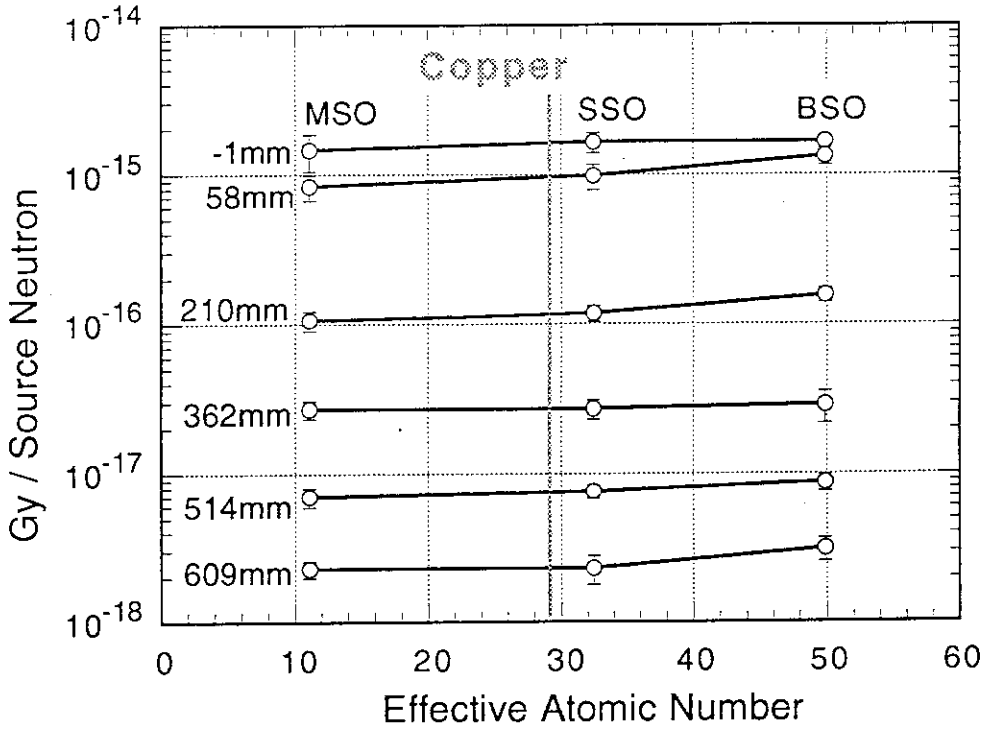

Fig. 3.4.2 Figure for explanation of derivation of gamma-ray heating rates of copper by interpolation.

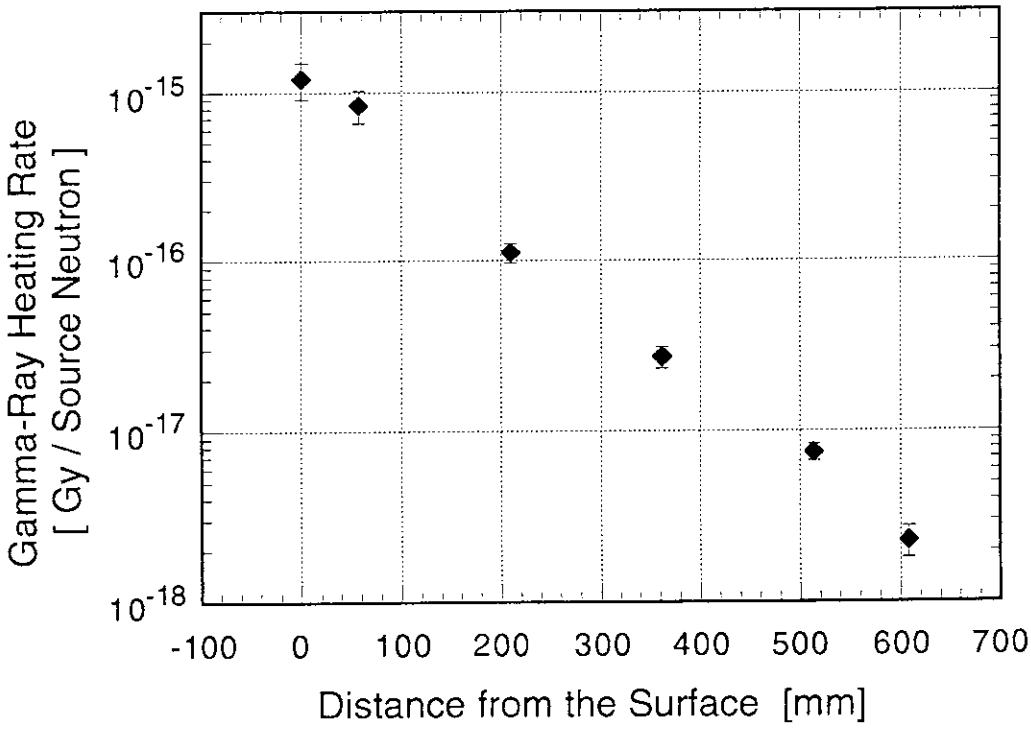

Fig. 3.4.3 Measured gamma-ray heating rates of copper in the copper assembly.

Appendix Example of Experimental Analysis

Since the experimental assembly has a cylindrical shape, the benchmark experiment can be analyzed by using two-dimensional SN transport codes and, of course, three-dimensional Monte Carlo codes. Two examples of input data for transport calculations, DOT and MCNP-4, are presented in the Appendix.

An example of input data of GRTUNCL for DOT calculation is shown in Fig. A.1. The GRTUNCL code calculate first collision sources to prevent the Ray-Effect. Figure A.2 is an input data for DOT calculation. Since some of measured data, that is, neutron spectra in the energy region of keV, non-threshold reaction rates, prompt gamma-ray spectra and gamma-ray heating rates, are influenced by the self-shielding effect of cross sections, multi-group cross section libraries in which self-shielding correction factors are considered should be used in analyses.

An input data for MCNP-4 calculation with neutron source is given in Fig. A.3. Since target gamma-rays are included in the measured prompt gamma-ray spectra, a calculation with target gamma-ray source is needed. Figure A.4 is an input data with target gamma-ray source.

```
FNS-GRTUNCL  Copper Slab Assembly  -- with JSSTDL Library
'  Run #4  Source MORSE(n) & MCNP(Gamma)
 O
1$$
          0          5          2         41         81        165
          4          5        169         18          0         42
         42          2          1      30000         10          0
          1          0         18          0          0          0
          1          1          1          0
2**
  0.0        0.0        0.0        0.0        0.0
 T
1**
 F0.0
2**
 1I0.0      6I2.0        16.0        17.0      3I18.0      5I20.0

54I23.0       78.0       78.8      1I79.4       80.4       80.84
3**
'         NWCT 125-Group Neutron Source   by MORSE-DD
   0.0          0.0          0.0          0.0          1.4419-01    2.2296-01
   4.0901-01    2.3565-01    3.0897-02    5.1474-03    9.5007-04    2.6083-03
   9.1020-04    4.6458-04    4.5938-04    5.1771-04    7.8183-04    7.4899-04
   4.1363-04    2.1025-04    1.6563-04    1.5985-04    1.6798-04    1.1227-04
   8.7841-05    8.8737-05    7.9567-05    9.3708-05    9.1407-05    9.2862-05
   8.2287-05    9.0768-05    3.5649-04    4.1280-04    5.1007-04    5.0750-04
   5.1710-04    6.2956-04    6.9228-04    7.5872-04    7.9293-04    7.9827-04
   8.8451-04    1.0018-03    1.0563-03    1.1937-03    1.1711-03    1.2741-03
   1.2861-03    1.4053-03    1.3518-03    1.4558-03    1.4329-03    1.3760-03
   1.4312-03    1.3820-03    1.3489-03    1.3270-03    1.4298-03    1.3898-03
   2.5945-03    2.8528-03    2.7699-03    2.5765-03    2.5872-03    2.5709-03
   2.5211-03    2.3040-03    2.2042-03    2.0605-03    1.8238-03    1.6473-03
   1.5803-03    1.3867-03    1.2232-03    1.0785-03    9.5392-04    8.0965-04
   7.0593-04    6.0762-04    5.3824-04    4.9933-04    3.7225-04    1.7906-04
   1.4874-04    1.2632-04    1.0531-04    9.7450-05    8.3190-05    8.0602-05
   6.9230-05    5.7202-05    5.0292-05    4.8831-05    5.3362-05    3.7185-05
   6.1572-05    4.6320-05    4.4237-05    3.7633-05    2.4899-05    2.8404-05
   1.7624-05    1.4791-05    1.6544-05    1.1820-05    1.4320-05    7.8013-06
   8.7622-06    7.2049-06    6.9372-06    2.2612-06    3.0541-06    3.8068-06
   2.9754-07    1.6817-07    1.3922-07    2.2450-07    1.8398-07    8.3975-08
   1.4264-08    7.4848-09    4.2225-09    2.2732-09    1.5142-07
         NWCT 40-Group Gamma-Ray Source   by MCNP
  0.0          1.8633E-04   2.4781E-04   2.6304E-04   1.0130E-03   9.4278E-04
  1.2635E-03   1.5887E-03   2.2136E-03   2.6026E-03   3.3959E-03   4.2346E-03
  5.0603E-03   6.1991E-03   6.8837E-03   3.0169E-03   5.4347E-03   5.5820E-03
  9.1277E-03   2.9512E-03   1.0412E-02   1.0790E-02   7.3978E-03   5.8107E-03
  6.8849E-03   8.5792E-03   6.3378E-03   2.4076E-03   2.8815E-03   5.9451E-03
  8.5598E-03   1.2291E-02   5.8376E-03   4.5651E-03   1.3289E-03   9.3110E-04
  1.9365E-04   2.8764E-04   5.0781E-05   0.0
4**
  0.0       3I0.2       2I1.4       2I2.9       22I5.0       1I28.0
2I29.4      1I30.9       31.5
6**
 1.0
7**
 1.0
8$$
  41R1       14Q41
  41R2       65Q41
9$$
  -13        -19
10$$
     4I13          18
     4I19          24         1Q6
11$$
 6Z
 6Z     4I7     12
12**
 6R0.0
 6R0.0        6R8.4627E-2
  T
```

Fig. A.1 An example of input data of GRTUNCL for DOT calculation.

```
FNS-DOT3.5  Copper Slab Assembly  -- with JSSTDL Library
'  Run #4  Source MORSE(n) & MCNP(Gamma)
  O
61$$
           0           5           2          41          81         165
           4           5         169          18           0           0
          42           1         160           1           1           0
           0           0           1          10          15           4
           6           2           0           0           0           0
           0           0           0           0           0           0
           0           0           0           0           3           0
           0           0           0           0           0           0
           0           0           2           1           1           0
           0           0           0           0           0           8
           0
62$$
           2           3           4          14          15           9
          10          11          12          13           8          60
           0           0
63**
   0.0          1.000E-02   0.0          0.0          0.0          0.0
   0.0          0.0         0.0          0.0          0.0          0.0
   0.0          0.0         0.0          0.0          0.0          0.0
  T
 7**
   -0.21082     -0.14907  1M1
   -0.42164     -0.39441     -0.14907  1M2
   -0.55777     -0.53748     -0.39441     -0.14907  1M3
   -0.66667     -0.64979     -0.53748     -0.39441     -0.14907  1M4
   -0.76012     -0.74536     -0.64979     -0.53748     -0.39441     -0.14907
 1M5
   -0.84327     -0.82999     -0.74536     -0.64979     -0.53748     -0.39441
   -0.14907  1M6
   -0.91894     -0.90676     -0.82999     -0.74536     -0.64979     -0.53748
   -0.39441     -0.14907  1M7
   -0.98883     -0.97753     -0.90676     -0.82999     -0.74536     -0.64979
   -0.53748     -0.39441     -0.14907  1M8
 1Q80
 3R-0.97753  5R-0.90676  7R-0.82999  9R-0.74536 11R-0.64979  13R-0.53748
15R-0.39441 17R-0.14907  3R0.97753   5R0.90676   7R0.82999   9R0.74536
11R0.64979  13R0.53748  15R0.39441  17R0.14907
  T
 6**
   0.0          2R0.13586-1                 0.0          4R0.97681-2
   0.0            0.64738-2   0.50390-2    0.64738-2 1N3
   0.0            0.64634-2 2R0.71124-2    0.64634-2 1N4
   0.0            0.64634-2   0.14381-2    0.36342-2    0.14381-2    0.64634-2
                1N5
   0.0            0.64738-2   0.71124-2    0.36342-2 1N3          1Q6
   0.0            0.97681-2   0.50390-2    0.71124-2    0.14381-2    0.71124-2
                  0.50390-2   0.97681-2 1N7
   0.0            0.13586-1   0.97681-2 2R0.64738-2 1N4          1Q8   1Q80
  T
 3**
  F0.0
  T
 1**
  F0.0
 2**
  1I0.0        6I2.0          16.0          17.0        3I18.0        5I20.0
 54I23.0         78.0          78.8        1I79.4          80.4          80.84
 4**
   0.0         3I0.2         2I1.4         2I2.9        22I5.0        1I28.0
 2I29.4        1I30.9         31.5
 5**
  F1.0
 8$$
   41R1        14Q41
   41R2        65Q41
 9$$
   -13         -19
10$$
      4I13          18
      4I19          24          1Q6
11$$
 6Z
 6Z      4I7    12
12**
 6R0.0
 6R0.0         6R8.4627E-2
  T
```

Fig. A.2 An example of input data for DOT calculation.

```
analysis of cylindrical copper assembly (63 diam. x 61 thick) 1993.12.6
c    ************************************
c    *   cell card                        *
c    ************************************
 1    2   4.9210-5    1   -2  -22
 2    2   4.9210-5    2   -3  -22
 3    1   8.4627-2    3   -4  -22
 4    1   8.4627-2    4   -5  -22
 5    1   8.4627-2    5   -6  -22
 6    1   8.4627-2    6   -7  -22
 7    1   8.4627-2    7   -8  -22
 8    1   8.4627-2    8   -9  -22
 9    1   8.4627-2    9  -10  -22
10    1   8.4627-2   10  -11  -22
11    1   8.4627-2   11  -12  -22
12    1   8.4627-2   12  -13  -22
13    1   8.4627-2   13  -14  -22
14    1   8.4627-2   14  -15  -22
15    1   8.4627-2   15  -16  -22
16    1   8.4627-2   16  -17  -22
17    1   8.4627-2   17  -18  -22
18    1   8.4627-2   18  -19  -22
19    2   4.9210-5   19  -20  -22
20    0              -1 : 20 : 22
c    ******* blank delimiter *******

c    ************************************
c    * surface card                     *
c    ************************************
c    ------------------------------< surfaces normal to z-axis >--
 1     pz   -21.00
 2     pz    -1.00      $ n & gamma spectrum
 3     pz     0.00      $ foil & tld
 4     pz     5.77      $ tld
 5     pz     7.605     $ n & gamma spectrum
 6     pz    10.11      $ foil
 7     pz    15.00      $ change cell importance
 8     pz    20.37      $ foil
 9     pz    20.98      $ tld
10     pz    22.815     $ n & gamma spectrum
11     pz    30.00      $ change cell importance
12     pz    35.61      $ foil
13     pz    36.19      $ tld
14     pz    38.025     $ n & gamma spectrum
15     pz    45.00      $ change cell importance
16     pz    50.85      $ foil
17     pz    51.40      $ tld
18     pz    53.235     $ n & gamma spectrum
19     pz    60.84      $ foil & tld
20     pz    61.84      $ n & gamma spectrum
c    ------------------------------< cylinders centered on z-axis >--
21     cz     3.00
22     cz    31.50
c    ******* blank delimiter *******

c    ************************************
c    *  mode card      - neutron & photon *
c    ************************************
mode  n p
c    ************************************
c    *   cell importance card           *
c    ************************************
imp:n   1   1   1   1   1   1   2   2   2   2
        4   4   4   4   8   8   8   8   8   0
imp:p   1   1   1   1   1   1   2   2   2   2
        4   4   4   4   8   8   8   8   8   0
pwt   0.1 0.1 0.1 0.1 0.1 0.1 0.1 0.1 0.1 0.1
      0.1 0.1 0.1 0.1 0.1 0.1 0.1 0.1 0.1   0
c    ****************************************************
c    *  source specificatio cards                       *
c    *  si(eng.) and sp(prob.) are taken from 125 group *
c    *     spectrum of 1tr new water cooled target      *
c    ****************************************************
sc1   fns 1tr new water cooled target (125-g) by morce-dd
sdef  erg=d1  dir=d2  vec=0 0 1  pos=0 0 -20  wgt=1.1261
sb2   -31  4.0
si1   1.0010-11  3.2241-07
      5.3156-07  8.7640-07  1.4449-06  2.3823-06  3.9278-06
      6.4758-06  1.0677-05  1.7603-05  2.9023-05  4.7850-05
      7.8891-05  1.3007-04  2.1445-04  3.5357-04  5.8293-04
```

Fig. A.3 An example of input data for MCNP-4 calculation with neutron source.

```
      9.6110-04  1.2341-03  1.5846-03  2.0346-03  2.6125-03
      3.3546-03  4.3073-03  5.5307-03  7.1016-03  9.1186-03
      1.1709-02  1.5034-02  1.9304-02  2.1874-02  2.4787-02
      2.8087-02  3.1827-02  3.6065-02  4.0867-02  4.6308-02
      5.2474-02  5.9461-02  6.7378-02  7.6349-02  8.6515-02
      9.8035-02  1.1109-01  1.2588-01  1.4264-01  1.6163-01
      1.8315-01  2.0754-01  2.3517-01  2.6649-01  3.0197-01
      3.4217-01  3.8774-01  4.3936-01  4.9786-01  5.6415-01
      6.3927-01  7.2438-01  8.2084-01  9.3013-01  1.0540+00
      1.1943+00  1.3533+00  1.5335+00  1.7377+00  1.8498+00
      1.9691+00  2.0961+00  2.2313+00  2.3752+00  2.5284+00
      2.6914+00  2.8650+00  3.0498+00  3.2465+00  3.4559+00
      3.6787+00  3.9160+00  4.1686+00  4.4374+00  4.7236+00
      5.0282+00  5.3525+00  5.6978+00  6.0652+00  6.4564+00
      6.8728+00  7.3161+00  7.7879+00  8.2902+00  8.8249+00
      9.3940+00  9.9999+00  1.0157+01  1.0317+01  1.0480+01
      1.0645+01  1.0812+01  1.0983+01  1.1156+01  1.1331+01
      1.1510+01  1.1691+01  1.1875+01  1.2062+01  1.2252+01
      1.2445+01  1.2641+01  1.2840+01  1.3042+01  1.3248+01
      1.3456+01  1.3668+01  1.3883+01  1.4102+01  1.4324+01
      1.4550+01  1.4779+01  1.5012+01  1.5248+01  1.5488+01
sp1   0.0        1.5142-07
      2.2732-09  4.2225-09  7.4848-09  1.4264-08  8.3975-08
      1.8398-07  2.2450-07  1.3922-07  1.6817-07  2.9754-07
      3.8068-06  3.0541-06  2.2612-06  6.9372-06  7.2049-06
      8.7622-06  7.8013-06  1.4320-05  1.1820-05  1.6544-05
      1.4791-05  1.7624-05  2.8404-05  2.4899-05  3.7633-05
      4.4237-05  4.6320-05  6.1572-05  3.7185-05  5.3362-05
      4.8831-05  5.0292-05  5.7202-05  6.9230-05  8.0602-05
      8.3190-05  9.7450-05  1.0531-04  1.2632-04  1.4874-04
      1.7906-04  3.7225-04  4.9933-04  5.3824-04  6.0762-04
      7.0593-04  8.0965-04  9.5392-04  1.0785-03  1.2232-03
      1.3867-03  1.5803-03  1.6473-03  1.8238-03  2.0605-03
      2.2042-03  2.3040-03  2.5211-03  2.5709-03  2.5872-03
      2.5765-03  2.7699-03  2.8528-03  2.5945-03  1.3898-03
      1.4298-03  1.3270-03  1.3489-03  1.3820-03  1.4312-03
      1.3760-03  1.4329-03  1.4558-03  1.3518-03  1.4053-03
      1.2861-03  1.2741-03  1.1711-03  1.1937-03  1.0563-03
      1.0018-03  8.8451-04  7.9827-04  7.9293-04  7.5872-04
      6.9228-04  6.2956-04  5.1710-04  5.0750-04  5.1007-04
      4.1280-04  3.5649-04  9.0768-05  8.2287-05  9.2862-05
      9.1407-05  9.3708-05  7.9567-05  8.8737-05  8.7841-05
      1.1227-04  1.6798-04  1.5985-04  1.6563-04  2.1025-04
      4.1363-04  7.4899-04  7.8183-04  5.1771-04  4.5938-04
      4.6458-04  9.1020-04  2.6083-03  9.5007-04  5.1474-03
      3.0897-02  2.3565-01  4.0901-01  2.2296-01  1.4419-01
c     ********************************************
c     *  material specification cards              *
c     ********************************************
c     ---------------------------------< copper >--
m1    29000.41c  1.0
c     ---------------------------------< air >--
m2     7014.34c  3.8810-5   8016.34c  1.0400-5
c     ---------------------------------< materials for reaction rate>--
m3     5010.03y  1.0   $ B-10      (n,a)
m4    13027.03y  1.0   $ Al-27     (n,a)
m5    22000.03y  1.0   $ Ti-0      (n,x)Sc-46  (n,x)Sc-47  (n,x)Sc-48
m6    25055.03y  1.0   $ Mn-55     (n,g)
m7    26054.03y  1.0   $ Fe-54     (n,p)
m8    26056.03y  1.0   $ Fe-56     (n,p)
m9    27059.34c  1.0   $ Co-59     (n,2n)  (n,g)  (n,a)  (n,p)
m10   28058.03y  1.0   $ Ni-58     (n,2n)  (n,p)
m11   29063.34c  1.0   $ Cu-63     (n,2n)  (n,g)   (n,a)
m12   29065.34c  1.0   $ Cu-65     (n,2n)  (n,g)
m13   30064.03y  1.0   $ Zn-64     (n,p)
m14   40090.03y  1.0   $ Zr-90     (n,2n)
m15   41093.03y  1.0   $ Nb-93     (n,2n)Nb-92m
m16   49115.03y  1.0   $ In-115    (n,n')In-115m
m17   79197.03y  1.0   $ Au-197    (n,g)
m18   92235.03y  1.0   $ U-235     (n,f)
c     ********************************************
c     *  tally specification cards                 *
c     ********************************************
fc2   --  neutron spectrum        surface  ------------------------------
f2:n    2   3   4   5   6   7   8   9  10  11
       12  13  14  15  16  17  18  19  20
fs2   -21
fc12  --  neutron reaction rate   surface  ------------------------------
f12:n   2   3   4   5   6   7   8   9  10  11
       12  13  14  15  16  17  18  19  20
```

Fig. A.3 Continued

```
fm12   (1  1 102)  (1  3 107)  (1  4 107)  (1  5 210)  (1  5 211)
       (1  5 212)  (1  6 102)  (1  7 103)  (1  8 103)  (1  9  16)
       (1  9 102)  (1  9 103)  (1  9 107)  (1 10  16)  (1 10 103)
       (1 11  16)  (1 11 102)  (1 11 107)  (1 12  16)  (1 12 102)
       (1 13 103)  (1 14  16)  (1 15  16)  (1 16  51)  (1 17 102)
       (1 18  18)
fs12   -21
e12    15.488
fq12     s  e  f  m
fc22   --  neutron e-dependent reaction rate   surface  ----------------
f22:n   3   6   8  12  16
fm22   (1)          (1  1   2)  (1  1 102)  (1 11   2)  (1 11 102)
       (1 12   2)  (1 12 102)  (1  3 107)  (1  6 102)  (1 18  18)
fs22   -21
fc32   --  gamma-ray spectrum      surface  ----------------------------
f32:p   2   3   4   5   6   7   8   9  10  11
       12  13  14  15  16  17  18  19  20
fs32   -21
e32    1.0000-02  2.0000-02  3.0000-02  4.5000-02  6.0000-02
       8.0000-02  1.0000-01  1.5000-01  2.0000-01  3.0000-01
       4.0000-01  5.0000-01  5.2000-01  6.0000-01  7.0000-01
       8.0000-01  9.0000-01  1.0000+00  1.1300+00  1.2500+00
       1.3800+00  1.5000+00  1.7500+00  2.0000+00  2.2500+00
       2.5000+00  3.0000+00  3.5000+00  4.0000+00  4.5000+00
       5.0000+00  5.5000+00  6.0000+00  6.5000+00  7.0000+00
       7.5000+00  8.0000+00  9.0000+00  1.0000+01  1.2000+01
       1.4000+01
c      ---------------------------------------------------------------------
fq0      s  m  e  f
e0     1.0010-11  3.2241-07
       5.3156-07  8.7640-07  1.4449-06  2.3823-06  3.9278-06
       6.4758-06  1.0677-05  1.7603-05  2.9023-05  4.7850-05
       7.8891-05  1.3007-04  2.1445-04  3.5357-04  5.8293-04
       9.6110-04  1.2341-03  1.5846-03  2.0346-03  2.6125-03
       3.3546-03  4.3073-03  5.5307-03  7.1016-03  9.1186-03
       1.1709-02  1.5034-02  1.9304-02  2.1874-02  2.4787-02
       2.8087-02  3.1827-02  3.6065-02  4.0867-02  4.6308-02
       5.2474-02  5.9461-02  6.7378-02  7.6349-02  8.6515-02
       9.8035-02  1.1109-01  1.2588-01  1.4264-01  1.6163-01
       1.8315-01  2.0754-01  2.3517-01  2.6649-01  3.0197-01
       3.4217-01  3.8774-01  4.3936-01  4.9786-01  5.6415-01
       6.3927-01  7.2438-01  8.2084-01  9.3013-01  1.0540+00
       1.1943+00  1.3533+00  1.5335+00  1.7377+00  1.8498+00
       1.9691+00  2.0961+00  2.2313+00  2.3752+00  2.5284+00
       2.6914+00  2.8650+00  3.0498+00  3.2465+00  3.4559+00
       3.6787+00  3.9160+00  4.1686+00  4.4374+00  4.7236+00
       5.0282+00  5.3525+00  5.6978+00  6.0652+00  6.4564+00
       6.8728+00  7.3161+00  7.7879+00  8.2902+00  8.8249+00
       9.3940+00  9.9999+00  1.0157+01  1.0317+01  1.0480+01
       1.0645+01  1.0812+01  1.0983+01  1.1156+01  1.1331+01
       1.1510+01  1.1691+01  1.1875+01  1.2062+01  1.2252+01
       1.2445+01  1.2641+01  1.2840+01  1.3042+01  1.3248+01
       1.3456+01  1.3668+01  1.3883+01  1.4102+01  1.4324+01
       1.4550+01  1.4779+01  1.5012+01  1.5248+01  1.5488+01
c      ***********************************************
c      * problem cutoff cards                        *
c      ***********************************************
phys:n  20  0
phys:p  20  1  0
phys:e  20  1  1  1  1  1  1  1  1
cut:n   0  0.0        -0.5   -0.25   0
cut:p   0  0.999-02   -0.5   -0.25   0
nps      2500000
ctme     1000000000
c      ***********************************************
c      * peripheral cards                            *
c      ***********************************************
prdmp   1000000    1000000   1  1
lost     10        10
print
c      ******* blank terminator *******
```

Fig. A.3 Continued

```
analysis of cylindrical copper assembly (target gamma-ray only) 1992.11.30
c    ************************************
c    *   cell card                        *
c    ************************************
 1    2   4.9210-5    1   -2  -22
 2    2   4.9210-5    2   -3  -22
 3    1   8.4627-2    3   -4  -22
 4    1   8.4627-2    4   -5  -22
 5    1   8.4627-2    5   -6  -22
 6    1   8.4627-2    6   -7  -22
 7    1   8.4627-2    7   -8  -22
 8    1   8.4627-2    8   -9  -22
 9    1   8.4627-2    9  -10  -22
10    1   8.4627-2   10  -11  -22
11    1   8.4627-2   11  -12  -22
12    1   8.4627-2   12  -13  -22
13    1   8.4627-2   13  -14  -22
14    1   8.4627-2   14  -15  -22 .
15    1   8.4627-2   15  -16  -22
16    1   8.4627-2   16  -17  -22
17    1   8.4627-2   17  -18  -22
18    1   8.4627-2   18  -19  -22
19    2   4.9210-5   19  -20  -22
20    0              -1 : 20 : 22
c    ******* blank delimiter *******

c    ************************************
c    * surface card                     *
c    ************************************
c    ------------------------------< surfaces normal to z-axis >--
 1     pz   -21.00
 2     pz    -1.00     $ n & gamma spectrum
 3     pz     0.00     $ foil & tld
 4     pz     5.77     $ tld
 5     pz     7.605    $ n & gamma spectrum
 6     pz    10.11     $ foil
 7     pz    15.00     $ change cell importance
 8     pz    20.37     $ foil
 9     pz    20.98     $ tld
10     pz    22.815    $ n & gamma spectrum
11     pz    30.00     $ change cell importance
12     pz    35.61     $ foil
13     pz    36.19     $ tld
14     pz    38.025    $ n & gamma spectrum
15     pz    45.00     $ change cell importance
16     pz    50.85     $ foil
17     pz    51.40     $ tld
18     pz    53.235    $ n & gamma spectrum
19     pz    60.84     $ foil & tld
20     pz    61.84     $ n & gamma spectrum
c    ----------------------------< cylinders centered on z-axis >--
21     cz     3.00
22     cz    31.50
c    ******* blank delimiter *******

c    ************************************
c    *  mode card      - neutron & photon *
c    ************************************
mode  p
c    ************************************
c    *   cell importance card           *
c    ************************************
imp:p   1   1   1   1   1   1   2   2   2   2
        4   4   4   4   8   8   8   8   8   0
c    ************************************************
c    *  source specificatio cards                   *
c    *  si(eng.) and sp(prob.) are taken from 125 group *
c    *     spectrum of 1tr new water cooled target  *
c    ************************************************
```

Fig. A.4 An example of input data for MCNP-4 calculation with gamma-ray source.

```
sc1   fns 1tr new water cooled target (40-g) by mcnp
sdef  erg=d1  dir=d2  vec=0 0 1  pos=0 0 -20  wgt=0.1637
sb2   -31  4.0
si1    0.01   0.02   0.03   0.045  0.06   0.08   0.10   0.15
       0.20   0.30   0.40   0.50   0.52   0.60   0.70   0.80
       0.90   1.00   1.13   1.25   1.38   1.50   1.75   2.00
       2.25   2.50   3.00   3.50   4.00   4.50   5.00   5.50
       6.00   6.50   7.00   7.50   8.00   9.00  10.00  12.00
      14.00
sp1    0.0    0.0013 0.0043 0.0250 0.0696 0.2318 0.5007 2.5609
       3.4125 7.2808 5.7247 3.7319 1.8434 2.0816 4.7853 5.7954
       5.3656 3.1294 4.6562 6.1254 6.3671 2.3627 4.9191 3.1199
       2.4592 2.2063 4.1378 3.7776 3.2119 2.6491 2.0481 1.5872
       1.2038 1.0247 0.7557 0.5420 0.3557 0.4102 0.2306 0.1075
       0.0054
c     ********************************************
c     *  material specification cards             *
c     ********************************************
c     ---------------------------------< copper >--
m1    29000.  1.0
c     ---------------------------------< air >--
m2     7014.  3.8810-5   8016.  1.0400-5
c    ********************************************
c    *  tally specification cards                 *
c    ********************************************
fc32  --  gamma-ray spectrum      surface  ------------------------------
f32:p   2   3   4   5   6   7   8   9  10  11
       12  13  14  15  16  17  18  19  20
fs32  -21
e32   1.0000-02  2.0000-02  3.0000-02  4.5000-02  6.0000-02
      8.0000-02  1.0000-01  1.5000-01  2.0000-01  3.0000-01
      4.0000-01  5.0000-01  5.2000-01  6.0000-01  7.0000-01
      8.0000-01  9.0000-01  1.0000+00  1.1300+00  1.2500+00
      1.3800+00  1.5000+00  1.7500+00  2.0000+00  2.2500+00
      2.5000+00  3.0000+00  3.5000+00  4.0000+00  4.5000+00
      5.0000+00  5.5000+00  6.0000+00  6.5000+00  7.0000+00
      7.5000+00  8.0000+00  9.0000+00  1.0000+01  1.2000+01
      1.4000+01
fq32    s  m  e  f
c    ********************************************
c    * problem cutoff cards                      *
c    ********************************************
phys:p  20  1  0
phys:e  20  1  1  1  1  1  1  1  1
cut:p   0  0.999-02  -0.5   -0.25   0
nps      100000000
ctme     10
c    ********************************************
c    * peripheral cards                          *
c    ********************************************
prdmp   99999999   99999999   1  1
lost     10        10
print
c    ******* blank terminator *******
```

Fig. A.4 Continued